



Research and Development Technical Report
ECOM-4357

12
B.S.

ROTOR BLADE EFFECTS ON L-BAND SIGNALS RECEIVED BY
HELICOPTER ANTENNAS MOUNTED ABOVE THE ROTOR BLADE:
CW EXPERIMENTS

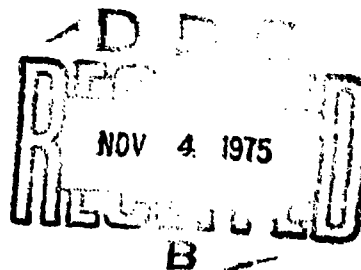
ADA 016866

C. M. DeSantis
F. Schwering

Communications/Automatic Data Processing Laboratory

October 1975

DISTRIBUTION STATEMENT
Approved for public release;
distribution unlimited.



ECOM

US ARMY ELECTRONICS COMMAND FORT MONMOUTH, NEW JERSEY 07703

| | |
|---------------|--------------------------------------|
| ACCESSION for | |
| NTIS | WASH DC 100 <input type="checkbox"/> |
| DDC | FORN ACQ <input type="checkbox"/> |
| UNCLASSIFIED | 10 |
| DATE | |
| BY | |
| DATE | INITIALS |

NOTICES

Disclaimers

The findings in this report are not to be construed as an official Department of the Army position, unless so designated by other authorized documents.

The citation of trade names and names of manufacturers in this report is not to be construed as official Government indorsement or approval of commercial products or services referenced herein.

Disposition

Destroy this report when it is no longer needed. Do not return it to the originator.

UNCLASSIFIED

SECURITY CLASSIFICATION OF THIS PAGE (When Data Entered)

| REPORT DOCUMENTATION PAGE | | READ INSTRUCTIONS BEFORE COMPLETING FORM |
|--|--|---|
| 1. REPORT NUMBER ECOM-4357 | 2. GOVT ACCESSION NO. | 3. RECIPIENT REPORT NUMBER |
| 4. TITLE (and Subtitle) ROTOR BLADE EFFECTS ON L-BAND SIGNALS RECEIVED BY HELICOPTER ANTENNAS MOUNTED ABOVE THE ROTOR BLADE: CW EXPERIMENTS. | 5. TYPE OF REPORT Final Experimental Report | 6. PERFORMING ORGANIZATION NAME |
| 7. AUTHOR(s) C. M. De Santis F. Schwering | 8. CONTRACT OR GRANT NUMBER(s) | 9. PERFORMING ORGANIZATION NAME AND ADDRESS Communications/Automatic Data Proc. Lab. AMSEL-NL-RH Fort Monmouth, New Jersey 07703 |
| 10. PROGRAM ELEMENT OR PROJECT TITLE 1161102861A Q1 451 | 11. CONTROLLING OFFICE NAME AND ADDRESS Communications/Automatic Data Processing Lab. U. S. Army Electronics Command Fort Monmouth, N. J. 07703 | 12. REPORT DATE 11 Oct 75 |
| 13. NUMBER OF PAGES 113 | 14. MONITORING AGENCY NAME & ADDRESS (if different from Controlling Office) | 15. SECURITY CLASSIFICATION UNCLASSIFIED |
| 16. DISTRIBUTION STATEMENT (of this Report) Approved for public release; distribution unlimited | 17. DISTRIBUTION STATEMENT (of the abstract entered in Block 20, if different from Report) | 18. SUPPLEMENTARY NOTES |
| 19. KEY WORDS (Continue on reverse side if necessary and identify by block number) Rotor modulation; L-band navigation system; Helicopter antennas; Shielding effect of rotor. | 20. ABSTRACT (Continue on reverse side if necessary and identify by block number) Rotor effects on L-Band signals received by helicopter antennas have been examined experimentally. CW data for two receiving-antenna locations above the rotor blade, viz. at the turning axis of the blade and on the tail, is presented. This data shows the amplitude and phase variations to be expected as a function of the direction of the incident signal. The effects of counterpoise size and height above the main rotor are also studied. In general it is shown that the signal variations were typically $\leq 3\text{ dB}$ for polar and | 15a. DECLASSIFICATION/DOWNGRADING SCHEDULE |

over

UNCLASSIFIED

SECURITY CLASSIFICATION OF THIS PAGE(When Data Entered)

$\theta < 90^\circ$ data $> 90^\circ$ des

of arrival $\theta \leq 70^\circ$; but that for greater angles, the signal amplitude changes by as much as ± 7 dB. For $\theta > 90^\circ$ (an arrival angle obtained, for instance, during a turning and banking maneuver) signal levels can decrease by -15 dB and the phase variation can exceed 180° . The tail location appears to be a better choice for the antenna than the center location. A worst-case analysis of CW rotor effects is presented in Appendix I. Appendices II and III contain some of the data measured at both antenna locations and should be referred to for a better understanding of the signal variations involved.



UNCLASSIFIED

SECURITY CLASSIFICATION OF THIS PAGE(When Data Entered)

CONTENTS

| | <u>Page</u> |
|--|-------------|
| 1. INTRODUCTION | 1 |
| 2. TEST FACILITIES AND INSTRUMENTATION | 1 |
| A. Mechanical Aspects | 1 |
| B. Electrical Aspects | 2 |
| C. Receiving Antenna and Mounting | 2 |
| 3. TEST RESULTS | 2 |
| A. Test Series | 2 |
| B. Amplitude Variations | 3 |
| C. Phase Variations | 3 |
| 4. DATA ANALYSIS | 6 |
| 5. CONCLUSIONS | 7 |
| ACKNOWLEDGMENTS | 7 |

APPENDICES

| | |
|---|----|
| I. WORST-CASE ANALYSIS OF ROTOR-BLADE EFFECTS ON ANTENNAS MOUNTED ABOVE THE ROTOR AT THE TURNING AXIS | 21 |
| II. EXPERIMENTAL DATA CHARACTERIZING THE SIGNAL FLUCTUATIONS AT THE CENTER LOCATION ABOVE THE ROTOR | 28 |
| III. SELECTED EXPERIMENTAL DATA CHARACTERIZING THE SIGNAL FLUCTUATIONS AT THE TAIL ABOVE THE ROTOR | 74 |

TABLES

| | |
|--|---|
| I. Azimuth and Polar Angles Considered for CW Rotor Blade Modulation Tests; Antenna at Center Position | 4 |
| II. Azimuth and Polar Angles Considered for CW Rotor Blade Modulation Tests; Antenna on Tail | 5 |

FIGURES

| | |
|-------------------------|----------|
| Figures 1 to 12 | 8 - 20 |
| Figures I-1 to I-4 | 24 - 27 |
| Figures II-1 to II-44 | 30 - 73 |
| Figures III-1 to III-38 | 76 - 113 |

ROTOR BLADE EFFECTS ON L-BAND SIGNALS RECEIVED BY HELICOPTER ANTENNAS MOUNTED ABOVE THE ROTOR BLADE: CW EXPERIMENTS

1. INTRODUCTION

A satellite navigation system is capable of providing high-accuracy three-dimensional location, velocity, and time information to users anywhere in the world. A typical signal structure for such a system involves phase shift keying a microwave carrier with a pseudo-random binary code. Four such two-state phase modulated satellite signals (using the same carrier frequency, but orthogonal codes) are processed at the receiver together with other information to provide real-time position, velocity, and time information.

Antenna systems for the reception of navigation signals must be able to view a large sky area. The four signals required must be received simultaneously by the same ground-based or airborne antenna. These signals may arrive from satellites widely separated from each other.

Antennas to be mounted on Army helicopters must be designed and placed to minimize or eliminate phase and amplitude distortions caused by the rotor blade. In a recent report [1] it was theoretically shown that signals received from a satellite by an antenna mounted on the cabin roof of a helicopter are subjected to severe amplitude and phase variations which could cause large errors during signal processing in the receiver or prevent the receiver from achieving the lock-on state.* In order to reduce these errors, antenna locations above the rotor blade, namely on the tail and at the turning axis of the blade, have been investigated.

This report discusses measurements of rotor effects on the CW microwave carrier made at these positions. A brief theoretical worst-case analysis for the center location is included in Appendix I. The overall experimental results presented in the body of this report were deduced from the amplitude and phase curves presented in Appendices II and III. These curves are representative of the hundreds of measurements made to characterize the helicopter antenna environment at the two locations under consideration.

2. TEST FACILITIES AND INSTRUMENTATION

A. Mechanical Aspects

Tests were performed on a full-scale UH-1B helicopter at the Wayside Test Site. Figure 1 shows the 80' high wooden tower with a microwave antenna mounted on an elevating track which provides a simulated L-band navigation

[1] F. Schwering and C. M. De Santis, "Rotor effects on L-band signals received by helicopter antennas. A theoretical study. Part I: Amplitude reduction and phase shift (shielding effect)," Research and Development Technical Report ECOM-4254, U. S. Army Electronics Command, Fort Monmouth, N. J., September 1974 (AD 787363).

*These theoretical findings have been verified experimentally and will be published as Part III of reference [1].

signal arriving at a selected polar angle and polarization. The helicopter rests on a rotating platform which permits azimuth angle variation (see Fig. 2). The rotor blade of this helicopter is rotated by a slow-speed synchro-positioner which drives the recording equipment inside the cabin and thereby provides received signal information as a function of instantaneous rotor position. The helicopter used is a non-operational UH-1B, stripped inside to provide room for the instrumentation and operators.

B. Electrical Aspects

The transmitting and receiving equipment were located inside the helicopter (see Fig. 3). The CW transmitter signal is split by means of a directional coupler: one branch feeds the transmitting antenna on the tower via a coaxial cable ($l = \sim 120$ ft.) and the other branch feeds the receiver as the reference signal. The phase and frequency locked receiver measures the amplitude and phase of a test signal as a function of this reference signal. Outputs from the receiver drive a 2-channel strip chart recorder, and thus provide amplitude and phase curves as a function of rotor position.

C. Receiving Antenna and Mounting

A simple dipole antenna tuned for operation at ~ 1.575 GHz was used to receive either horizontally or vertically polarized test signals. To minimize excitation of the feedline and supporting structure, a sleeve choke was incorporated with the antenna support post. The antenna was mounted a quarter wavelength above a removable counterpoise. The effectiveness of counterpoise shielding was indicated by the differences in the received amplitude and phase as a function of a 1λ and a 2λ diameter counterpoise. The antenna is protected by a thin plexiglass bubble secured to the counterpoise.

The antenna, counterpoise, and protective bubble were mounted on a long supporting tube. This assembly was centered at the top of the hollow rotor shaft by a large teflon bearing [Fig. 4(a)] and secured at the stationary base of the synchro-positioner [Fig. 4(b)]. This allowed the rotor to turn freely while the antenna remained fixed. For measurement purposes, the tube length was sufficient to allow a $0-1\lambda$ change in the antenna height above the top surface of the rotor blade. Due to the physical constraints imposed by the blade control mechanisms, what is referred to in the data as the zero position of the antenna was actually a height of 1λ above the blade.

The antenna assembly mounted on the helicopter tail is shown in Fig. 5. The antenna-supporting and height-adjusting tube was mounted concentrically inside a 6-foot long metal tube which was fastened to the tail fin of the helicopter. This arrangement provided a $0-1\lambda$ height adjustment. As in the previous case, zero height was 1λ above the top surface of the main rotor. However, in this case the reason for the offset was that the large tail rotor had to be cleared by the antenna (see Fig. 6). This tail rotor could be rotated manually, and several tests to determine its influence were performed.

3. TEST RESULTS

A. Test Series

The amplitude and phase variations of a microwave carrier which would occur in actual flight can be determined from CW measurements. This

can be seen by considering that the propagation time of the field scattered from any portion of the rotor to the antenna is much smaller than the time required for an appreciable change in rotor position* to occur. Thus the signal fluctuations caused by the scattering have already stabilized before the rotor has moved far enough to cause significant changes in the received signal. Of course, time delay distortions resulting from multipath can still cause errors in the coded signal.

Tables I and II give a list of the parameters considered in the CW experiments for the center and tail locations, respectively. A cross-section of the measured curves is given by the figures of Appendices II and III. The coordinate system for the CW experiments is shown in Fig. 7. Polar angles from 45° to 105° with respect to the vertical axis were investigated (the former is the minimum angle considered since evaluation of the data indicated no unusual results to be expected at steeper angles). The 105° angle was selected to represent the conditions obtaining during banking maneuvers.

B. Amplitude Variations

Amplitude reductions as a function of direction of incidence are shown in the 3-dimensional presentations of Fig. 8 (for center position) and Fig. 9 (for tail position). These diagrams show the worst case reception for each direction of incidence. The numerical values represent the maximum reductions below undistorted level[†] observed during a series of tests to determine the effect of variations in polarization, counterpoise size, and height. In general, most of the worst case data for the center position resulted from tests with the small counterpoise. The large-counterpoise data exhibits somewhat smaller changes in signal level (1 to 3 dB less) for $\theta < 60^\circ$. For larger angles $\theta \geq 85^\circ$, the data is comparable to that for the 1λ diameter counterpoise. Peak-to-peak fluctuations in amplitude were even greater for some cases than the attenuation levels shown in Figs. 8 and 9. However, increased receiver sensitivity is more difficult to achieve than dynamic range in current GPS receivers, hence the attenuation data is a better indicator of receiver requirements.

C. Phase Variations

The 3-dimensional plots given in Fig. 10 (for center position) and Fig. 11 (for tail position) show the maximum phase shifts sustained by the received signals as a function of the direction of incidence. The phase variations, of course, are continuous functions of rotor position; in some cases these variations may be symmetrical about 0° while in others they may occur in one direction only. It is difficult to estimate the effect of these phase variations on receiver performance without additional knowledge of the receiver design. However, in those cases where a 180° shift occurs, an incorrect bit is introduced into the code and, even for somewhat smaller

* 1λ at the rotor tips.

† The level received when the rotor was moved to the position of least interference.

Table 1. Azimuth and Polar Angles Considered for CW Rotor Blade Modulation Tests; Antenna at Center Position

| <u>Direction of Incidence</u> | | <u>Polarization</u> | | <u>Counterpoise Diameter</u> | | <u>Height above Rotor</u> | |
|-------------------------------|--------|---------------------|-----------------|------------------------------|-------------|---------------------------|------------------|
| θ | ϕ | <u>Horizontal</u> | <u>Vertical</u> | 1λ | 2λ | <u>Range</u> | <u>Step Size</u> |
| (in degrees) | | (in ft) | | | | | |
| 45 | 0 | x | x | x | x | 0-1 | 0.1 |
| | 180 | x | x | x | NM | 0-1 | 0.1 |
| 60 | 0 | x | x | x | x | 0-1 | 0.1 |
| | 180 | x | x | x | NM | 0-1 | 0.1 |
| 55 | 0 | x | x | x | x | 0-1 | 0.1 |
| | 90 | x | x | x | NM | 0-1 | 0.1 |
| | 180 | x | x | x | NM | 0-1 | 0.1 |
| 105 | 90 | x | x | x | NM | 0-1 | 0.1 |

NM: not measured.

x : measured

Table 11. Azimuth and Polar Angles Considered for CW Rotor Blade Modulation Tests; Antenna on Tail

| <u>Direction of Incidence</u> | | <u>Polarization</u> | | <u>Counterpoise Diameter</u> | | <u>Height above Rotor</u> | |
|-------------------------------|--------|---------------------|-----------------|---------------------------------|-------------------------------|---------------------------------|------------------|
| θ (in degrees) | ϕ | <u>Horizontal</u> | <u>Vertical</u> | <u>1 λ^+</u> | <u>2 λ</u> | <u>Range</u> (in λ) | <u>Step Size</u> |
| 55 | 0 | x | x | + | x | 0-1 | 0.3 |
| | 45 | x | x | + | x | 0-1 | 0.3 |
| | 90 | x | x | + | x | 0-1 | 0.3 |
| | 180 | x | x | + | x | 0-1 | 0.3 |
| 70 | 0 | x | x | + | x | 0-1 | 0.3 |
| | 90 | x | x | + | x | 0-1 | 0.3 |
| | 180 | x | x | + | NM | NM | NM |
| 85 | 0 | x | x | + | x | 0-1 | 0.2 |
| | 90 | x | x | + | x | 0-1 | 0.2 |
| | 180 | x | x | + | x | 0-1 | 0.2 |
| 105 | 0 | x | x | + | x | 0-1 | 0.2 |
| | 45 | x | x | + | x | 0-1 | 0.1 |
| | 90 | x | x | + | x | 0-1 | 0.2 |
| | 135 | x | x | + | x | 0-1 | 0.1 |
| | 180 | x | x | + | x | 0-1 | 0.1 |
| 45 | -110 | x | x | + | NM | NM | NM |
| | -45 | x | x | + | x | NM | NM |
| | 110 | x | x | + | x | NM | NM |
| 60 | -110 | x | x | + | x | NM | NM |
| | -45 | x | x | + | x | NM | NM |
| | 110 | x | x | + | x | NM | NM |
| 85 | -110 | x | x | + | x | NM | NM |
| | -45 | x | x | + | x | NM | NM |
| | 110 | x | x | + | x | NM | NM |
| 105 | -110 | x | x | + | x | NM | NM |
| | -45 | x | x | + | x | NM | NM |

NM: not measured; x: measured; +: only zero position measured.

phase deviations, long integration intervals in the receiver could result in the detection of a large number of bits with incorrect coding information. For $\theta > 85^\circ$, phase variations increase drastically and, in some directions, phase reversals ($> 180^\circ$ shifts) occur.

4. DATA ANALYSIS

It is apparent from Figs. 8 to 11 that the tail position is a better location for the antenna than the center position. Consider in particular the data for $\theta = 105^\circ$, which simulates a turning and banking maneuver. For this polar angle, regardless of antenna placement (center or tail position on helicopter), signal degradation is severe. Although this degradation obtains for all azimuth angles at the center location, severe fluctuations at the tail location occur only over an azimuth range of $\sim 60^\circ$ around $\phi = 0^\circ$. In the former case, the rotor always intercepts the signal at the polar angle $\theta = 105^\circ$ regardless of the azimuth; for this reason loss of lock in the receiver is a distinct possibility. At the tail location, however, the blade does not intercept the signal directly except over the azimuth range just mentioned. Furthermore, most helicopters normally fly in a pitched-forward attitude, so that the directions of incidence in the tests where large signal perturbations occurred, such as $\theta = 105^\circ$ and $\phi = 0^\circ$, may not occur in practice.

Considerably different responses were observed between horizontally and vertically polarized signals. In general, the horizontally polarized signals exhibited greater amplitude and phase fluctuations over all angles of incidence and, in particular, near grazing incidence. The reason for this behavior can be seen from the following argument. The tangential component of the electric field in the incident wave must be zero at the metal surface of the rotor blade. It is apparent that the greatest disturbance in the received field will occur when the blade is in the plane of incidence, rather than perpendicular to it. In the latter case, the effective scatter area of the blade, from which significant contributions to the received field strength are made, is considerably reduced, as shown qualitatively in Fig. 12(a). Figure 12(b) shows the increased blade area from which scattering contributes to the receiving antenna when the blade is parallel to the plane of incidence. This is indeed the case as shown by the data presented in Appendices II and III.

The following description pertains to the parallel orientation of the blade. In this case, for horizontal polarization of the incident signal, the electric field of the incident wave is entirely tangential to the blade, and the reflection coefficient at the metal surface is -1 , i.e., total reflection with a phase reversal. Thus, near grazing incidence, $\theta \approx 90^\circ$, where the path lengths of the direct and reflected field are approximately equal, the two field components tend to cancel at the receiving antenna, producing zero signal. On the other hand, the tangential component of a vertically polarized signal is a function of incidence angle and approaches zero near grazing incidence. The reflection coefficient at the blade surface is $+1$, i.e., total reflection but no phase reversal, and the equal path lengths occurring at shallow incidence angles result in reinforcement of the received signal. At $\theta = 0^\circ$, the rotor causes a strong scatter field for both polarizations since there is essentially no difference in the tangential component of the incident wave. However, the counterpoise effectively shields the antenna from this disturbance. For angles of incidence between the two limiting cases ($\theta = 0^\circ$ and $\theta = 90^\circ$), the tangential component of the

horizontally polarized signal will always be greater than that of the vertically polarized signal, and the fluctuations due to scattering will be more severe. This behavior becomes more apparent at increasing angles of incidence.

Circular polarization should minimize some of the fluctuations observed since they are caused by reflections from metal surfaces and will have a polarization sense opposite to that of the incident radiation. The helicopter antennas, of course, should be designed for optimum reception of the latter radiation.

Similar phase and amplitude distortions were measured at the two antenna positions for polar angles $< 70^\circ$. Examination of the curves in Appendices II and III also shows that the worst-case conditions depicted in Figs. 8, 9, 10, and 11 actually occur over, at most, a 40° sector of rotor rotation for the tail position and a 60° sector for the center position. Two such disturbances occur for each complete rotation of a single-bladed helicopter. Since the rotor on the UH-1B turns at ~ 330 rpm, a disturbance of the signal occurs at an 11 Hz rate with a duration of ~ 20 to 30 msec per disturbance, depending on the location of the antenna. This fact coupled with the signal degradation levels given in Figs. 8 to 11 is indicative of the receiver sensitivity required at the present time.

5. CONCLUSIONS

The results of this study show that it is more advantageous from an electrical as well as from a mechanical standpoint to locate the antenna on the tail rather than at the center of the helicopter. However, an antenna assembly which is aerodynamically acceptable must be designed. Two electrical problems still exist for the tail location. Because of the long RF cable from the antenna on the tail to the receiver in the cabin, a low-noise pre-amplifier may be necessary to maintain an acceptable signal-to-noise ratio. The second problem involves the poor response of planar antennas to signals arriving at or near grazing incidence. In this case, antennas of nonplanar design or conical spirals are strongly recommended. However, such three-dimensional designs are subject to somewhat greater influence from the rotor and helicopter. In this regard, the counterpoise having a diameter of one wavelength was found to be sufficient to minimize rotor modulation of the type discussed previously. The larger diameter counterpoise is more effective at the center location. Follow-up studies to determine the proper single antenna configuration, and investigation of multiple antenna configurations using switching and/or phasing techniques should be undertaken as a next step.

ACKNOWLEDGMENTS

The authors wish to thank Mr. J. R. Wills of the Antenna Research Team of the Communications/Automatic Data Processing Laboratory, ECOM, for his able assistance in performing the numerous and detailed measurements of this study. Thanks are also given Messrs. I. Levine and J. Gray of the Avionics Laboratory, ECOM, for their technical and administrative support, and to the U. S. Army Satellite Communications Agency, the sponsor of the program leading to the results given in this report and those given in reports ECOM-4254 and-4255, September 1974.

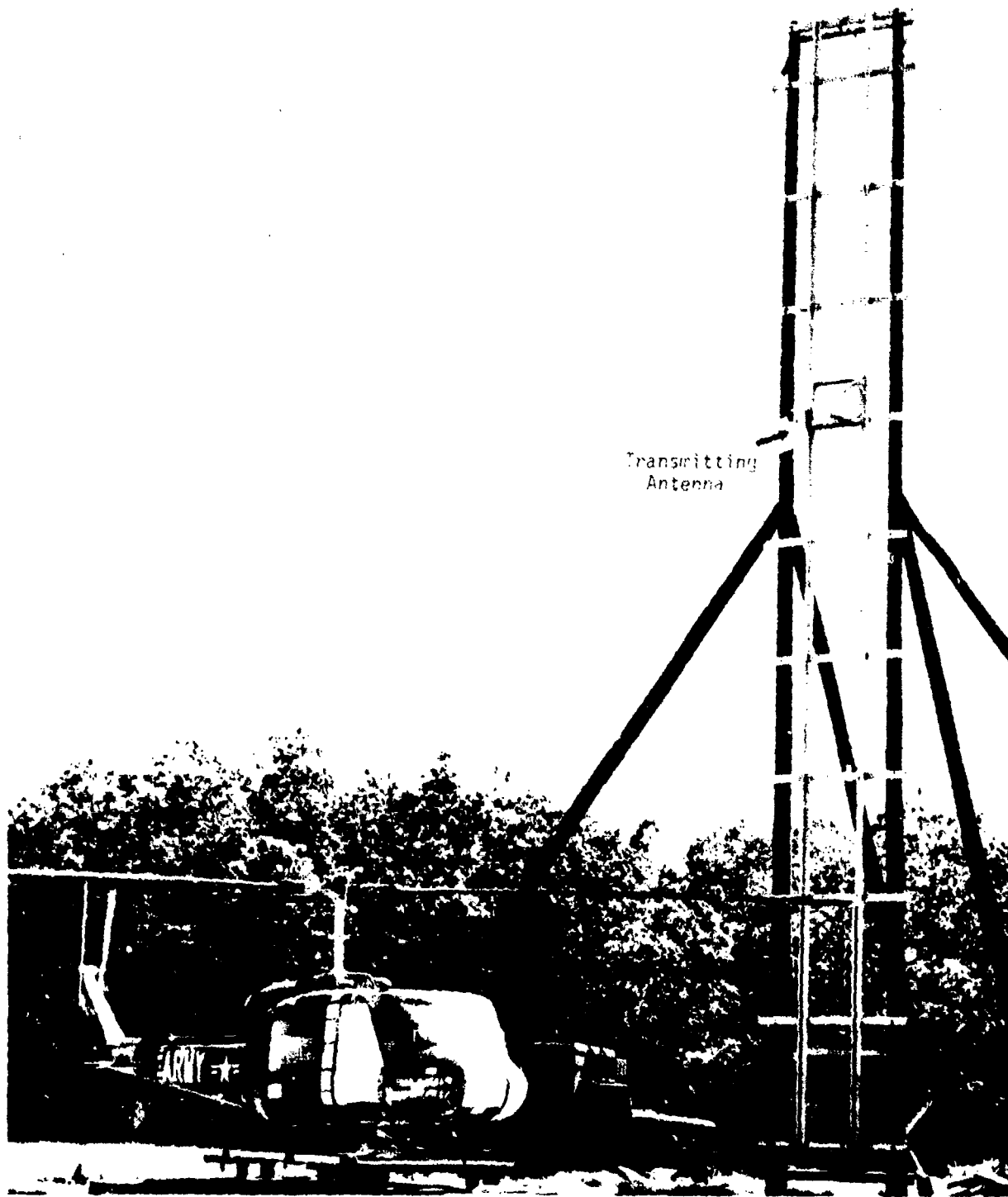


Fig. 1. Wayside test site.



Fig. 2. Helicopter and rotating platform for tests.

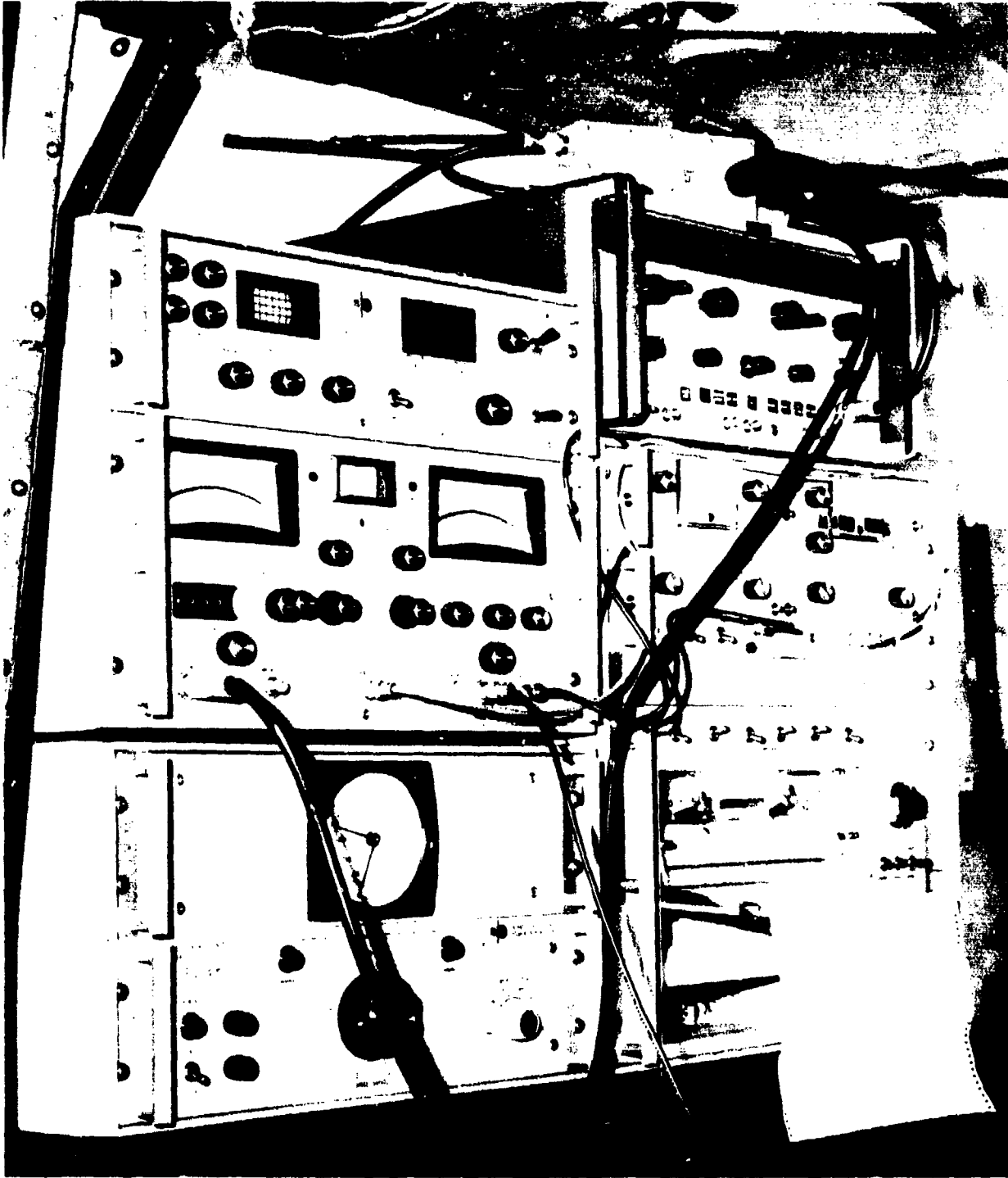


FIG. 3- CW TRANSMITTING, RECEIVING, RECORDING,
AND ROTOR POSITIONING EQUIPMENT

Receiving Antenna
and Counterpoise

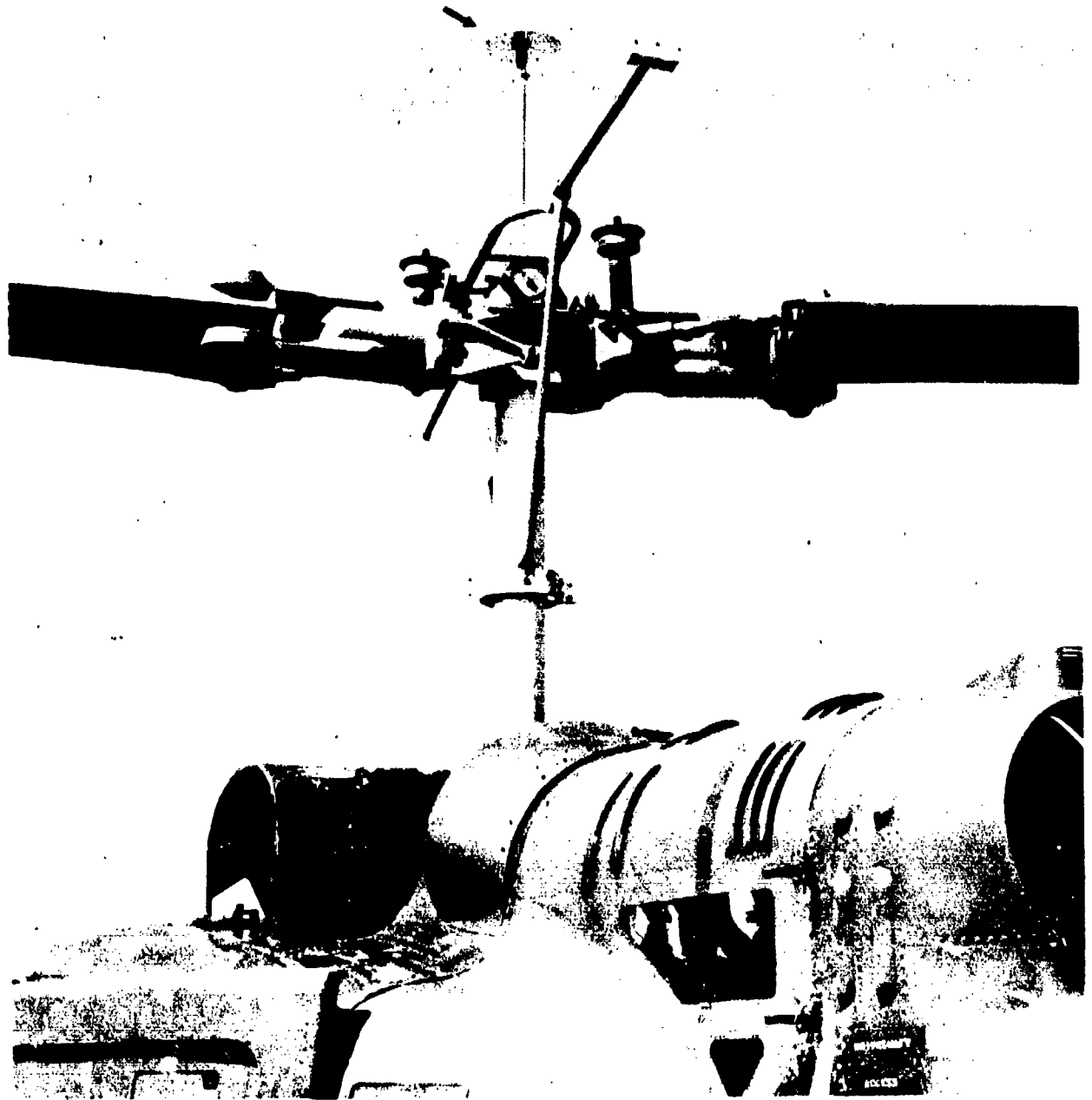


Fig. 4(a). RECEIVING ANTENNA ABOVE ROTOR (CENTER POSITION)

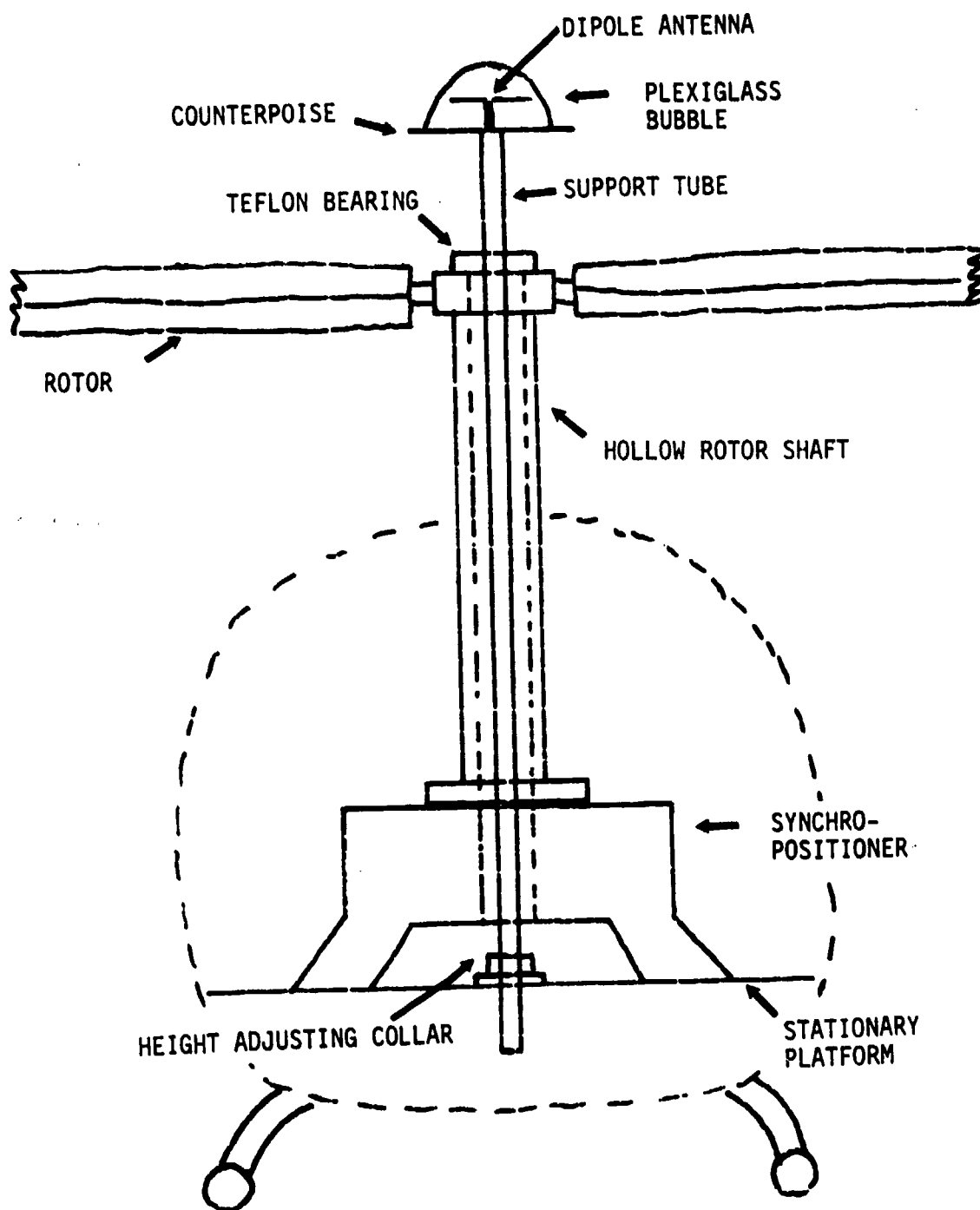


FIG. 4(b). ANTENNA AND SUPPORT TUBE MOUNTED IN THE HELICOPTER



FIG. 5- RECEIVING ANTENNA ABOVE ROTOR (TAIL POSITION)



FIG. 6- OVERALL VIEW OF RECEIVING ANTENNA ASSEMBLY AND TAIL ROTOR
SHOWING THE HEIGHT CONSTRAINT IMPOSED BY ROTOR LENGTH.

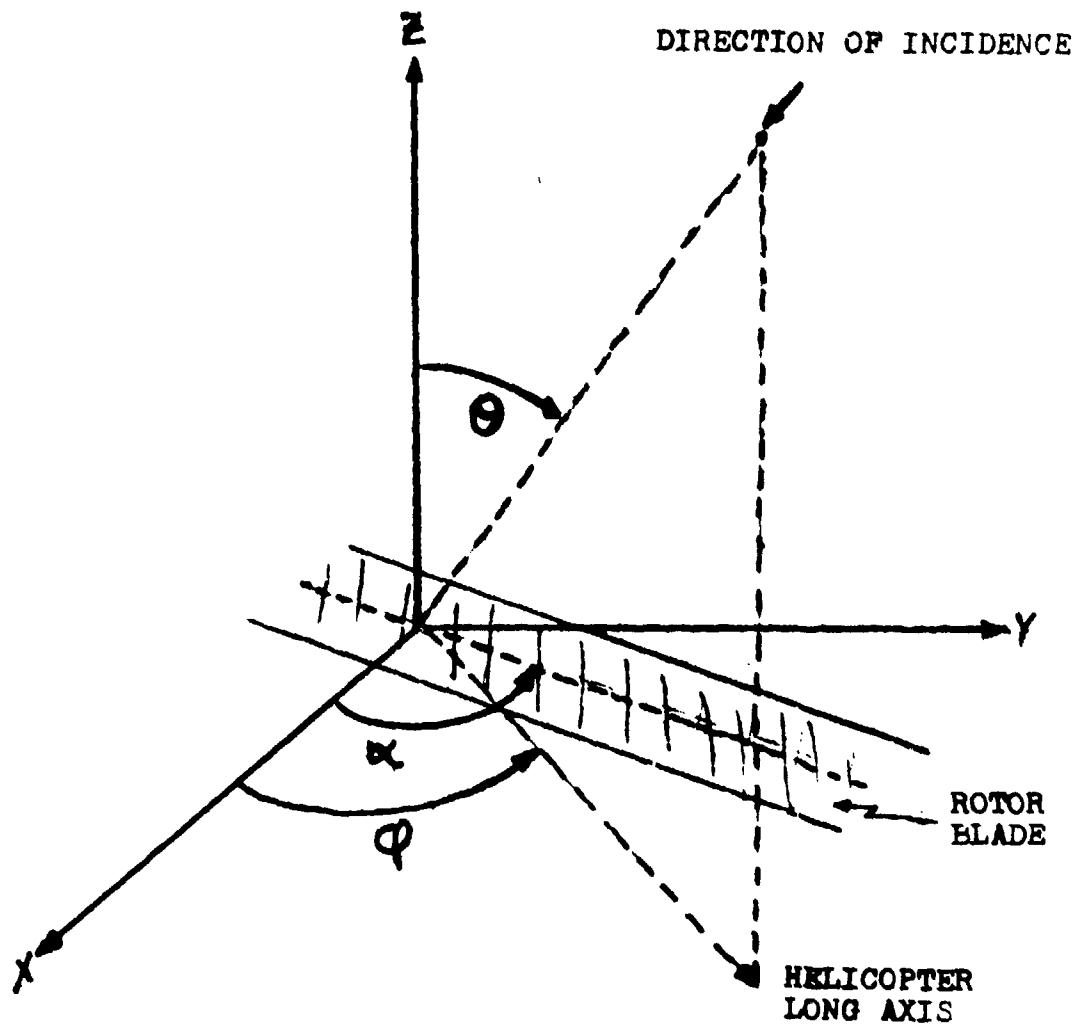
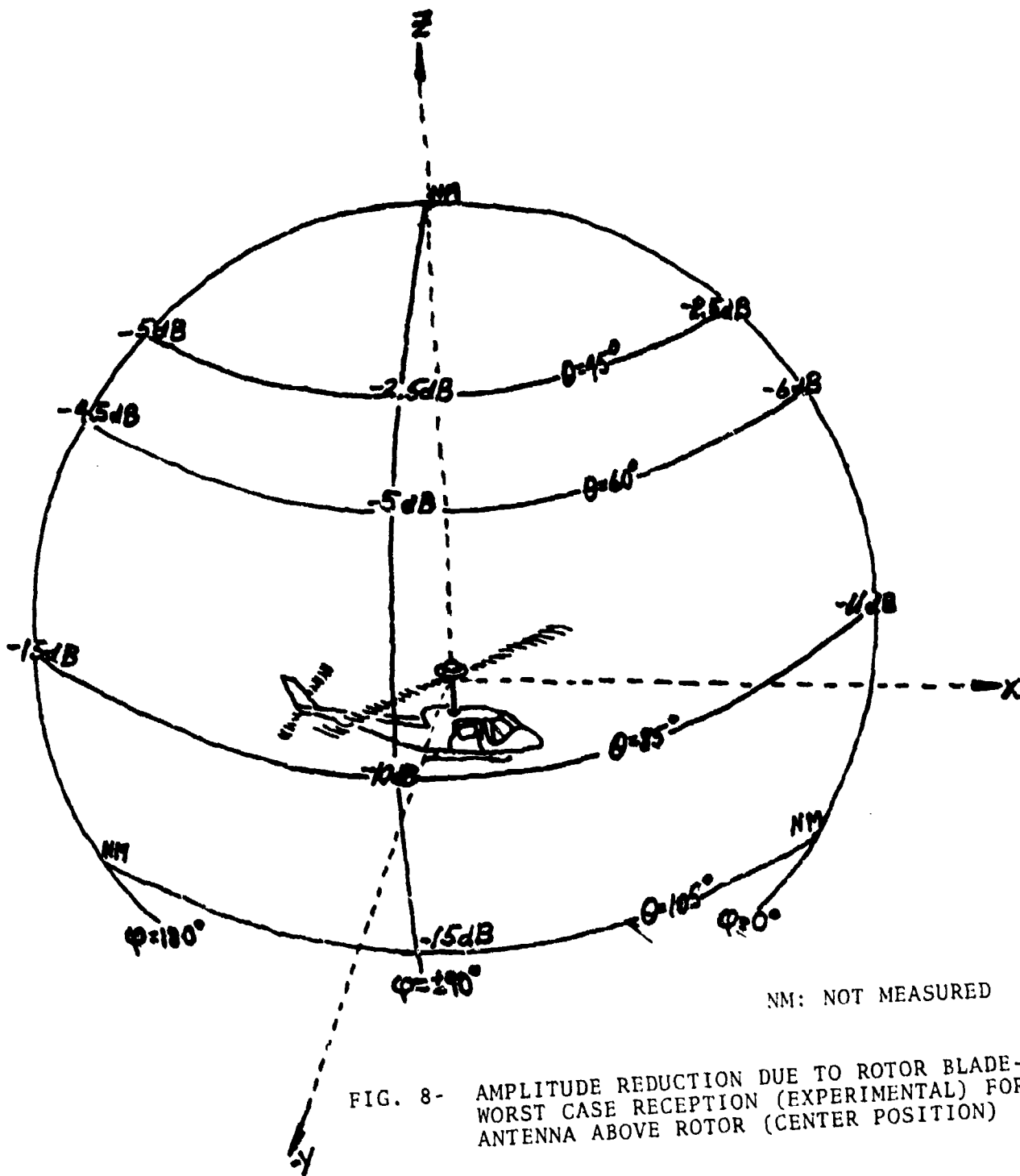


FIG. 7- COORDINATE SYSTEM FOR CW ROTOR BLADE MODULATION EXPERIMENTS



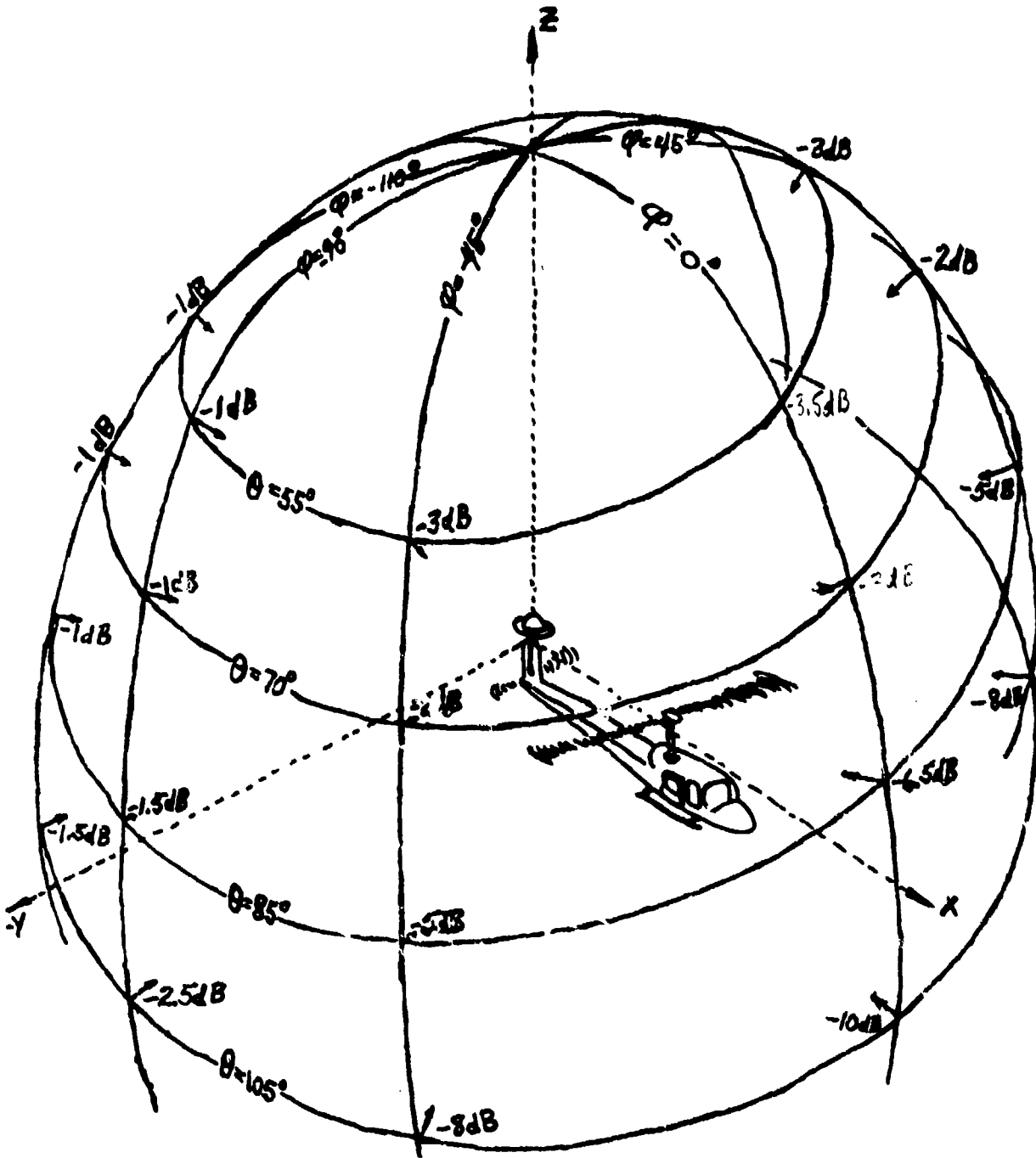
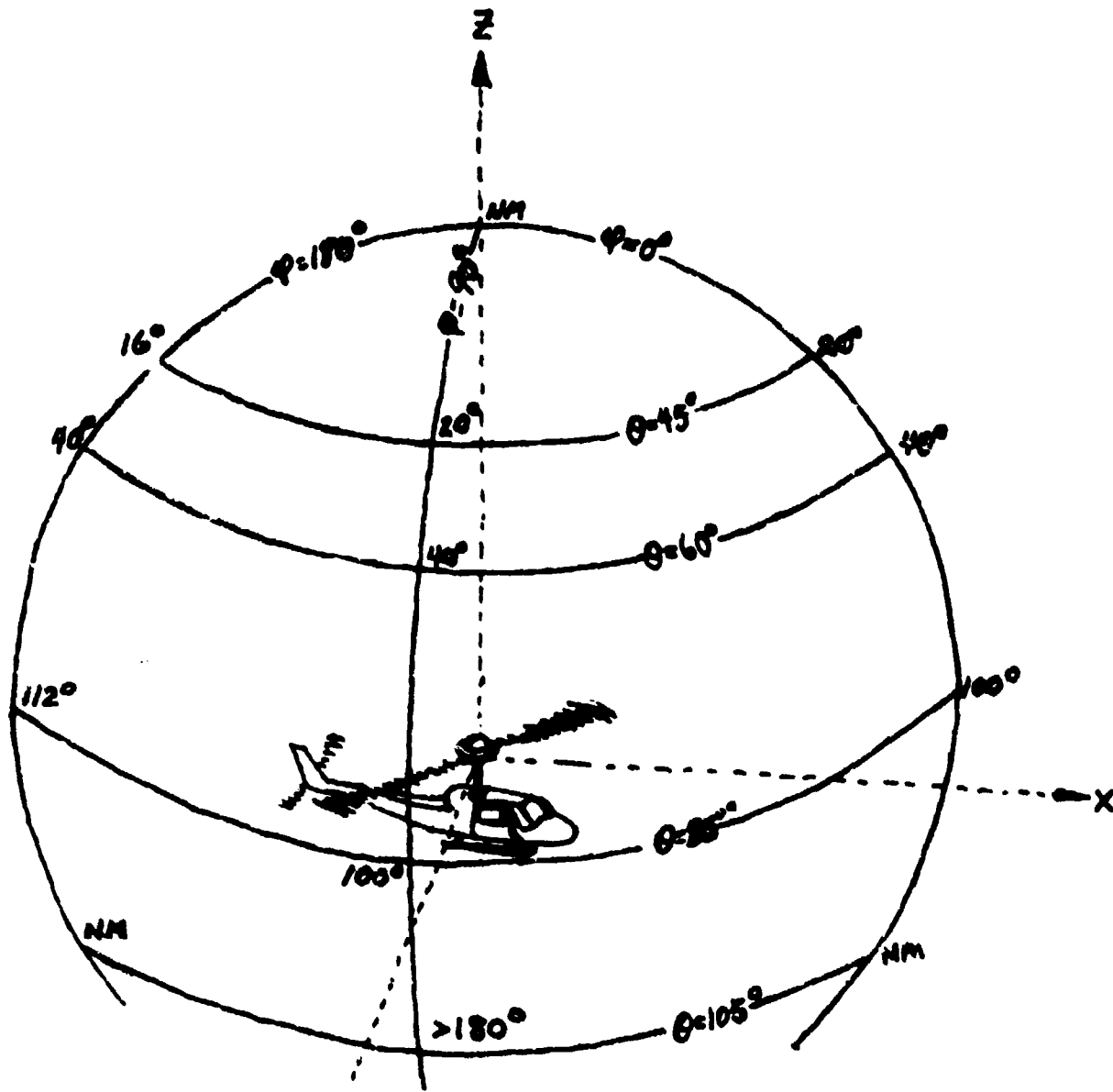


FIG. 9. AMPLITUDE REDUCTION DUE TO ROTOR BLADE-WORST CASE RECEPTION (EXPERIMENTAL) FOR ANTENNA ABOVE ROTOR (TAIL POSITION).



NM: NOT MEASURED

FIG. 10. PHASE DISTORTION DUE TO ROTOR BLADE-
 WORST CASE RECEPTION (EXPERIMENTAL) FOR
 ANTENNA ABOVE ROTOR (CENTER POSITION)

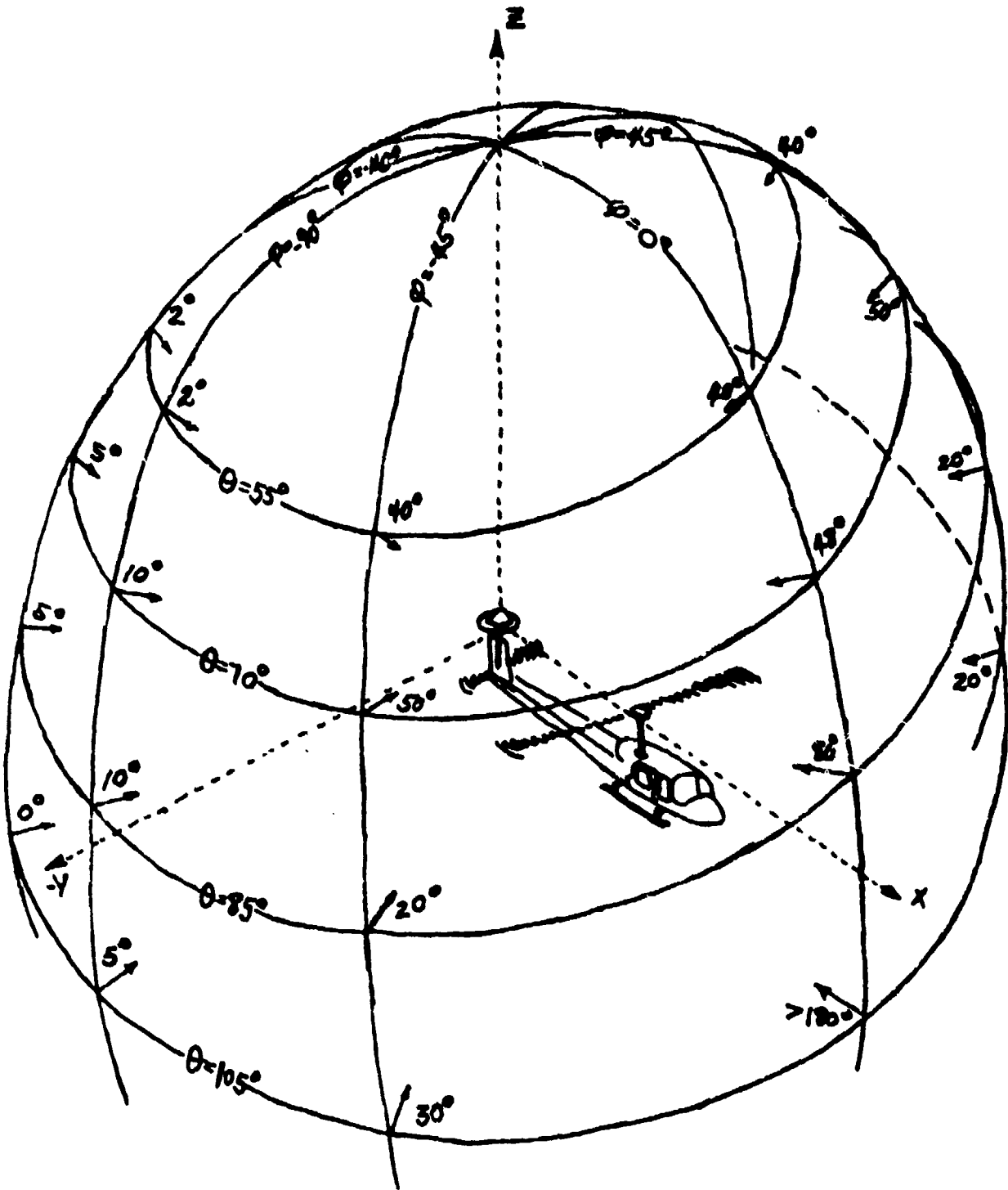


FIG. 11. PHASE DISTORTION DUE TO ROTOR BLADE-
 WORST CASE RECEPTION (EXPERIMENTAL) FOR
 ANTENNA ABOVE ROTOR (TAIL POSITION)

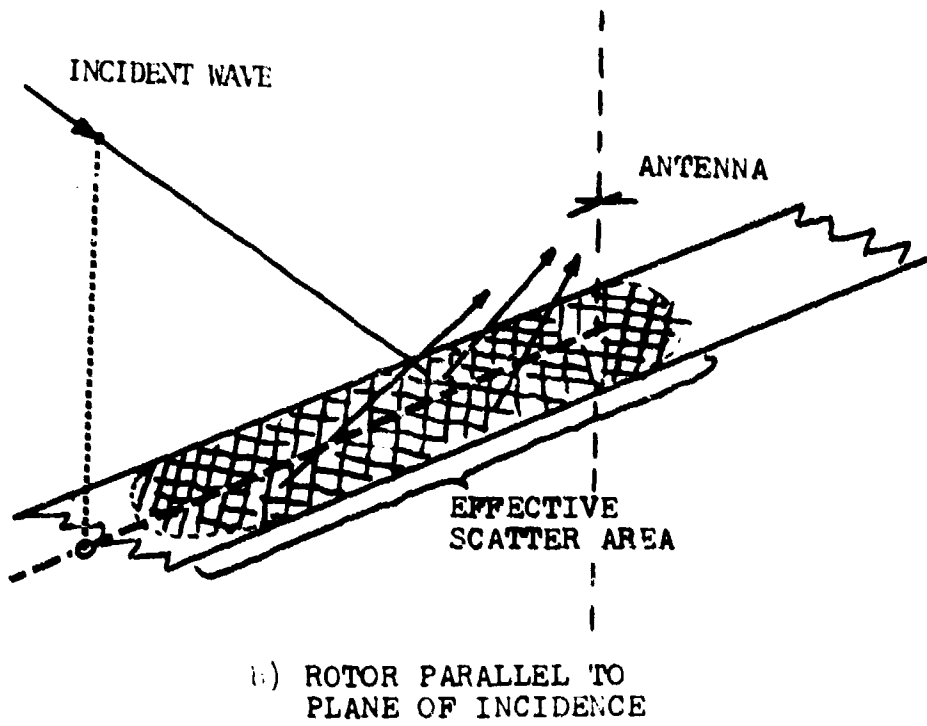
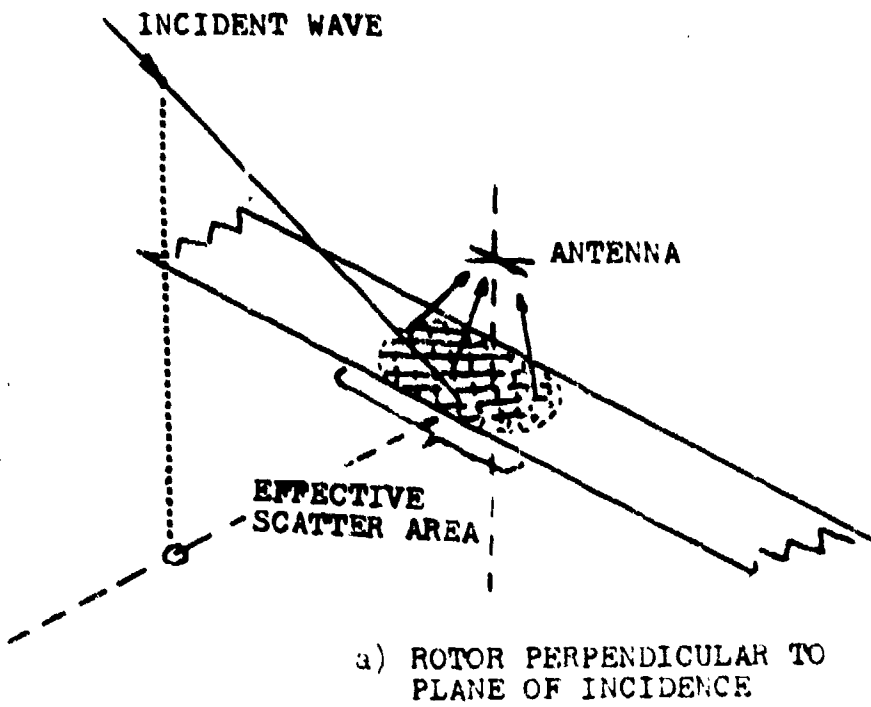


FIG. 12- EFFECTIVE SCATTER AREA OF THE ROTOR BLADE

APPENDIX I

WORST-CASE ANALYSIS OF ROTOR-BLADE EFFECTS ON ANTENNAS
MOUNTED ABOVE THE ROTOR AT THE TURNING AXIS

Consider the backscatter of the rotor blade and its effect on a signal received at the antenna in the configuration illustrated by Fig. I-1(a). Scattering will be greatest when the rotor blade is parallel to the plane of incidence, as depicted in Fig. I-1(b), the worst-case configuration. An incident plane wave field, in the two-dimensional case of Fig. I-1(b) given by

$$E_1 = E_0 \exp(-jk(ux + uz)) \quad (1)$$

where $u = -\sin\theta$, $w = -\cos\theta$ illuminates the antenna and rotor blade. To some extent, a counterpoise shields the antenna from the backscattered field of the rotor. This field according to [1] is:

$$E_2(x', z) = \left(\frac{jk}{2\pi}\right) \sqrt{1-u^2} \cdot E_0 \cdot z \cdot \exp(-jkux') \cdot \int_{-a}^a \exp\{-jk(r\sqrt{1-u^2})\} \frac{ds}{r^{3/2}} \quad (2)$$

where $r = \sqrt{(y'-c)^2 + z^2}$, a is the rotor blade half-width, and primed quantities denote observation points. What is the resultant field at the antenna? To simplify this problem, several assumptions will be made. We assume that: (1) the strongest distortion of the received field occurs only when the blade is in the plane of incidence (see the Sections "Data Analysis" and "Conclusions"); (2) the rotor blade surface is planar; (3) the blade extends to $\pm\infty$ in one dimension; (4) the effect of counterpoise shielding on the rotor is negligible [see Fig. I-1(b)]; and (5) the phase fronts of the scattered field at the location of the counterpoise are planar. Although these assumptions result in a somewhat greater reduction in the total field at the antenna than actually occurs, they provide an upper bound on the magnitude of the reduction and permit a simplification of Eq. (2):

$$E_2(x', z) = E_0 \cdot A(z) \cdot \exp(-jx' \sin\theta) \quad (3)$$

where

[1] F. Schwering and C. M. De Santis, "Rotor effects on L-band signals received by helicopter antennas. A theoretical study. Part I: Amplitude reduction and phase shift (shielding effect)," Research and Development Technical Report ECOM-4254, U. S. Army Electronics Command, Fort Monmouth, N. J., September 1974 (AD 787363).

$$A(z) = + \sqrt{\frac{2 \cos \theta}{\pi}} \cdot z \cdot \int_0^a \exp\left\{-j\left(\sqrt{z^2+s^2} \cos \theta + \frac{3\pi}{4}\right)\right\} \frac{ds}{(z^2+s^2)^{3/4}} \quad (4)$$

All linear dimensions have been normalized by multiplication with $k = 2\pi/\lambda$. The field expressed by Eq. (3) illuminates the counterpoise from below. When Eq. (3) and the appropriate Green's function for a plane surface are used in Green's Theorem, the field scattered by the counterpoise is

$$E_3(x', z) = \frac{1}{2\pi} \int_0^b \int_0^{2\pi} E_2(x', h) \frac{\partial}{\partial z} \left(\frac{e^{-jR}}{R} \right) r \, dr \, d\phi, \quad (5)$$

where $R = \sqrt{r^2 + (z-h)^2}$. The geometry for this aspect of the problem is shown in Fig. I-2(a). Integration with respect to ϕ and partial integration over r may be performed to give:

$$E_3(z) = +E_0 \cdot A(h) \cdot z \cdot \left\{ J_0(r \sin \theta) \cdot \frac{e^{-jR}}{R} \Big|_0^b + \sin \theta \cdot \int_0^b J_1(r \sin \theta) \frac{e^{-jR}}{R} \, dr \right\} \quad (6)$$

for $X' = 0$. J_0 and J_1 are the first- and second-order Bessel functions of the first kind. $A(h)$ is obtained from Eq. (4) for $Z = h$. Equations (3) and (6) are added to obtain the total field received at the antenna location when the field produced by the rotor is scattered by the counterpoise, i.e.,

$$E_{23}(z) = E_2(z) + E_3(z). \quad (7)$$

A further contribution to the total field at the antenna must be considered: the backscatter of the finite diameter counterpoise illuminated by the primary field. The coordinate system applicable to this problem is shown in Fig. I-2(b). Using Green's Theorem, the primary field of Eq. (1) and an approximate set of boundary conditions at $Z = h$,

$$-E_1(r, h) = E_{\text{Counterpoise}}(r, h) \quad \text{for } r \leq b$$

$$E_{\text{Counterpoise}}(r, h) = 0 \quad \text{for } r > b,$$

the backscatter field is:

$$E_{\text{Counterpoise}}(z) = + \frac{1}{2\pi} \int_0^{2\pi} \int_0^b E_1(r, h) \frac{\partial}{\partial z} \left(\frac{e^{-jR}}{R} \right) r \, dr \, d\phi \quad (8)$$

where $R = \sqrt{r^2 + z^2}$. Integration with respect to ϕ and partial integration over r yields

$$E_{\text{Counterpoise}}(z) = + E_0 \cdot z \cdot \exp(jh \cos\theta) \cdot \left\{ J_0(r \sin\theta) \frac{e^{-jR}}{R} \Big|_0^b + \sin\theta \cdot \int_0^b J_1(r \sin\theta) \frac{e^{-jR}}{R} \, dr \right\}. \quad (9)$$

The total field at the antenna due to this contribution is given by:

$$E_{c1}(z) = E_1(z) + E_{\text{Counterpoise}}(z). \quad (10)$$

The total field at the antenna from all sources can then be determined by adding Eqs. (7) and (10):

$$E_T = E_{23} + E_{c1}. \quad (11)$$

Equation (11) has been programmed for numerical evaluation, and some results for $\theta = 45^\circ$ and 85° are shown in Figs. I-3 to I-4.* Figure I-3 also illustrates the effect of counterpoise diameter. The amplitude curves are referenced to the theoretical value of the received field at the 0 position (i.e., 1λ above the rotor). Comparison of these curves with the appropriate data of Appendix II shows fairly good agreement with regard to the amplitude excursions and the slope of the phase variations. Further detail is lost in the experimental data. The abrupt change in phase shown in Fig. I-3 (a 360° phase jump) was caused by the automatic plotting routine and was not a true effect. A more exact theory of rotor modulation for the antenna at both positions above the rotor blade has been attempted, but no results are available at the present time.

* At or near grazing incidence, this theoretical description of counterpoise effects cannot be expected to be accurate. In fact, the curves in Fig. I-4 tend to diverge with increasing height. However, for $0 \leq h \leq 1\lambda$, the theory is in fair agreement with the measured results.

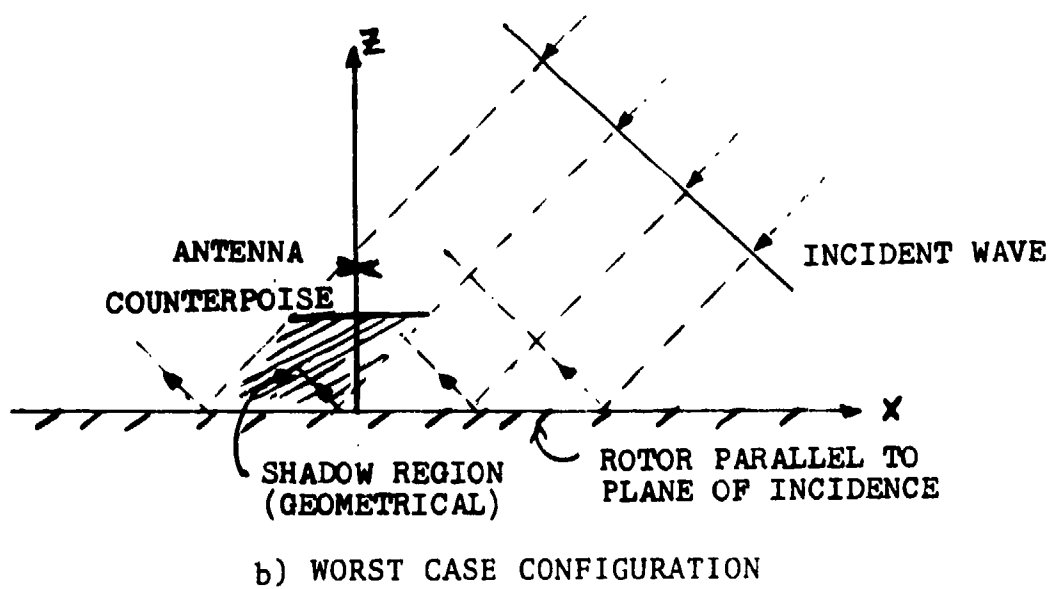
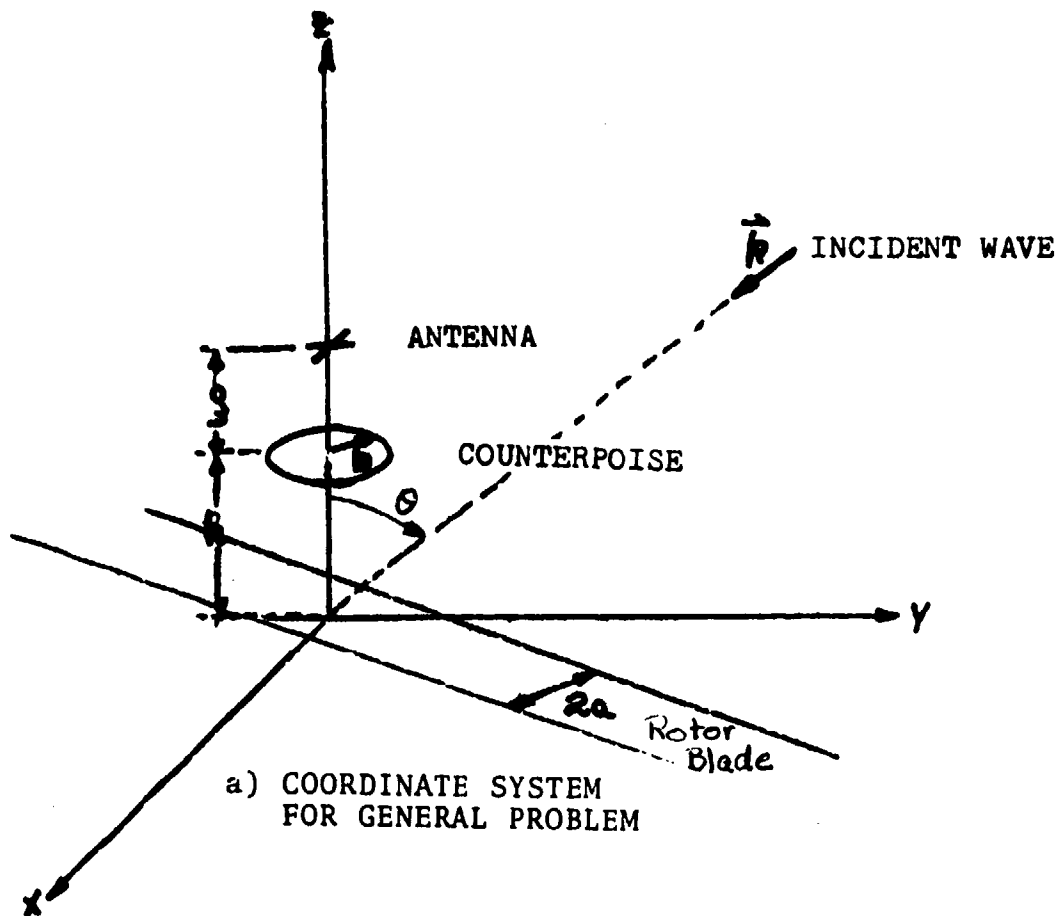
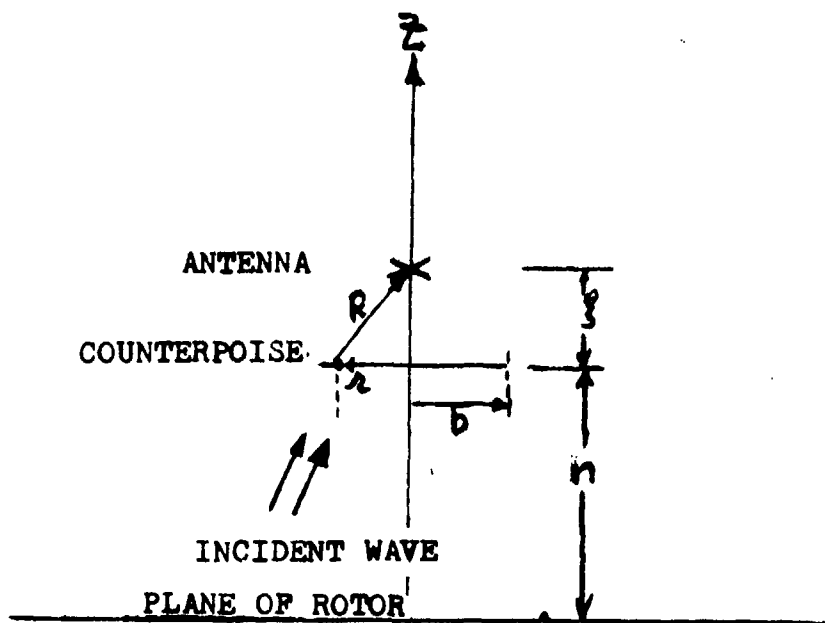
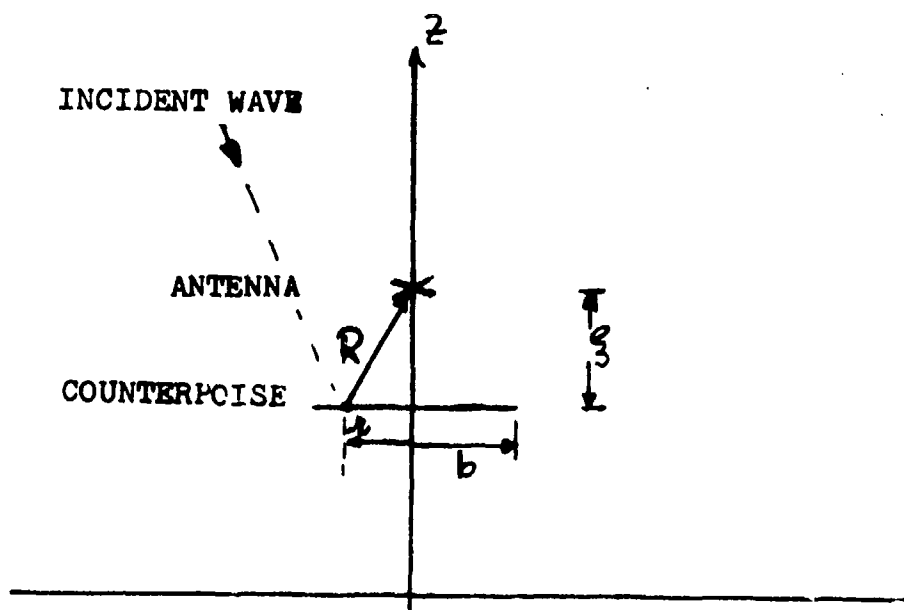


FIG. I-1- TYPICAL ROTOR SCATTERING PROBLEM



a) GEOMETRY FOR DETERMINATION OF COUNTERPOISE EFFECT ON FIELD SCATTERED FROM ROTOR



b) GEOMETRY FOR DETERMINATION OF BACKSCATTER FROM COUNTERPOISE IN PRIMARY FIELD

FIG. I-2- SCATTER EFFECTS CAUSED BY COUNTERPOISE

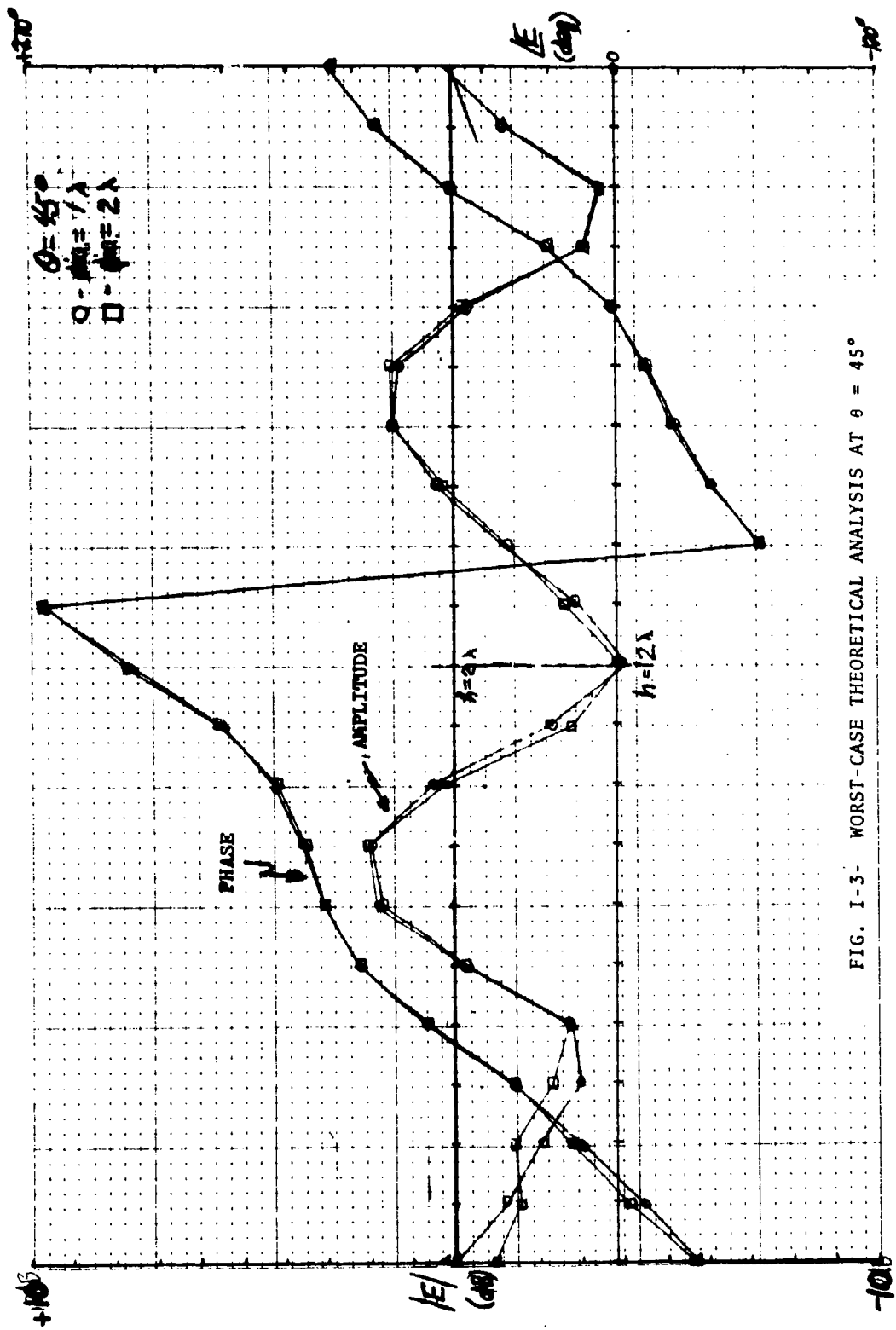


FIG. I-3- WORST-CASE THEORETICAL ANALYSIS AT $\theta = 45^\circ$

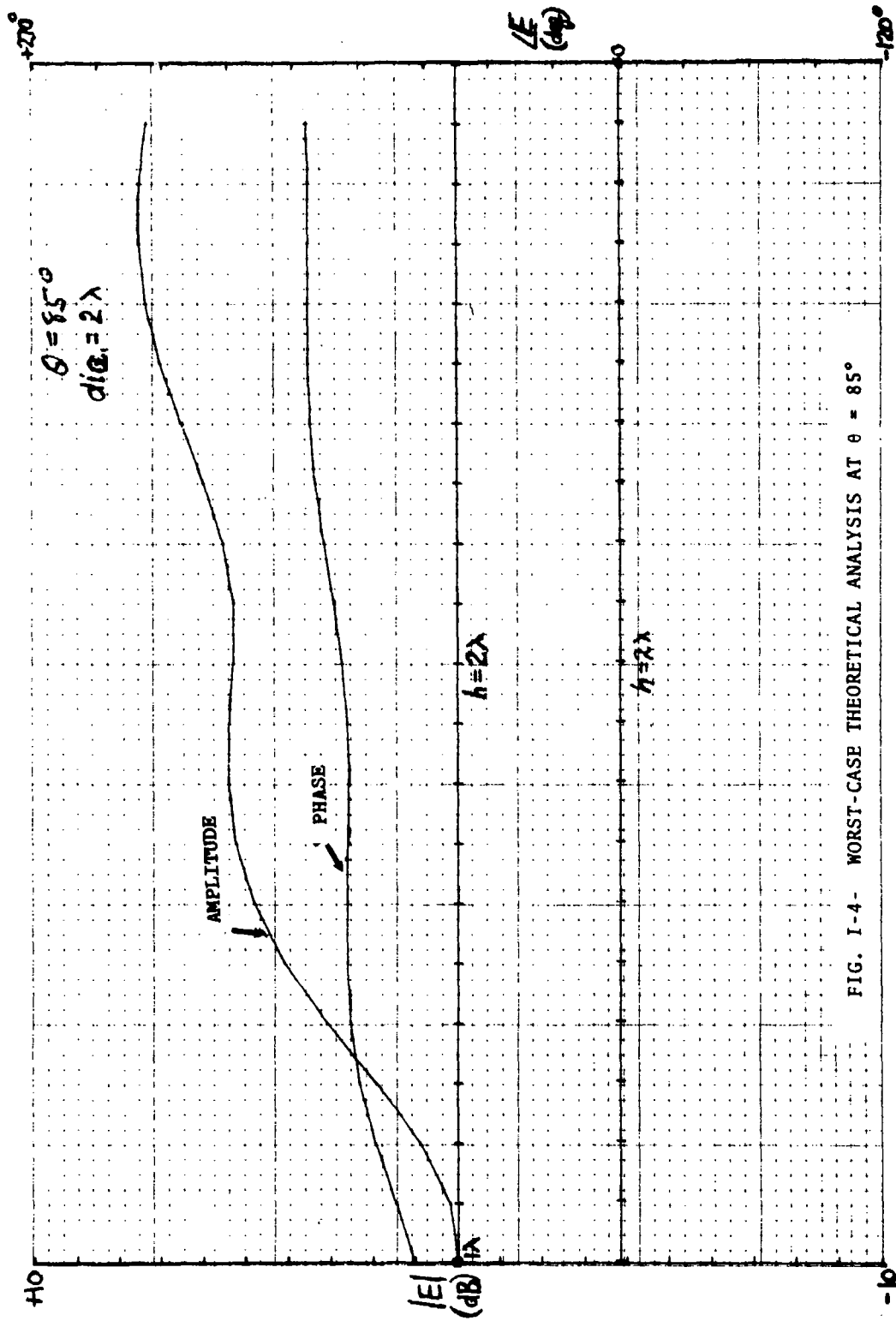


FIG. I-4- WORST-CASE THEORETICAL ANALYSIS AT $\theta = 85^\circ$

APPENDIX II

EXPERIMENTAL DATA CHARACTERIZING THE SIGNAL FLUCTUATIONS AT THE CENTER LOCATION ABOVE THE ROTOR

All of the data taken to characterize signal reception at the center location above the rotor blade is shown in the curves of this appendix. In general, eight such curves are required for each set of polar and azimuth angles (θ, ϕ) considered. Data for two different sized counterpoises (dia. = $1\lambda, 2\lambda$) is presented for horizontal and vertical polarization. Typically, four odd- and four even-numbered illustrations are presented for each direction of incidence. The odd-numbered figures show the amplitude and phase variations actually measured for the zero position whereas the even-numbered figures are composites generated from the measured data showing the signal variations as a function of height. Only small-counterpoise data for both polarizations is available at $\phi = 90^\circ, 180^\circ$ for all θ values considered. However, the small counterpoise is less effective as a shield against rotor scatter than the large counterpoise; thus the small-counterpoise data represents worst-case conditions at these azimuth angles.

The even-numbered figures for any given (θ, ϕ) set consist of multiple curves displaying amplitude and phase changes as a function of height for several fixed rotor positions. These fixed positions have been selected from the measured data to show the amplitude and phase variations to be expected over the full 360° rotation of the blade. Two rotor positions, $\alpha = 0^\circ$ and $\alpha = 90^\circ$, are shown in each of the even-numbered figures. In addition, a third rotor position, and sometimes a fourth- and a fifth position are shown for clarification of the variations which occurred for the various directions of incidence. The composite amplitude curves show that horizontally polarized incident signals undergo stronger scattering from the rotor than vertically polarized signals, especially at shallower angles of incidence.

The composite phase curves shown in the even-numbered figures require some explanation. First of all, some of the curves show an abrupt change of phase with height. These breaks are due to the method of plotting only and do not represent phase reversals of the signal. Since the phase variation measured as a function of height is greater than 360° for some directions of incidence and since the graph ordinate range is limited to 360° , some of the curves have been broken into two parts in order to show the entire variation. True phase reversals, i.e., $\Delta\phi \geq 180^\circ$, were observed only for horizontally polarized signals arriving at $\theta = 105^\circ, \phi = 90^\circ$. The slope of the phase curves, which gives an indication of the polar angle of arrival, are as anticipated (i.e., steeper for small polar angles than for near grazing incidence). This behavior agrees with the theoretical curves of Appendix I.

Some comments on the individual figures given in this Appendix are:

(1) Figures II-1 to II-12 show the set $\theta = 45^\circ, \phi = 0^\circ, 180^\circ$; only two azimuth angles were examined since these directions show helicopter body effects. Note that the larger counterpoise is a more effective shield than the smaller counterpoise. Note also that greater fluctuations result from horizontal polarization than from vertical polarization;

(2) Figures II-13 to II-24 show the set $\theta = 60^\circ$ and $\phi = 0^\circ, 180^\circ$. Differences in the shielding effectiveness of the large and small counterpoise become less significant for this direction of incidence. The general characteristic of all these curves is that there is a 1 to 2 dB increase in the amplitude variations as compared to those considered in (1) above;

(3) Figures II-25 to II-40 show the set $\theta = 85^\circ$ and $\phi = 0^\circ, 90^\circ, 180^\circ$. Note here that the ordinate for some of the amplitude curves is 10 dB per major division rather than 5 dB and that the slope of the phase curves is decreasing with increasing polar angle. Additional rotor positions have been included to indicate the increased scatter effects of the rotor at large polar angles; also note, in contrast to the previous cases of (1) and (2) above, that a change in height did not reduce the scatter effects of the rotor and that there was practically no difference in the shielding effectiveness of the large and the small counterpoise. The azimuth angle $\phi = 90^\circ$ is shown for comparison with $\phi = 0^\circ$ and 180° in order to indicate multipath effects of the helicopter body;

(4) Figures II-41 to II-44 show the set $\theta = 105^\circ$ and $\phi = 90^\circ$. This direction of incidence will occur during turning and banking maneuvers; it is apparent (although no measurements were made) that at $\theta = 105^\circ$ and $\phi = 180^\circ$, the antenna will be completely shielded from the direct signal by the tail boom, the tail fin, and the tail rotor resulting in complete signal drop-out. True 180° phase reversals in the received signal occurred for this direction of incidence.

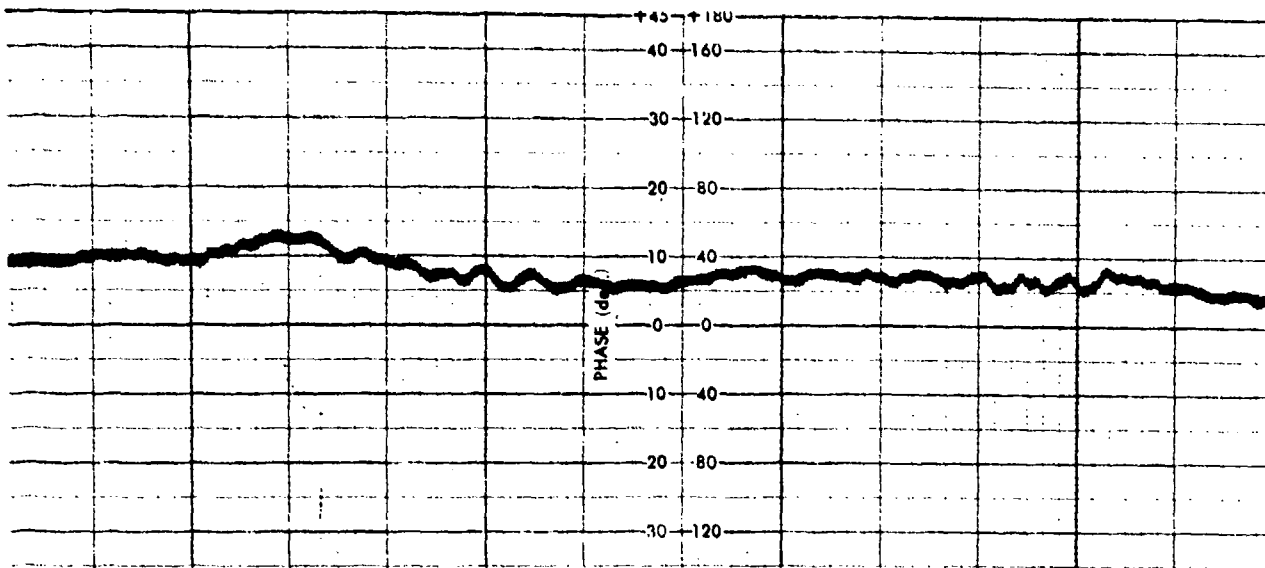
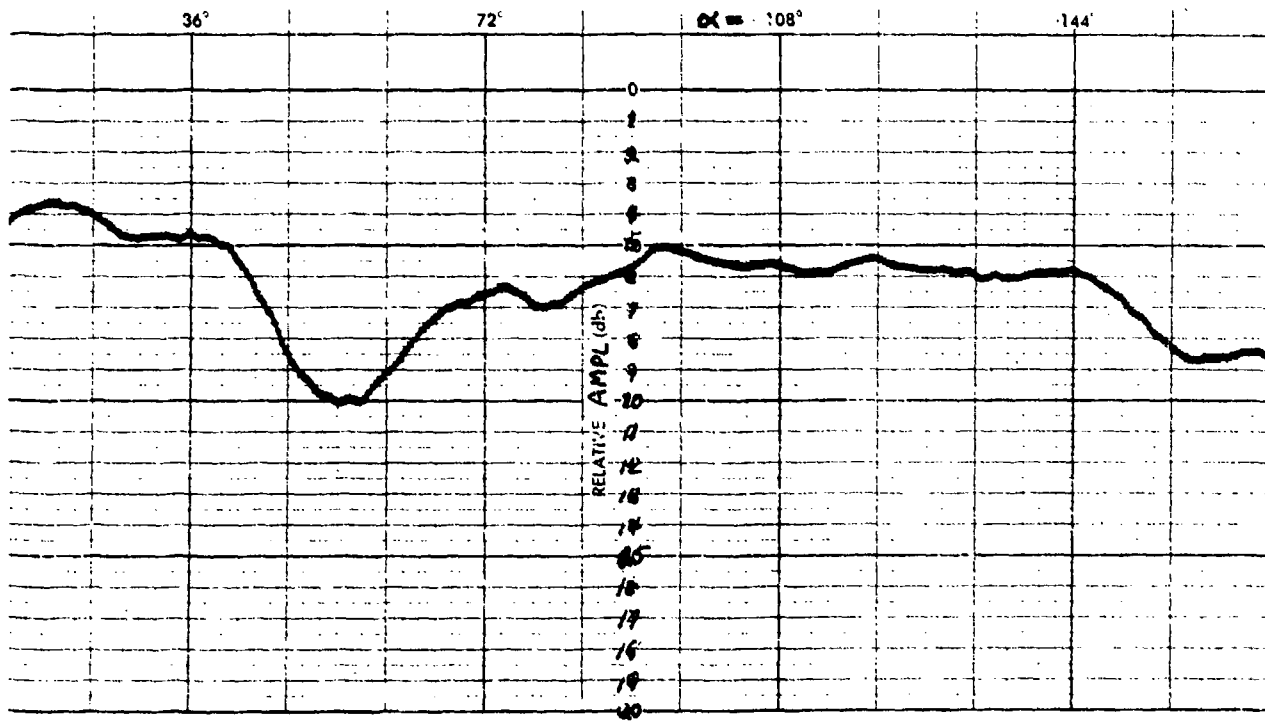


FIG. II-1. AMPLITUDE AND PHASE VARIATIONS
FOR SMALL COUNTERPOISE AND
HORIZONTAL POLARIZATION AT
 $\theta = 45^\circ$, $\phi = 0^\circ$



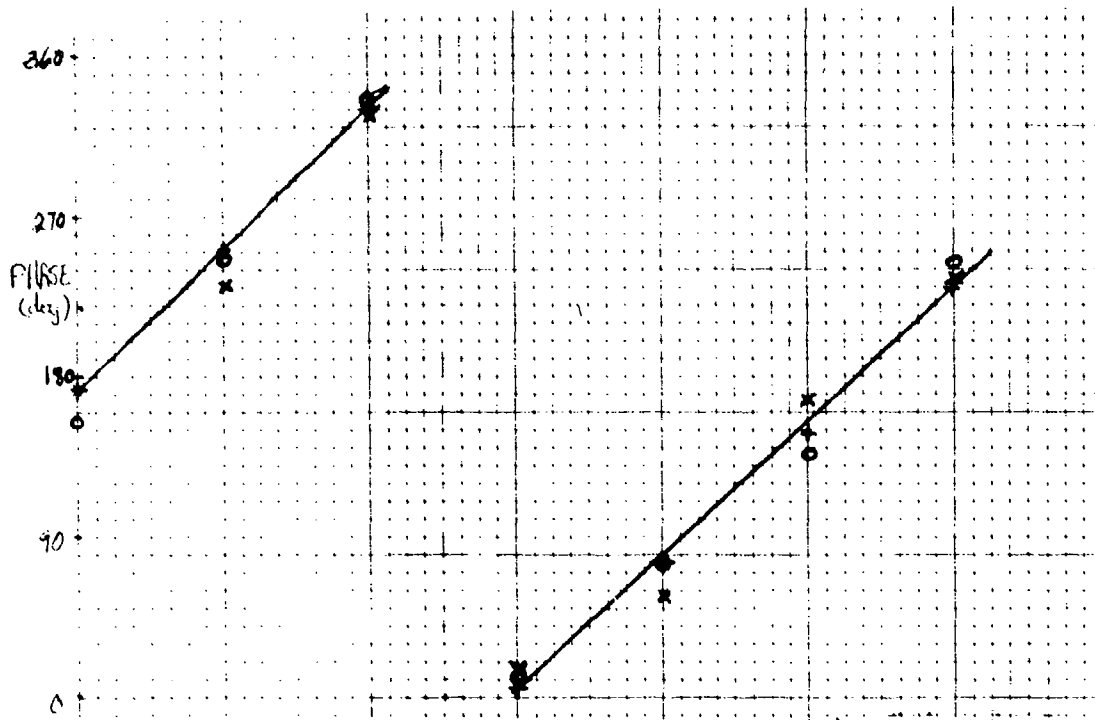
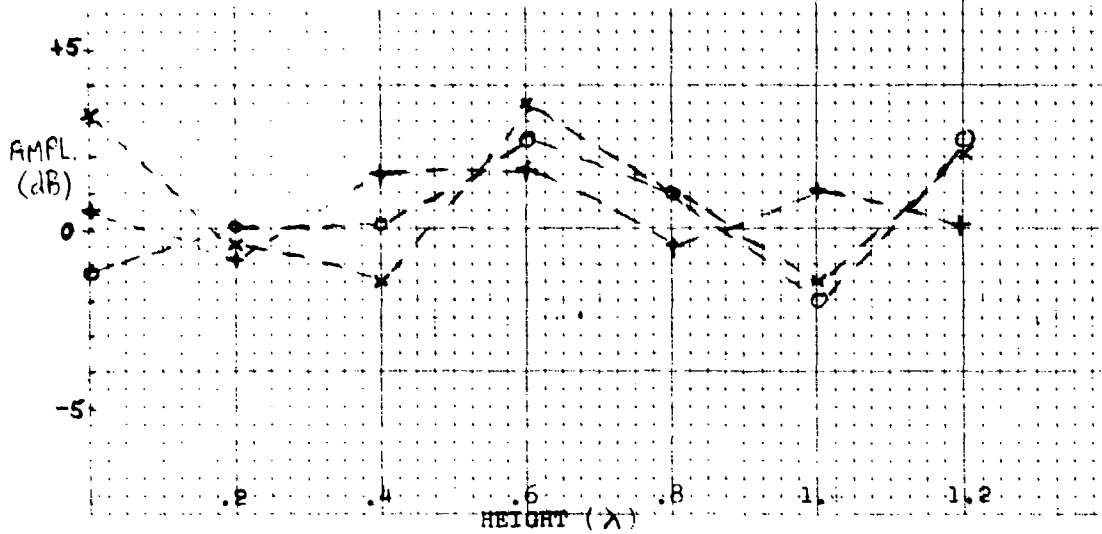


FIG. II-2. PHASE AND AMPLITUDE VARIATIONS FOR SMALL COUNTERPOISE AND HORIZONTAL POLARIZATION AT $\theta = 45^\circ, \phi = 0^\circ$

- + : BLADE AT 0
- O : BLADE AT 90
- X : BLADE AT 35



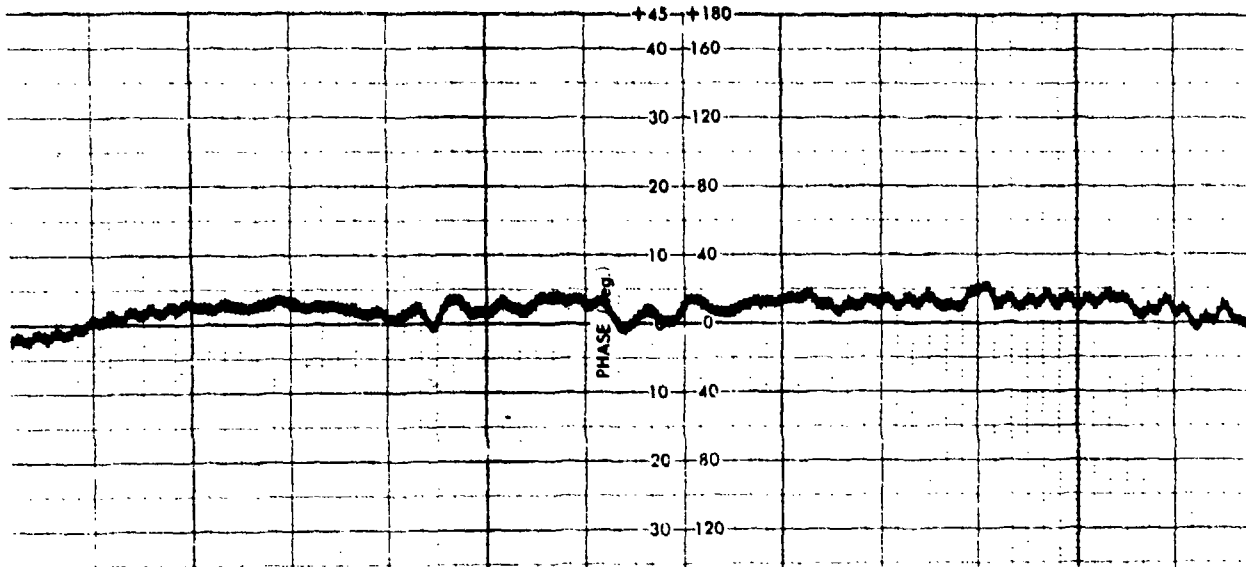
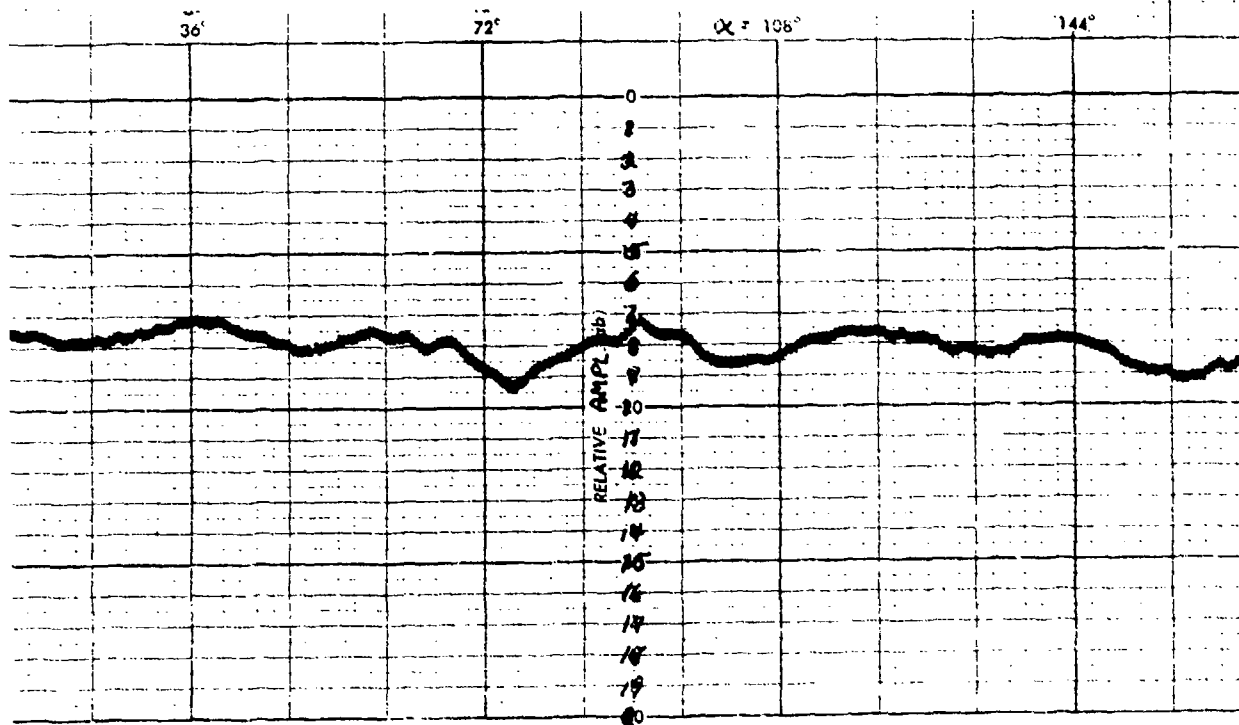


FIG. II-3. PHASE AND AMPLITUDE VARIATIONS
FOR SMALL COUNTERPOISE AND
VERTICAL POLARIZATION AT
 $\theta = 45^\circ, \phi = 0^\circ$



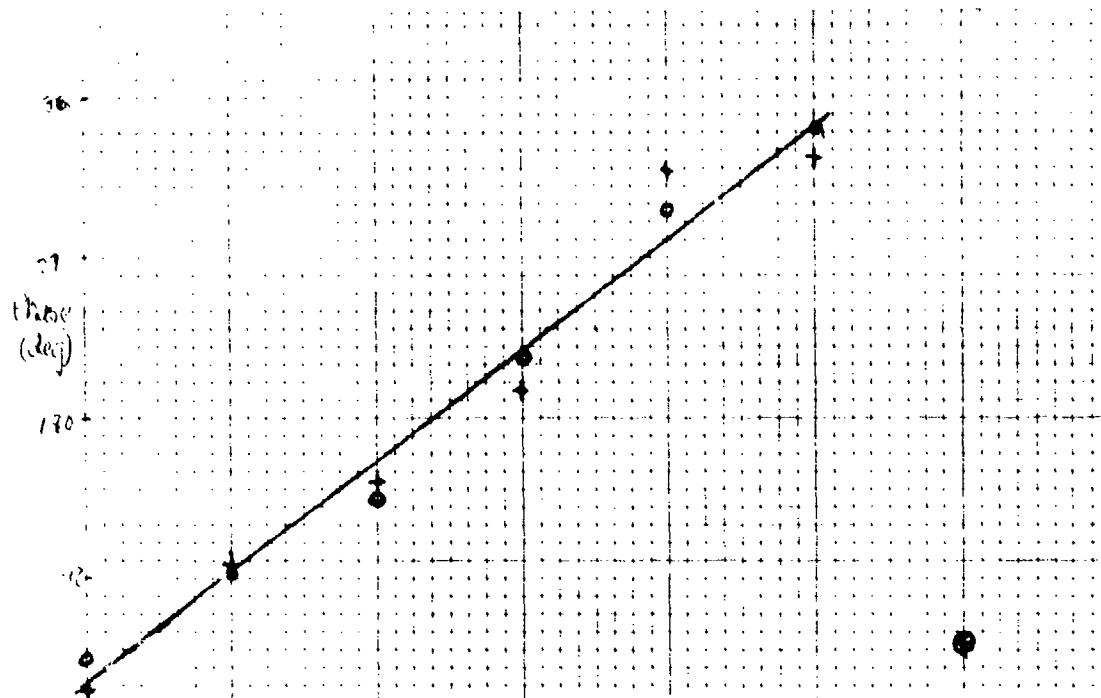
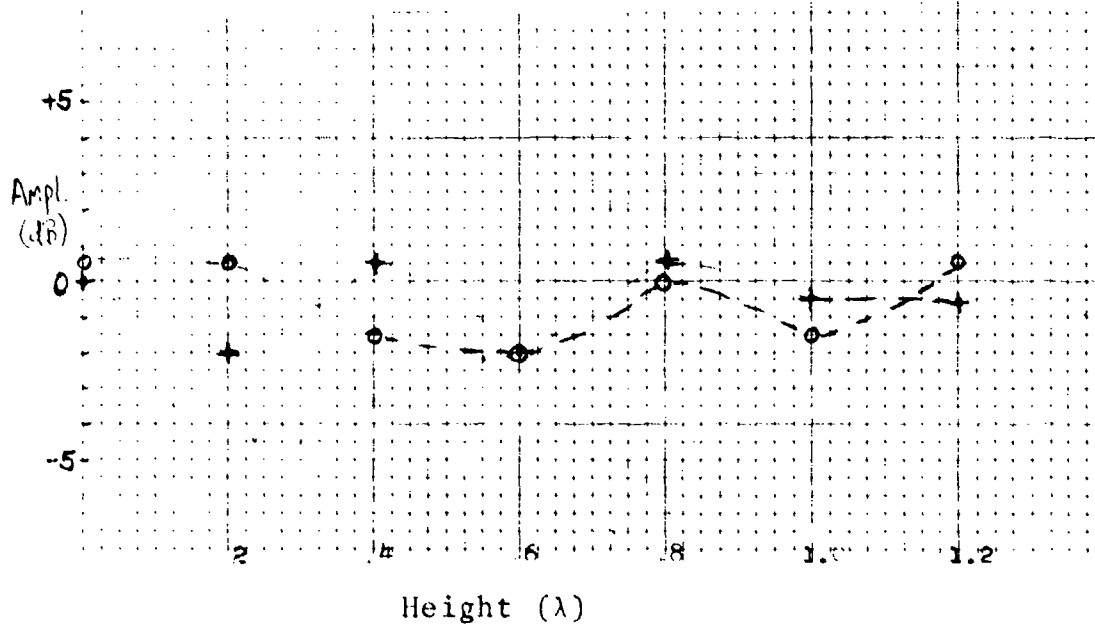


FIG. II-4. PHASE AND AMPLITUDE VARIATIONS FOR SMALL COUNTERPOISE AND VERTICAL POLARIZATION AT $\theta = 45^\circ, \phi = 0^\circ$

◆ - BLADE AT 0°
 ○ - BLADE AT 90°



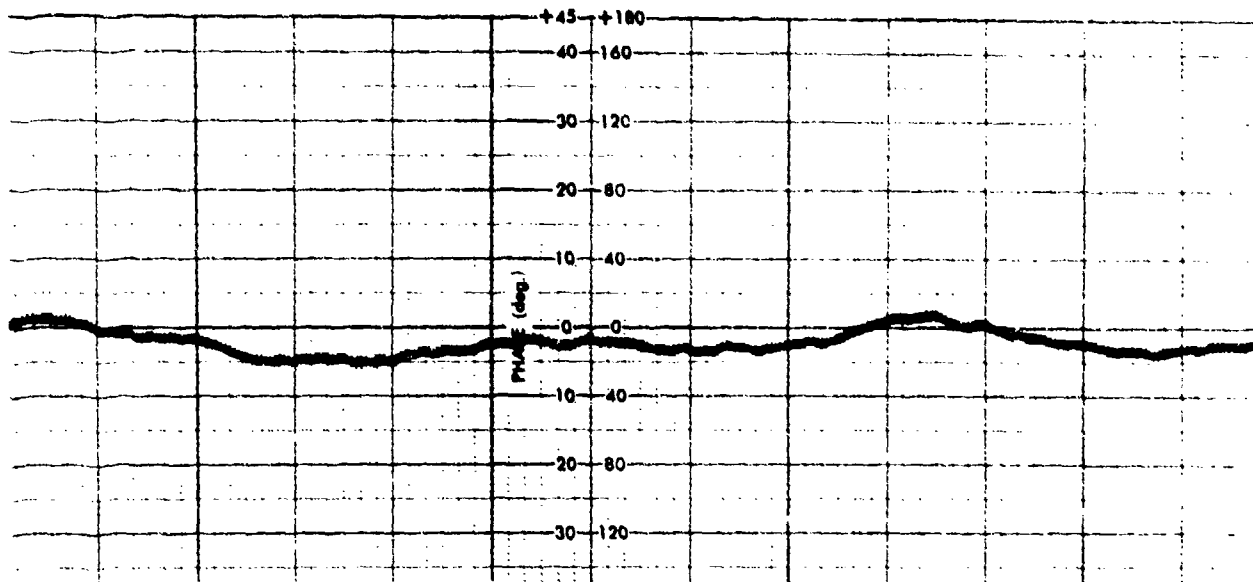
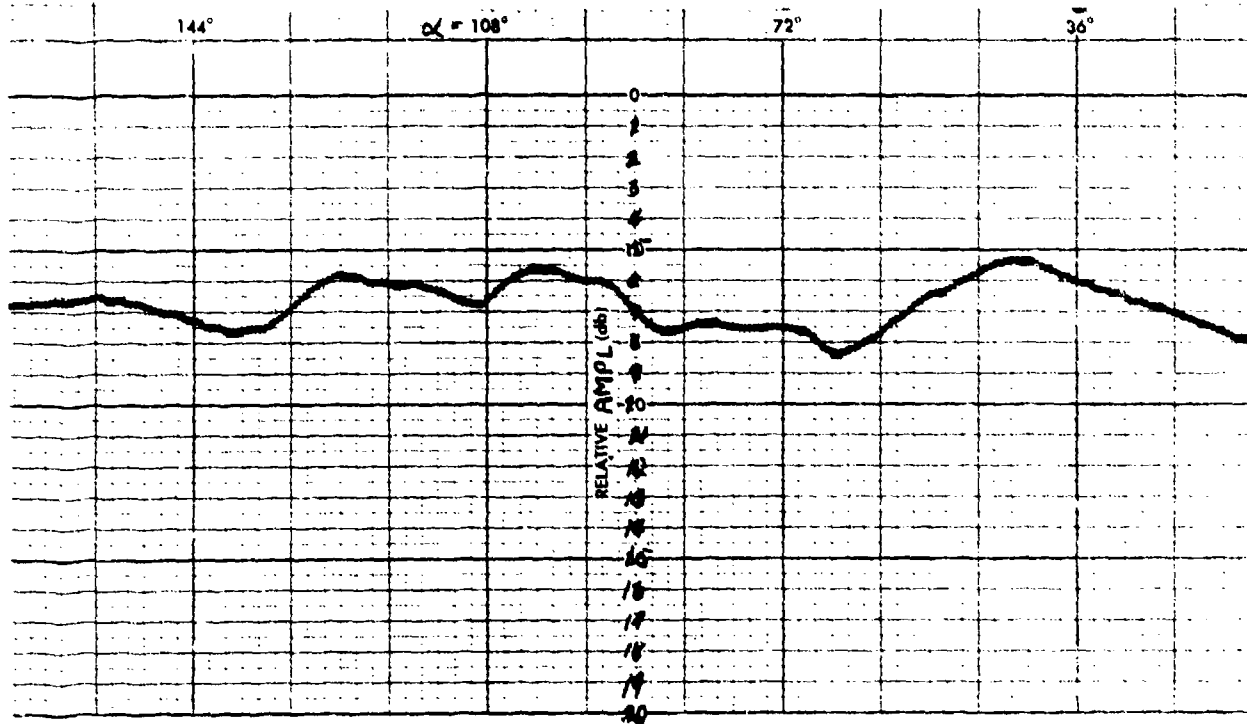


FIG. II-5. PHASE AND AMPLITUDE VARIATIONS FOR LARGE COUNTERPOISE AND HORIZONTAL POLARIZATION AT $\theta = 45^\circ$, $\phi = 0^\circ$



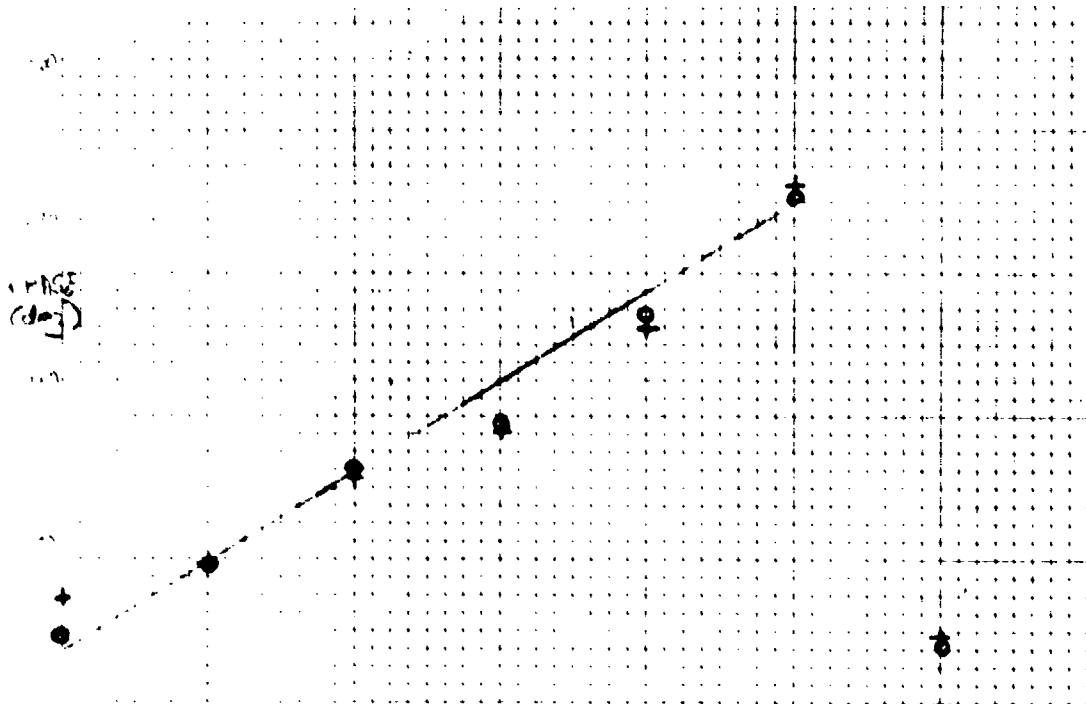
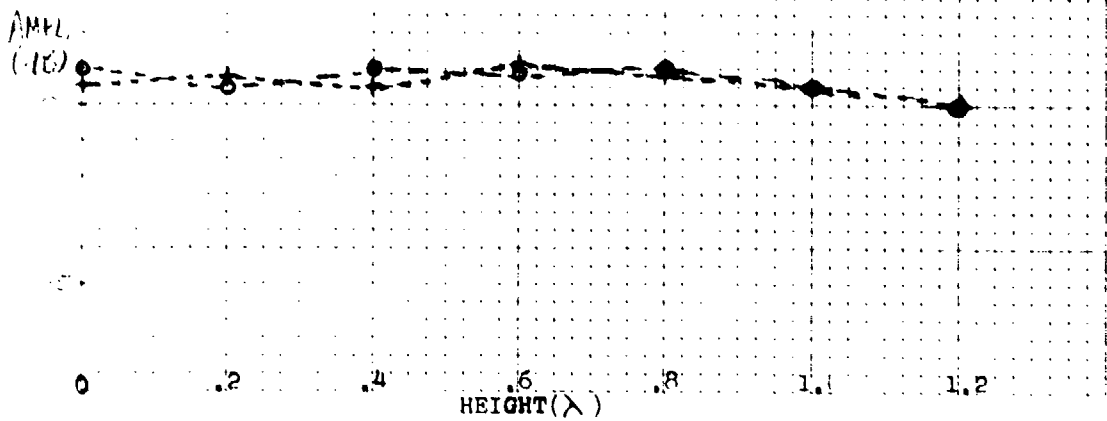


FIG. 11-6. PHASE AND AMPLITUDE VARIATIONS FOR LARGE COUNTERPOISE AND HORIZONTAL POLARIZATION AT $\theta = 45^\circ$, $\phi = 0^\circ$

+ - BLADE AT 0°
 o - BLADE AT 90°



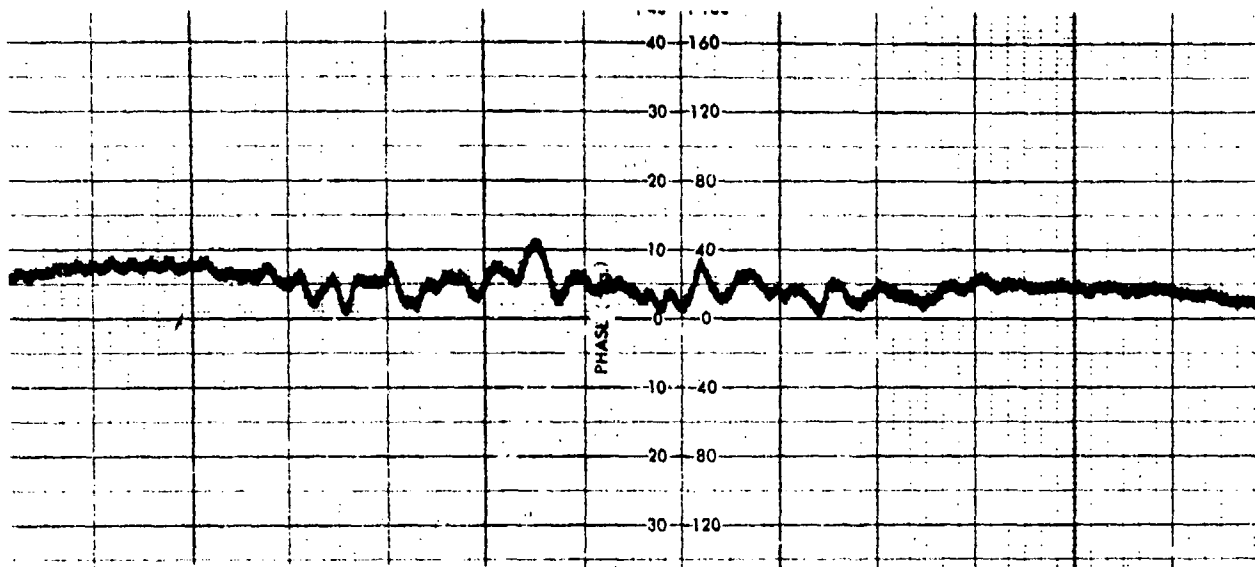
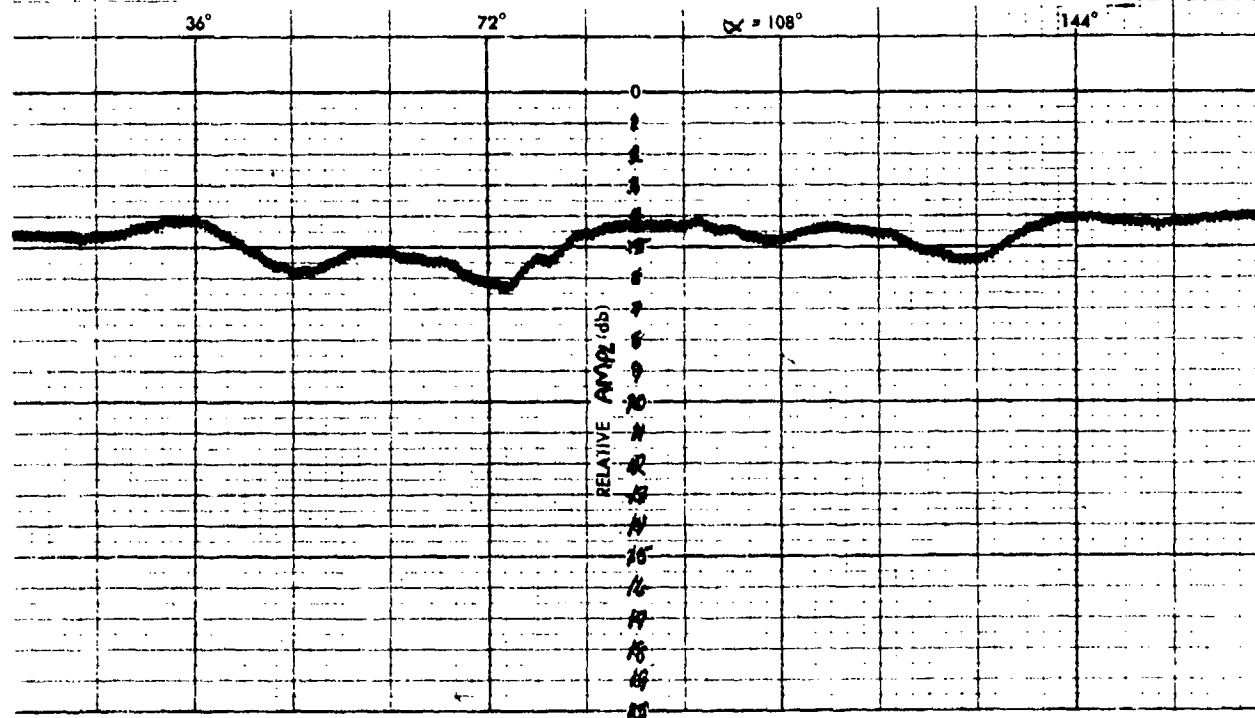


FIG. II-7. PHASE AND AMPLITUDE VARIATIONS
FOR LARGE COUNTERPOISE AND
VERTICAL POLARIZATION AT
 $\theta = 45^\circ$, $\phi = 0^\circ$



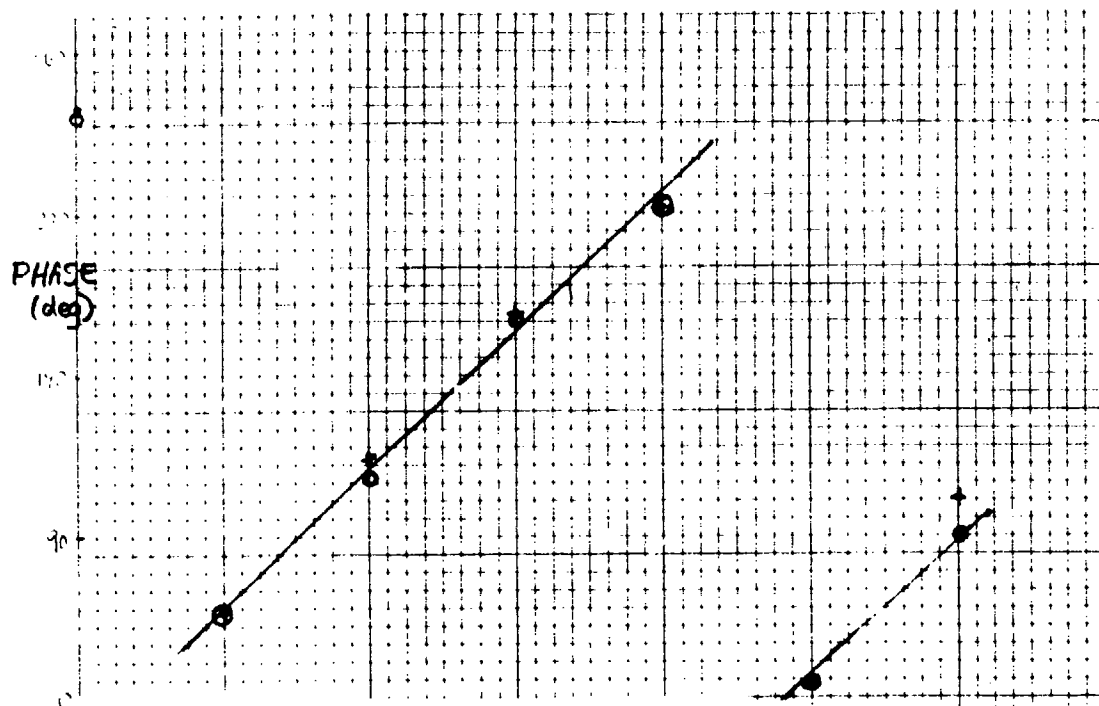
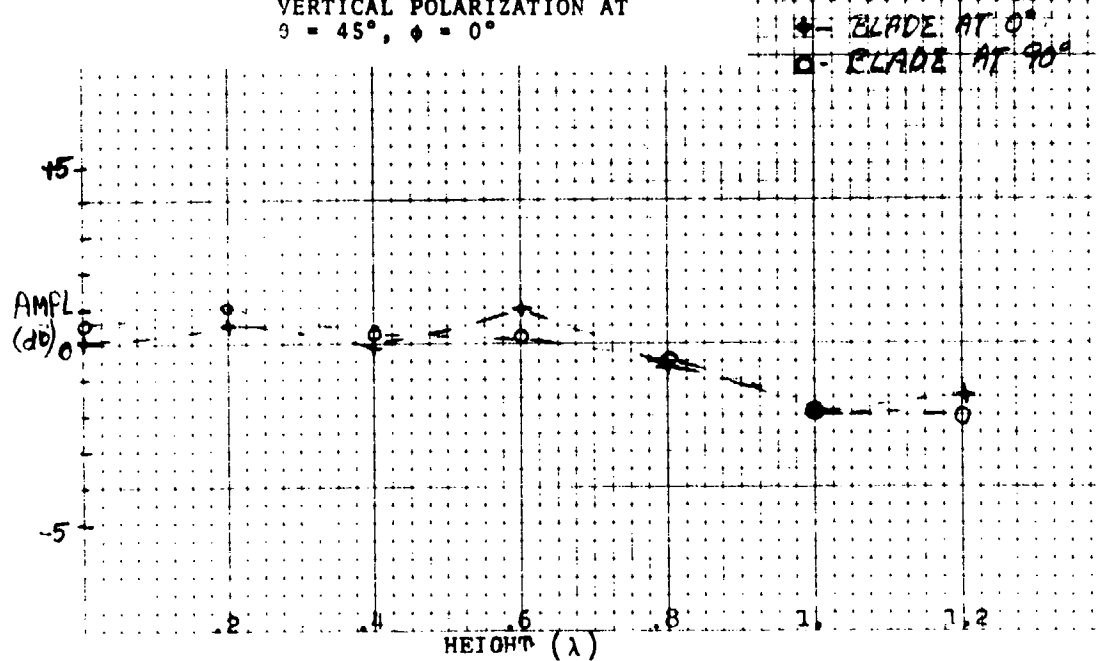


FIG. II-8. PHASE AND AMPLITUDE VARIATIONS FOR LARGE COUNTERPOISE AND VERTICAL POLARIZATION AT $\theta = 45^\circ$, $\phi = 0^\circ$



* - BLADE AT 0°
 ○ - BLADE AT 90°

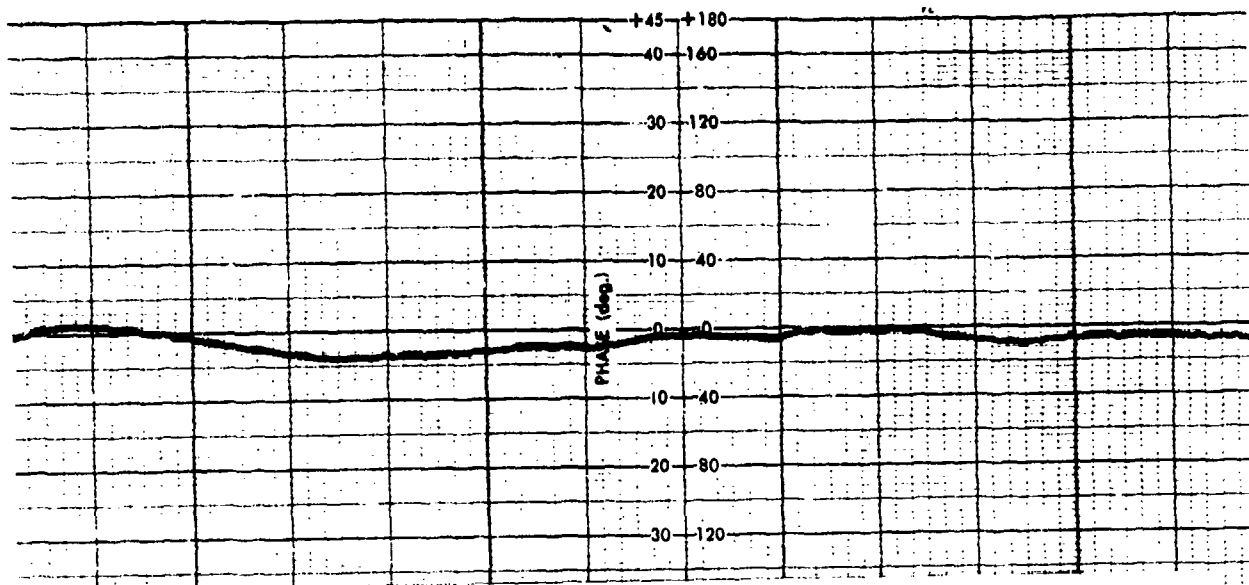
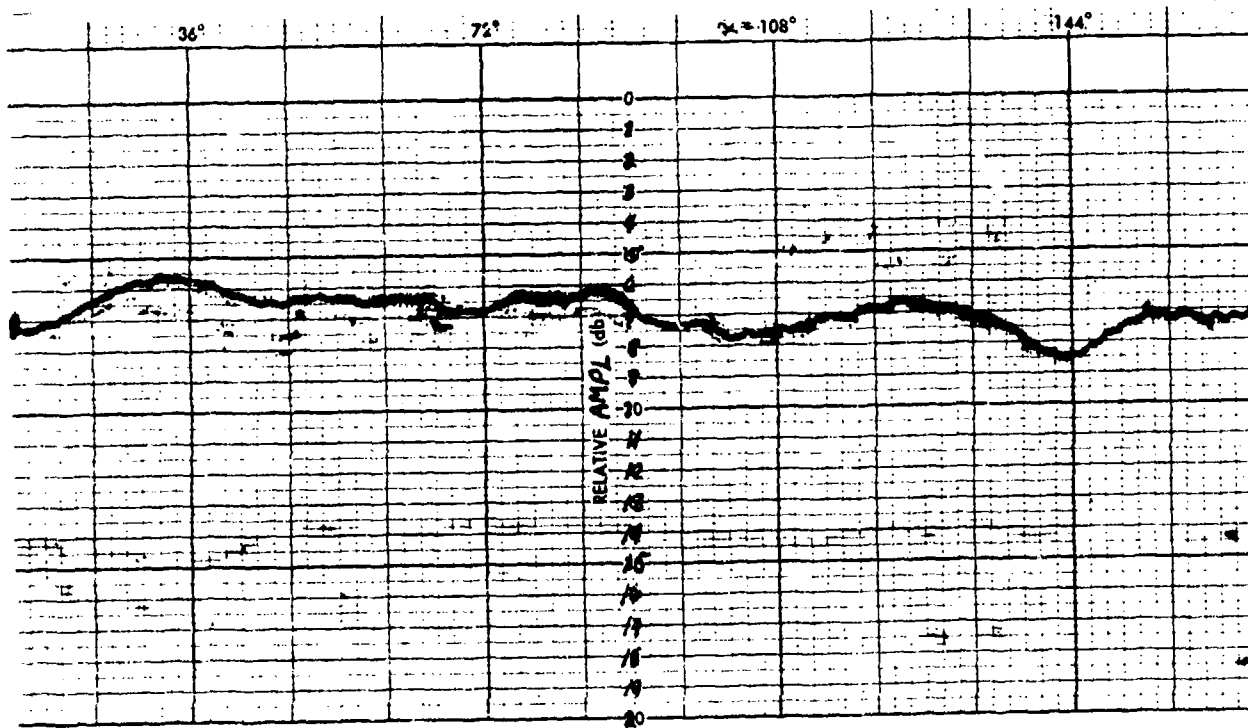
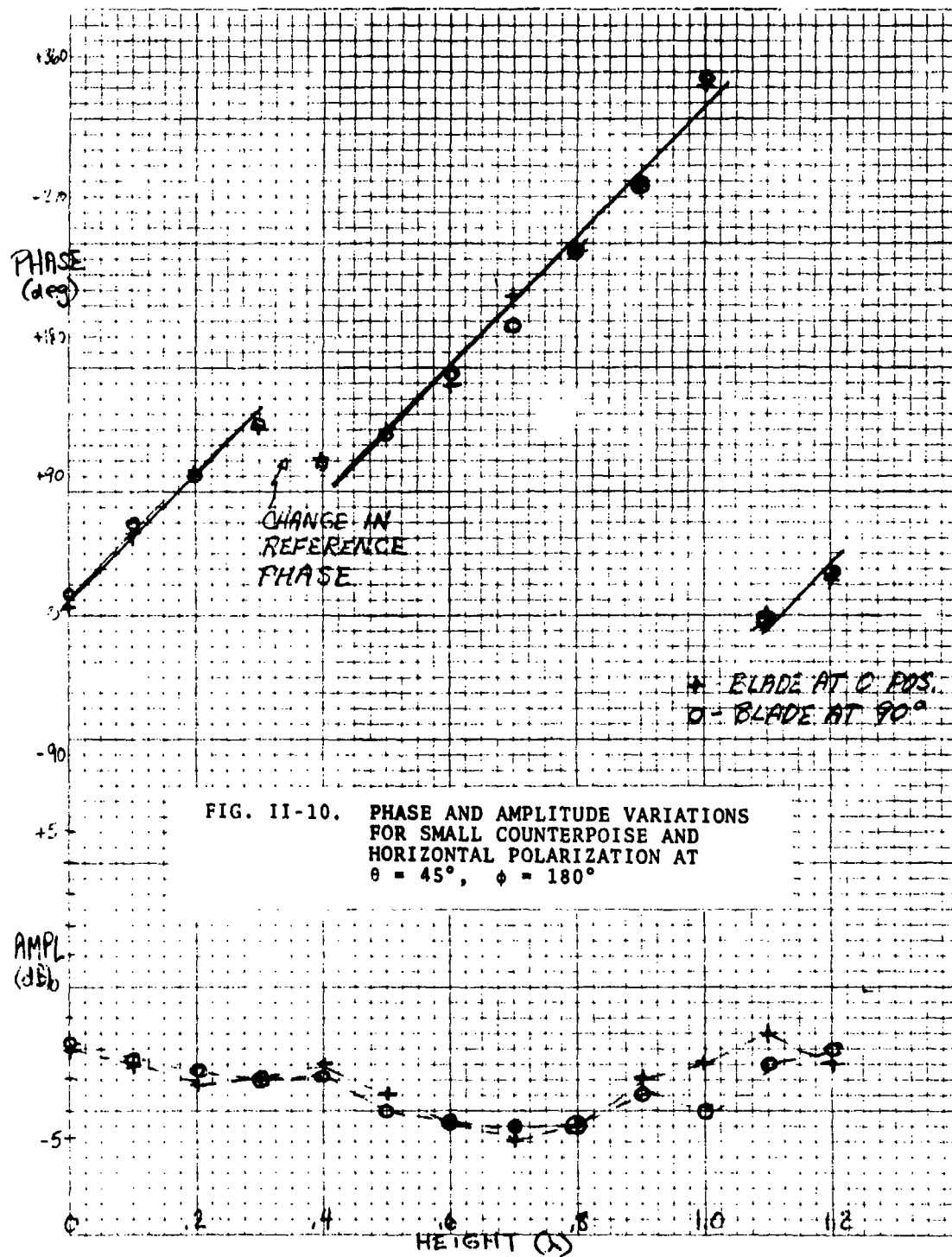


FIG. II-9. PHASE AND AMPLITUDE VARIATIONS
FOR SMALL COUNTERPOISE AND
HORIZONTAL POLARIZATION AT
 $\theta = 45^\circ$, $\phi = 180^\circ$





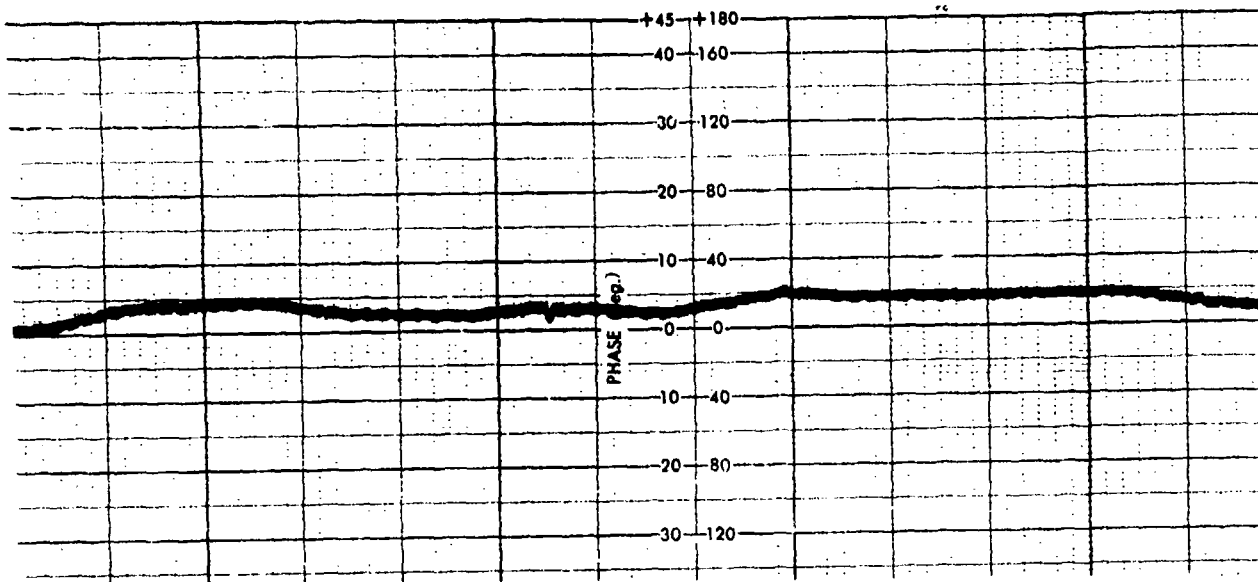
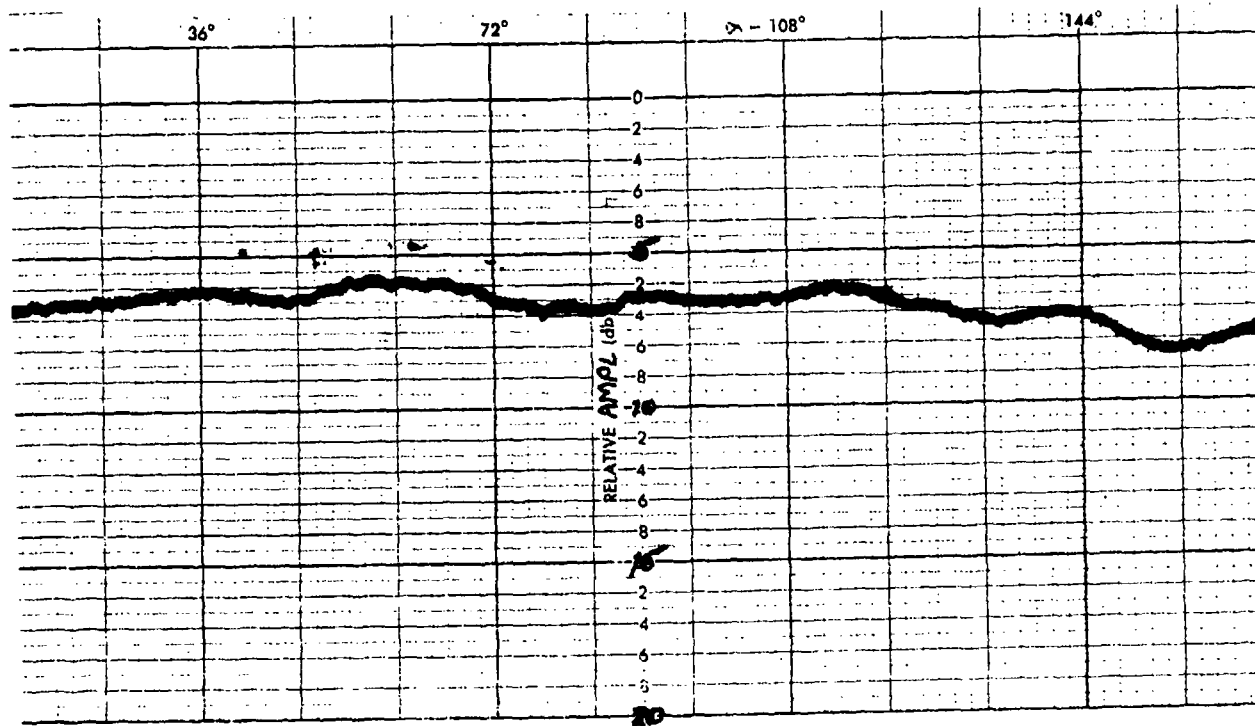


FIG. II-11. PHASE AND AMPLITUDE VARIATIONS
FOR SMALL COUNTERPOISE AND
VERTICAL POLARIZATION AT
 $\theta = 45^\circ$, $\phi = 180^\circ$



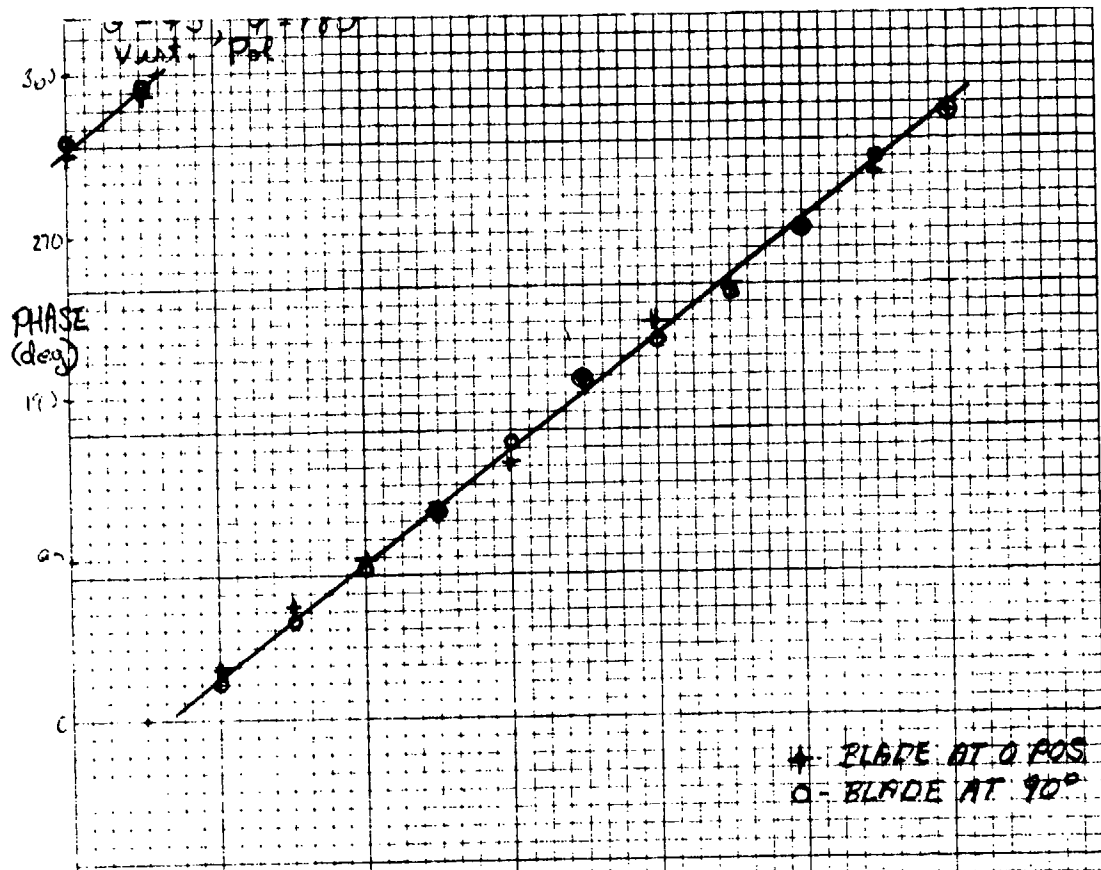
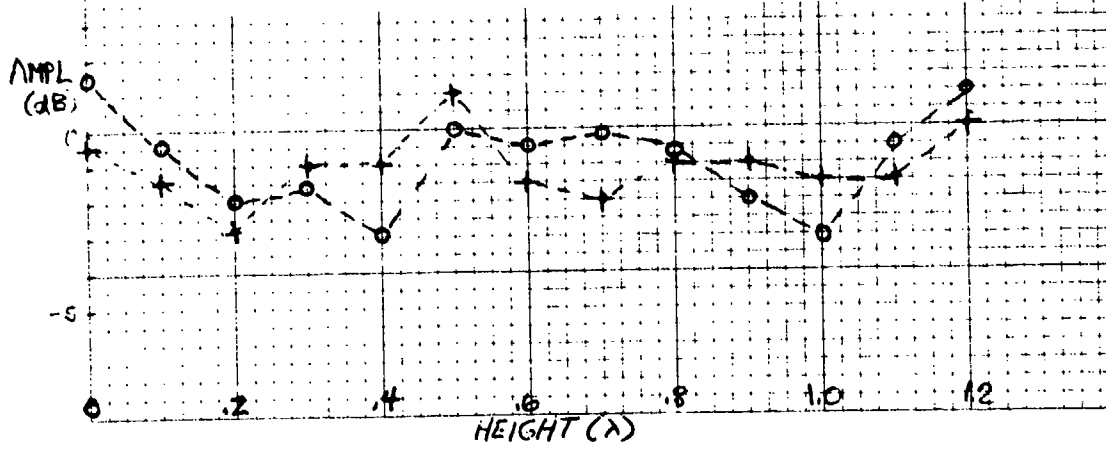


FIG. II-12. PHASE AND AMPLITUDE VARIATIONS FOR SMALL COUNTERPOISE AND VERTICAL POLARIZATION AT $\theta = 45^\circ$, $\phi = 180^\circ$



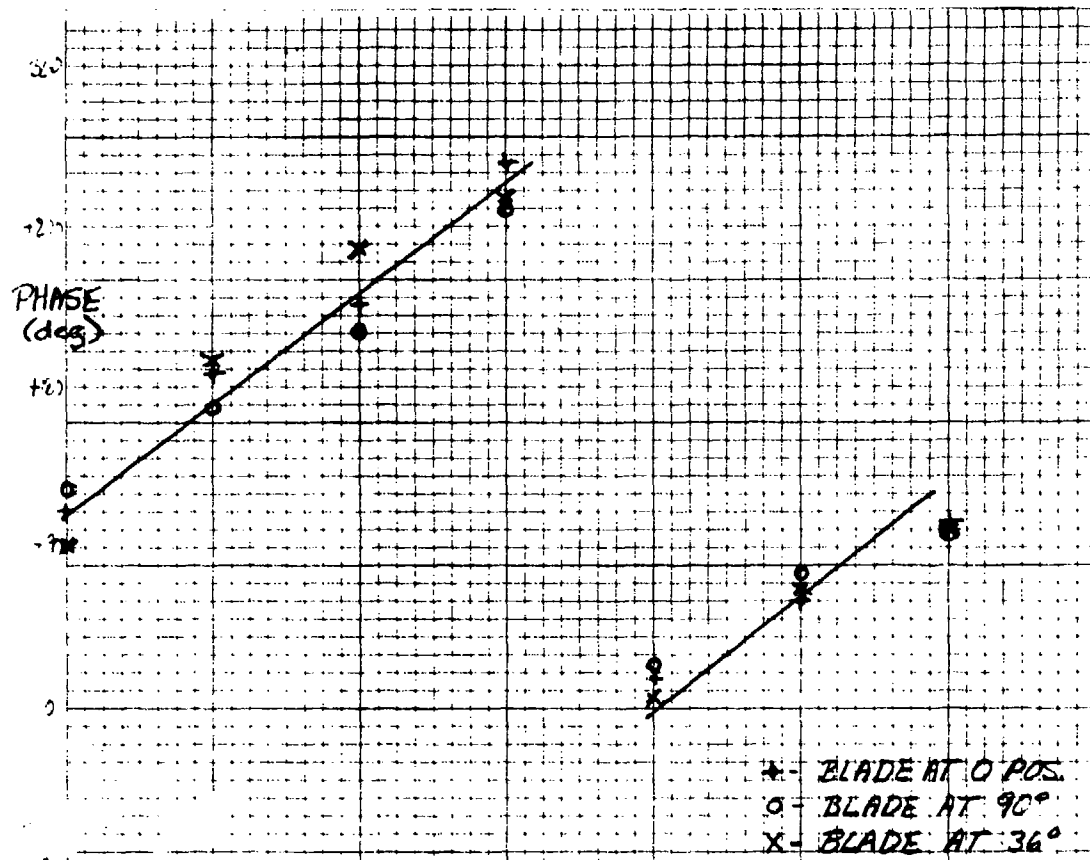
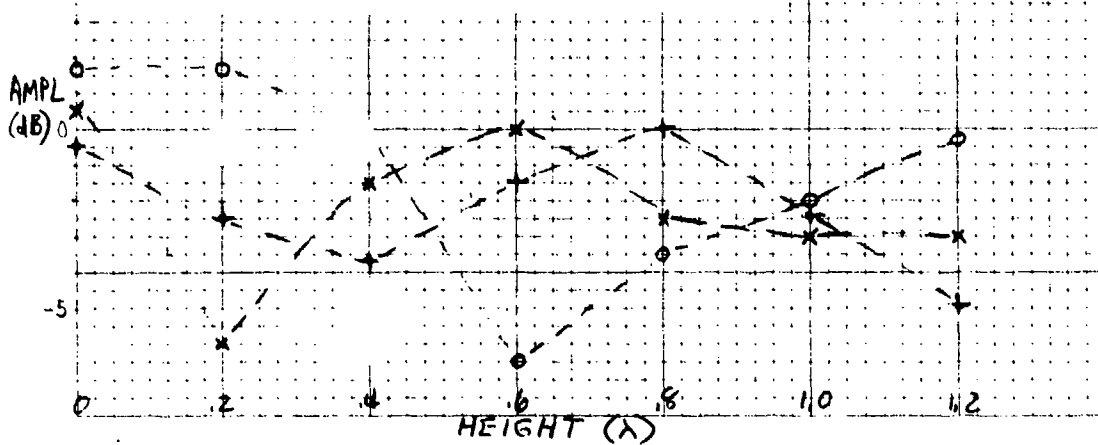


FIG. II-14. PHASE AND AMPLITUDE VARIATIONS FOR SMALL COUNTERPOISE AND HORIZONTAL POLARIZATION AT $\theta = 60^\circ$, $\phi = 0^\circ$



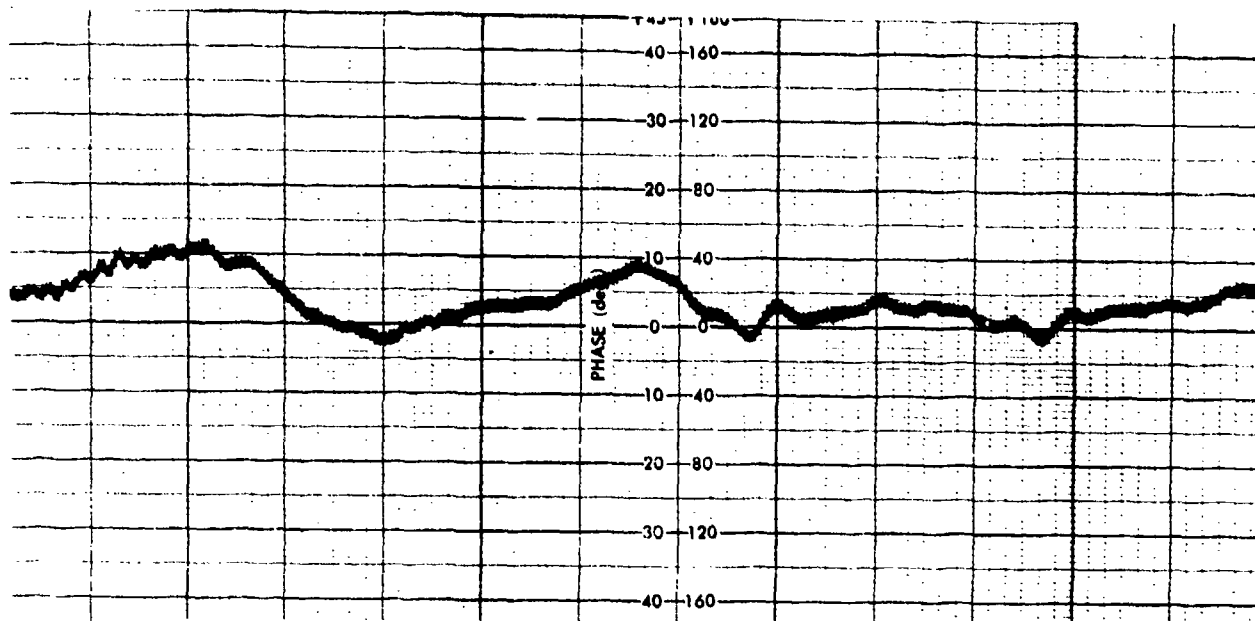
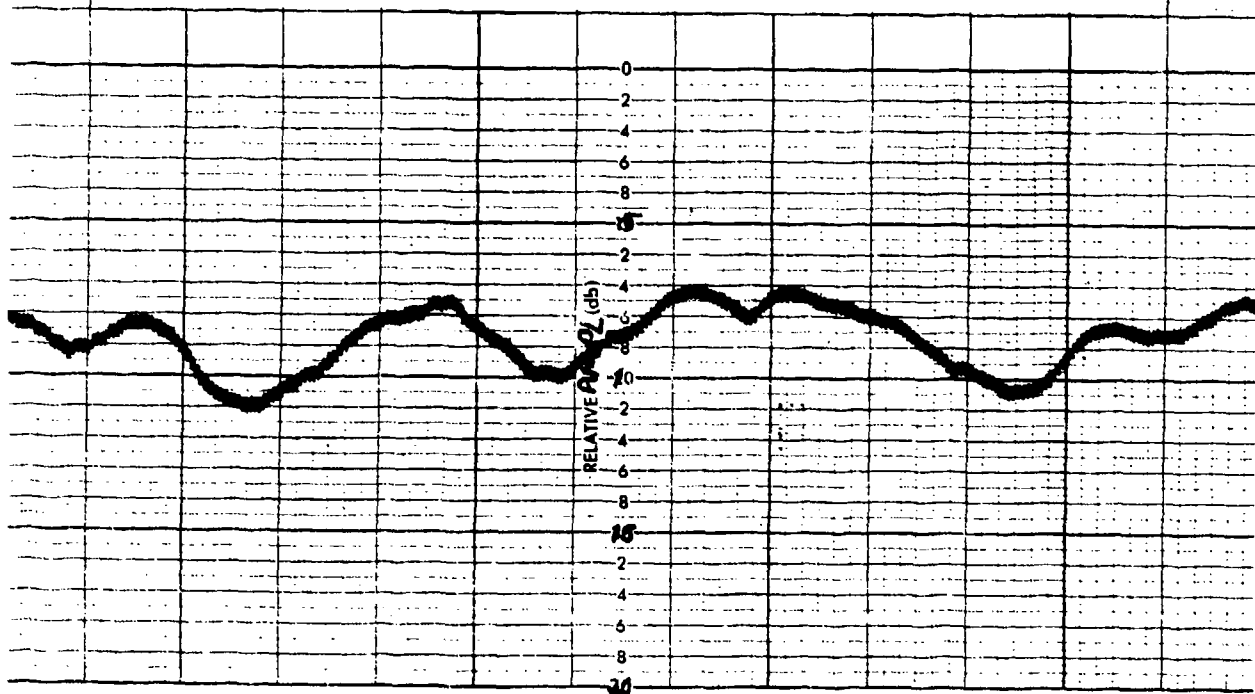


FIG. II-15. PHASE AND AMPLITUDE VARIATIONS
FOR SMALL COUNTERPOISE AND
VERTICAL POLARIZATION AT
 $\theta = 60^\circ, \phi = 0^\circ$



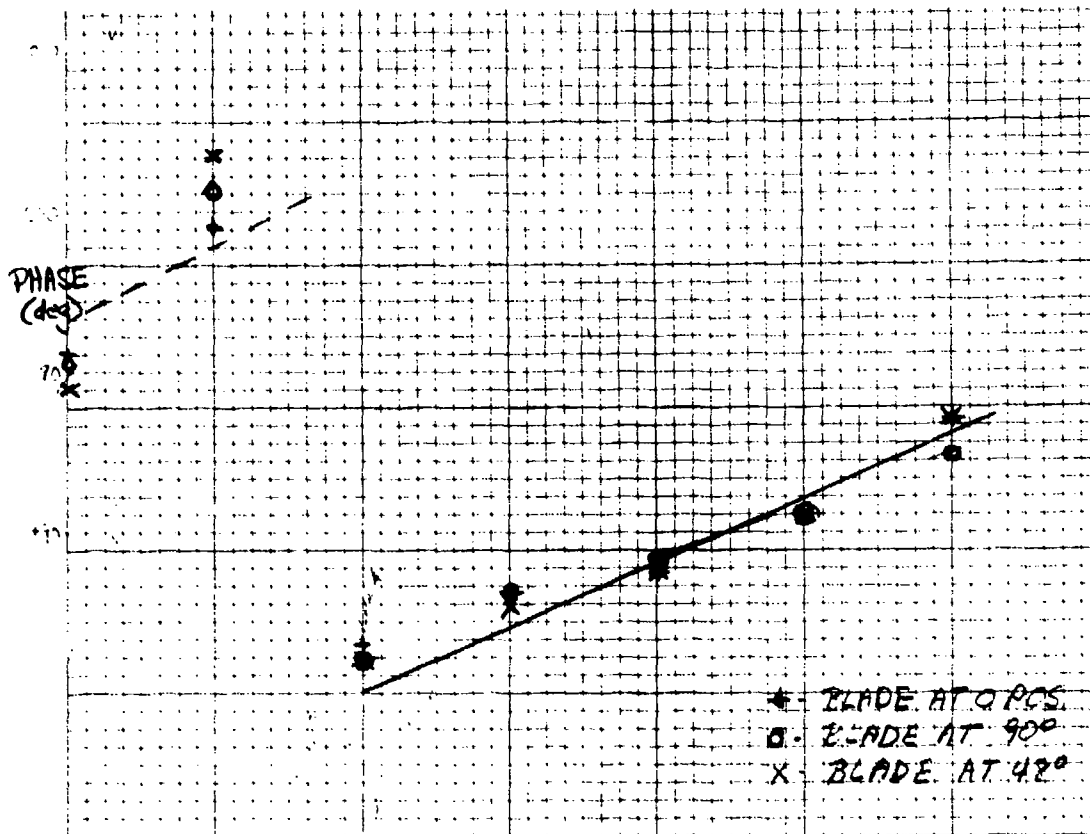
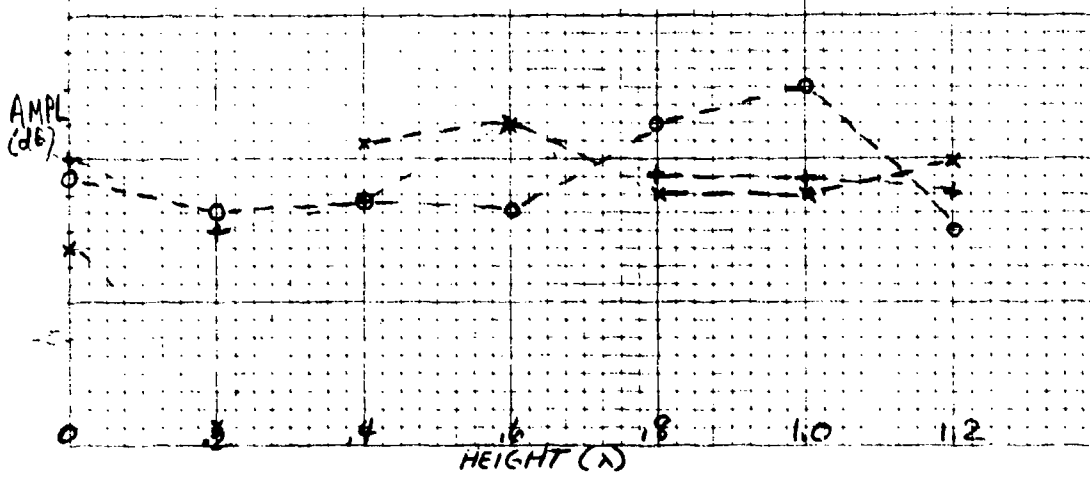


FIG. II-16. PHASE AND AMPLITUDE VARIATIONS FOR SMALL COUNTERPOISE AND VERTICAL POLARIZATION AT $\theta = 60^\circ$, $\phi = 0^\circ$



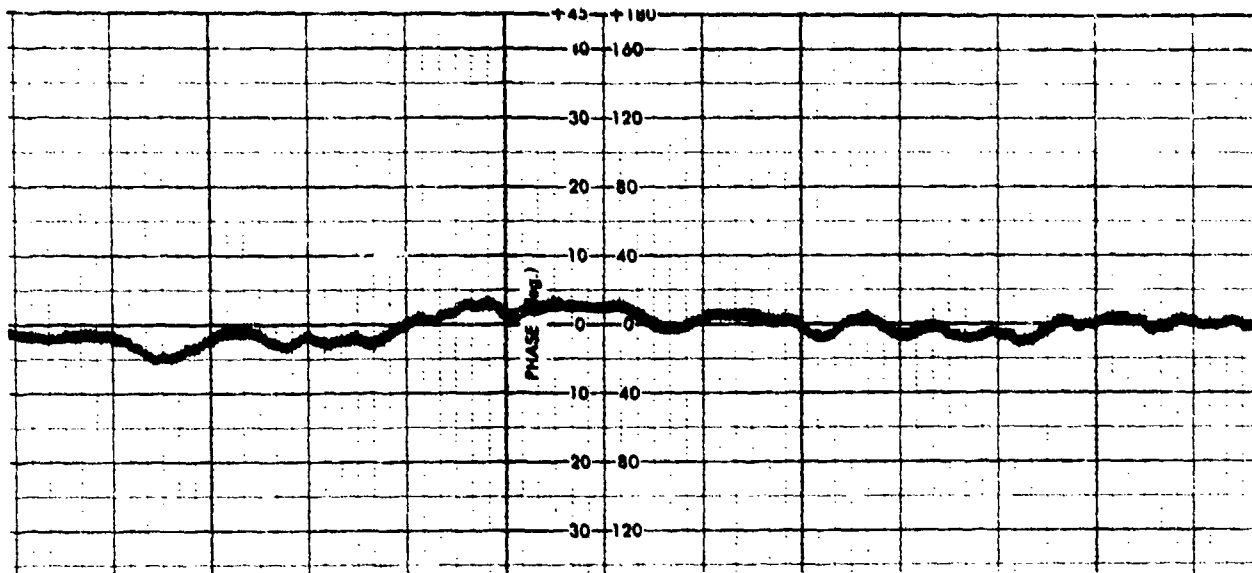
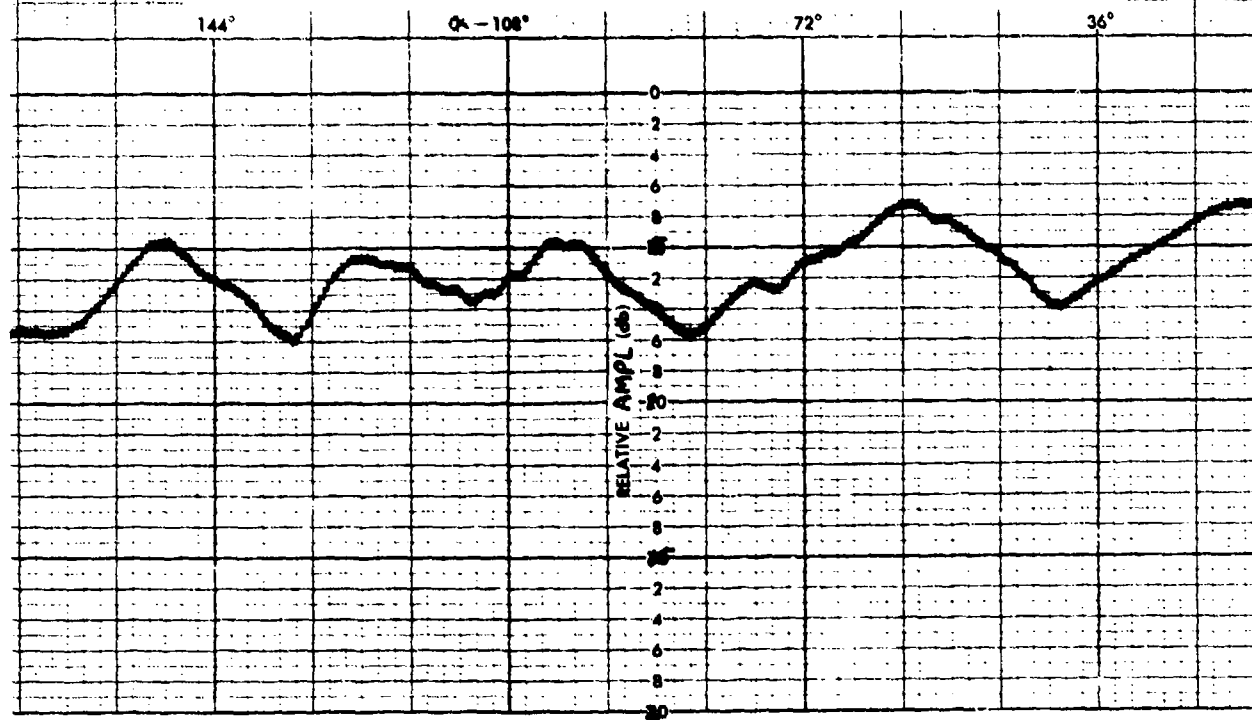


FIG. II-17. PHASE AND AMPLITUDE VARIATIONS FOR LARGE COUNTERPOISE AND HORIZONTAL POLARIZATION AT $\theta = 60^\circ$, $\phi = 0^\circ$



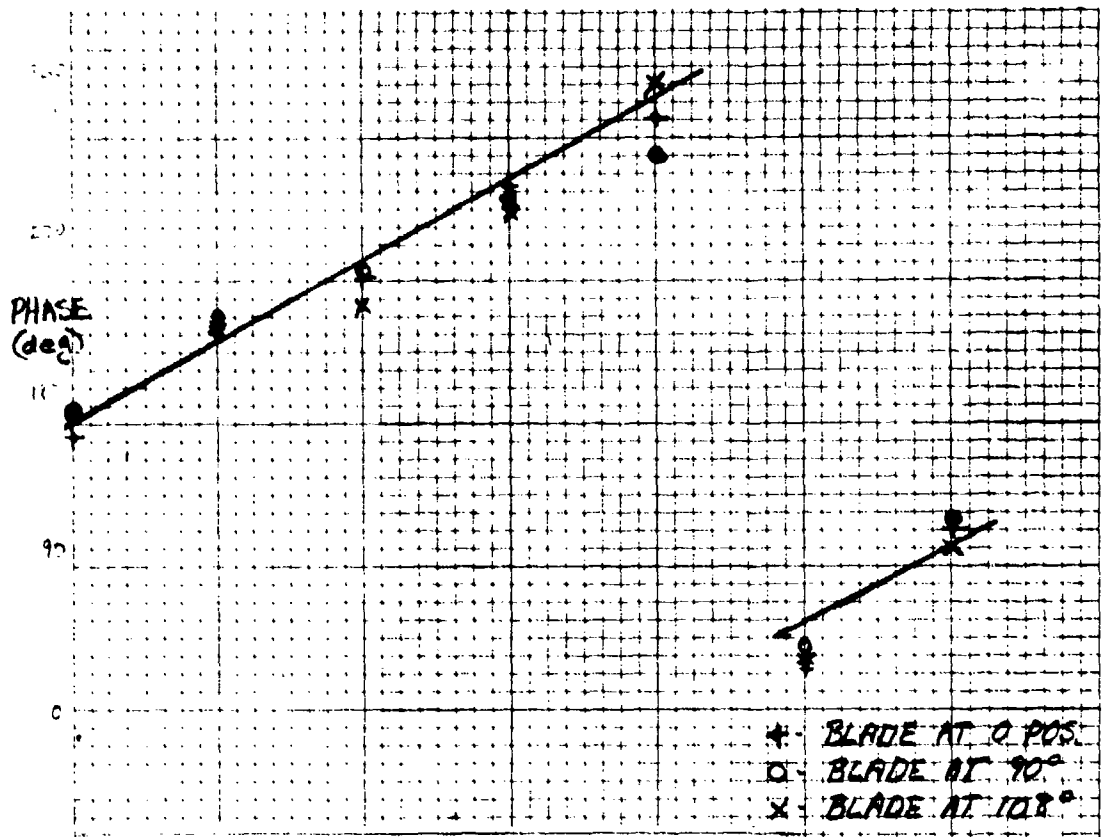
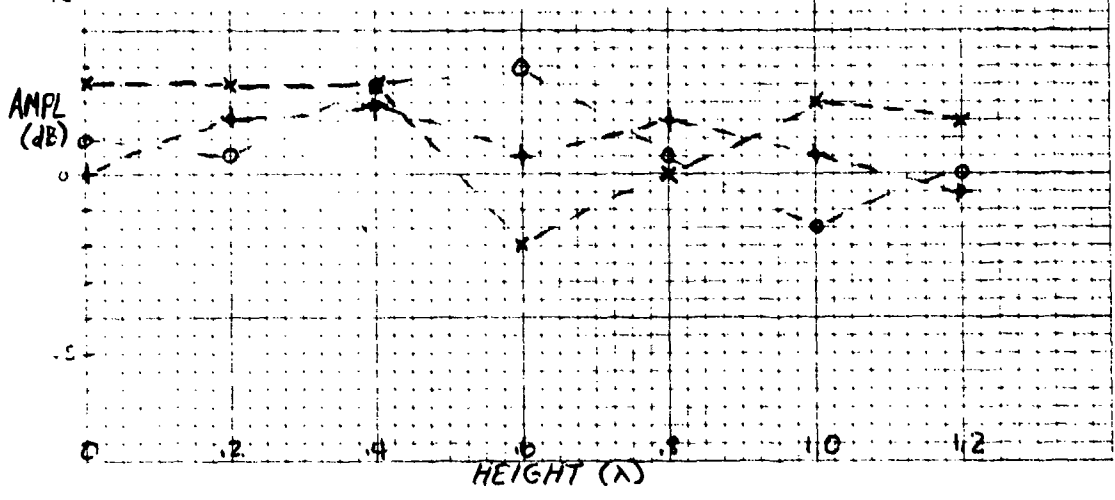


FIG. 11-18. PHASE AND AMPLITUDE VARIATIONS FOR LARGE COUNTERPOISE AND HORIZONTAL POLARIZATION AT $\theta = 60^\circ$, $\phi = 0^\circ$



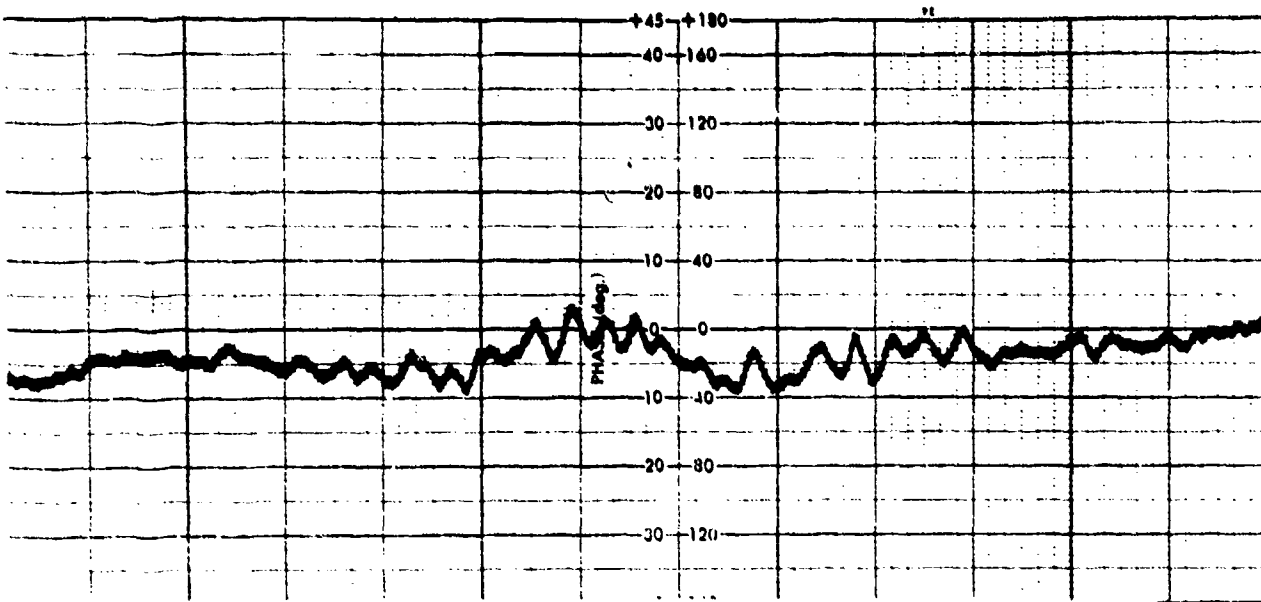
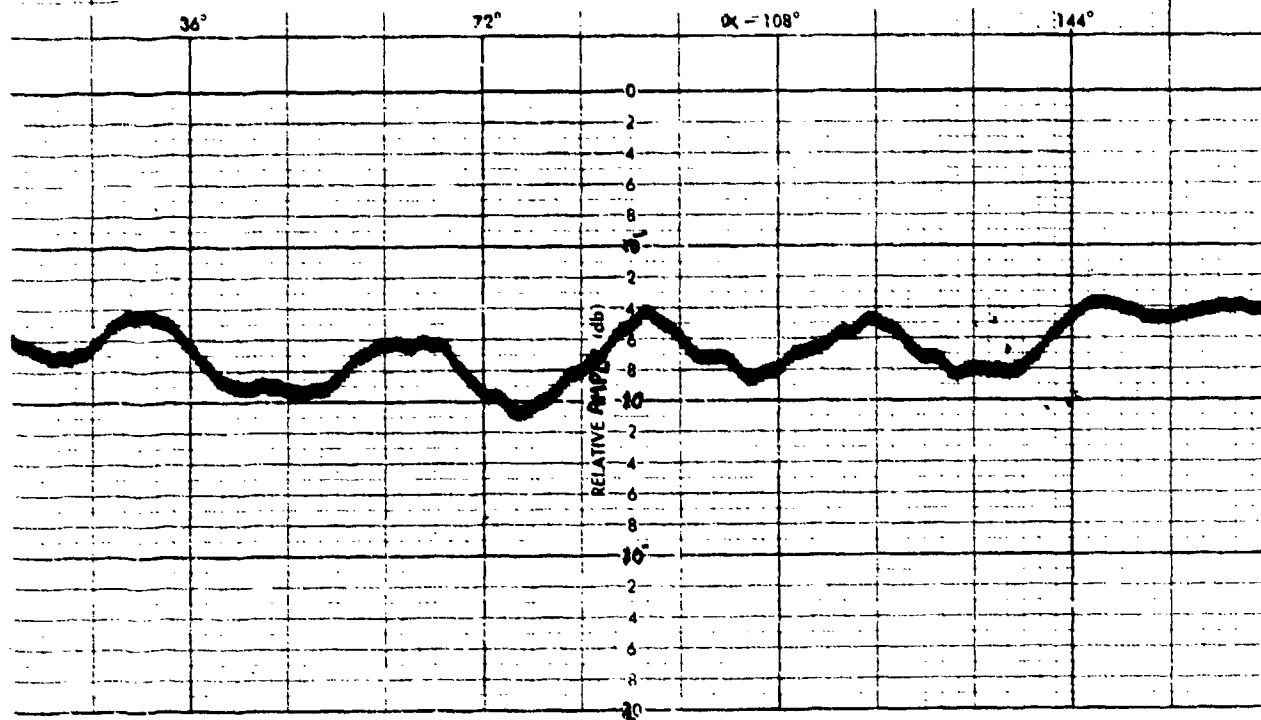


FIG. II-19. AMPLITUDE AND PHASE VARIATIONS
FOR LARGE COUNTERPOISE AND
VERTICAL POLARIZATION AT
 $\theta = 60^\circ$, $\phi = 0^\circ$



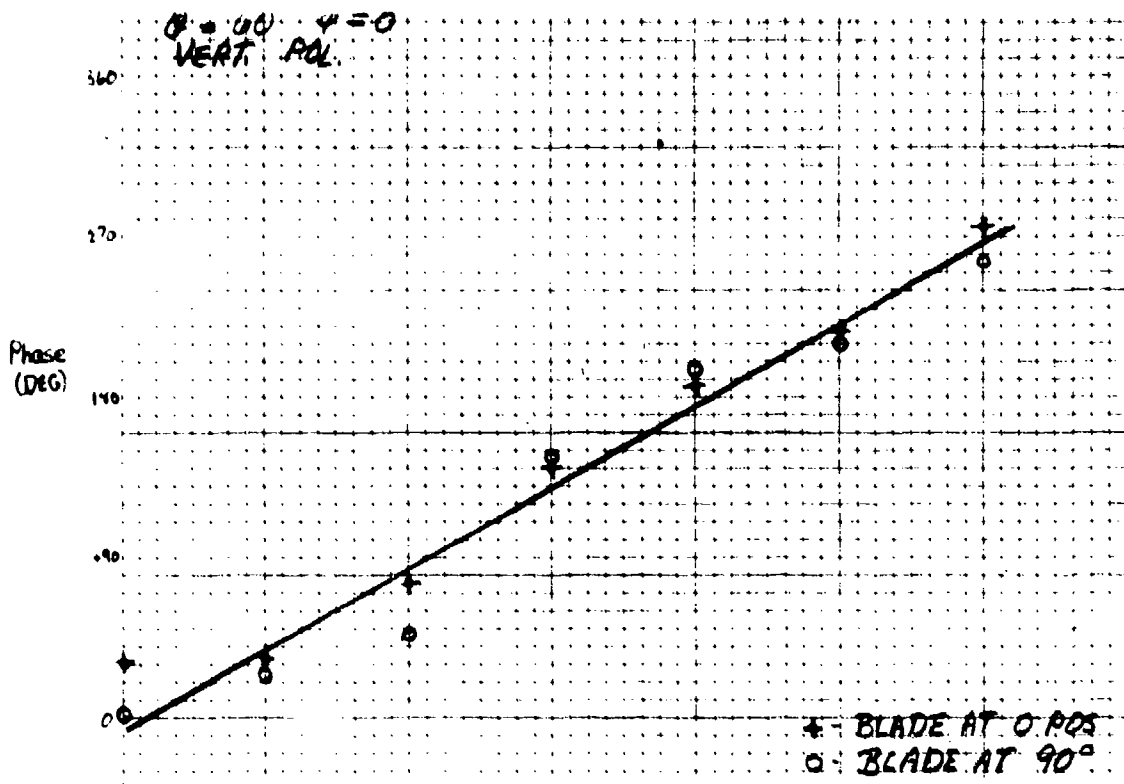
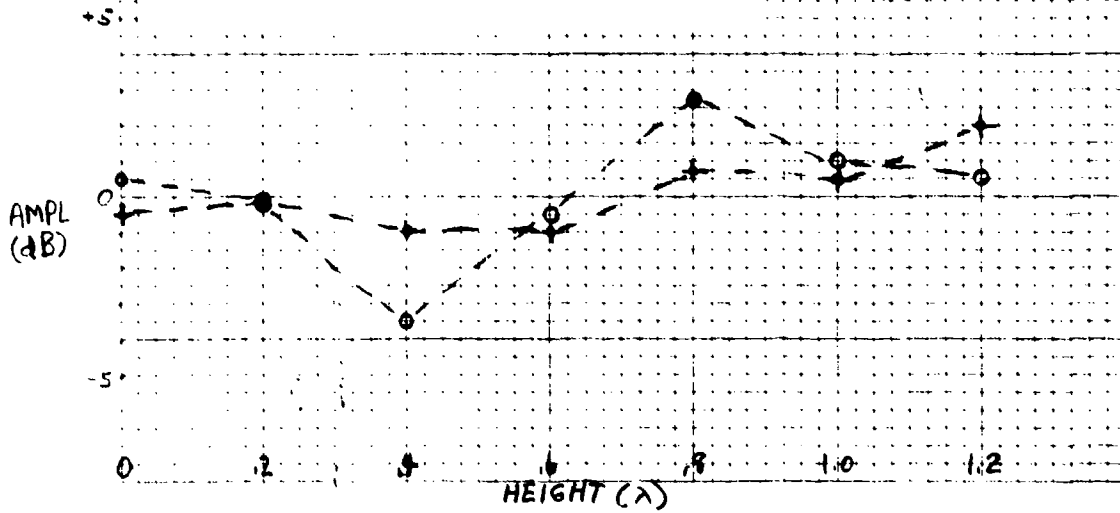


FIG. II-20. AMPLITUDE AND PHASE VARIATIONS FOR LARGE COUNTERPOISE AND VERTICAL POLARIZATION AT $\theta = 60^\circ$, $\phi = 0^\circ$



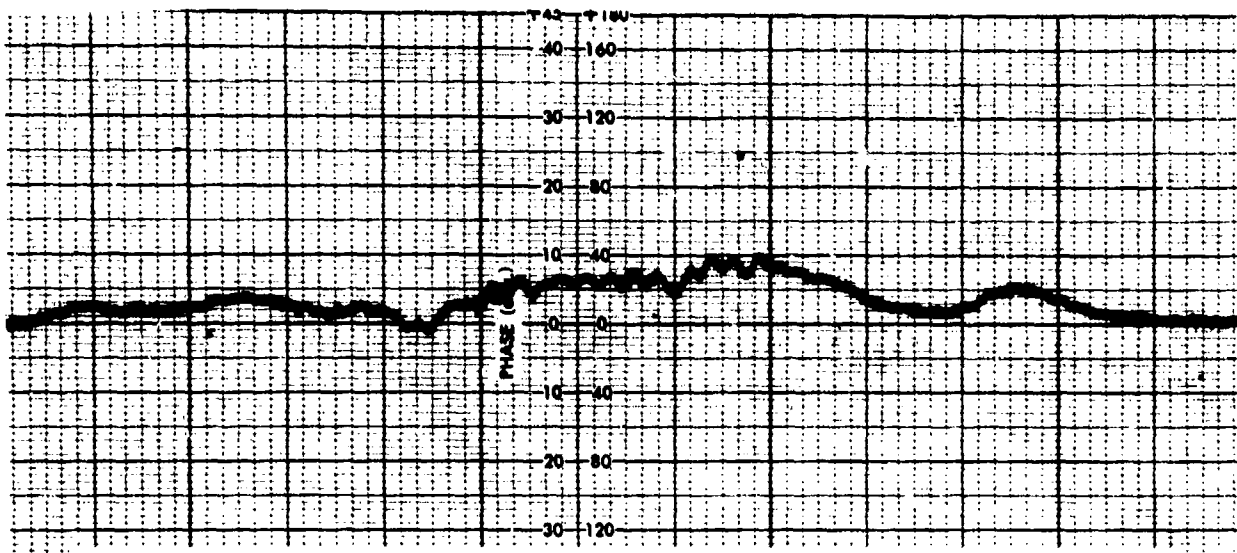
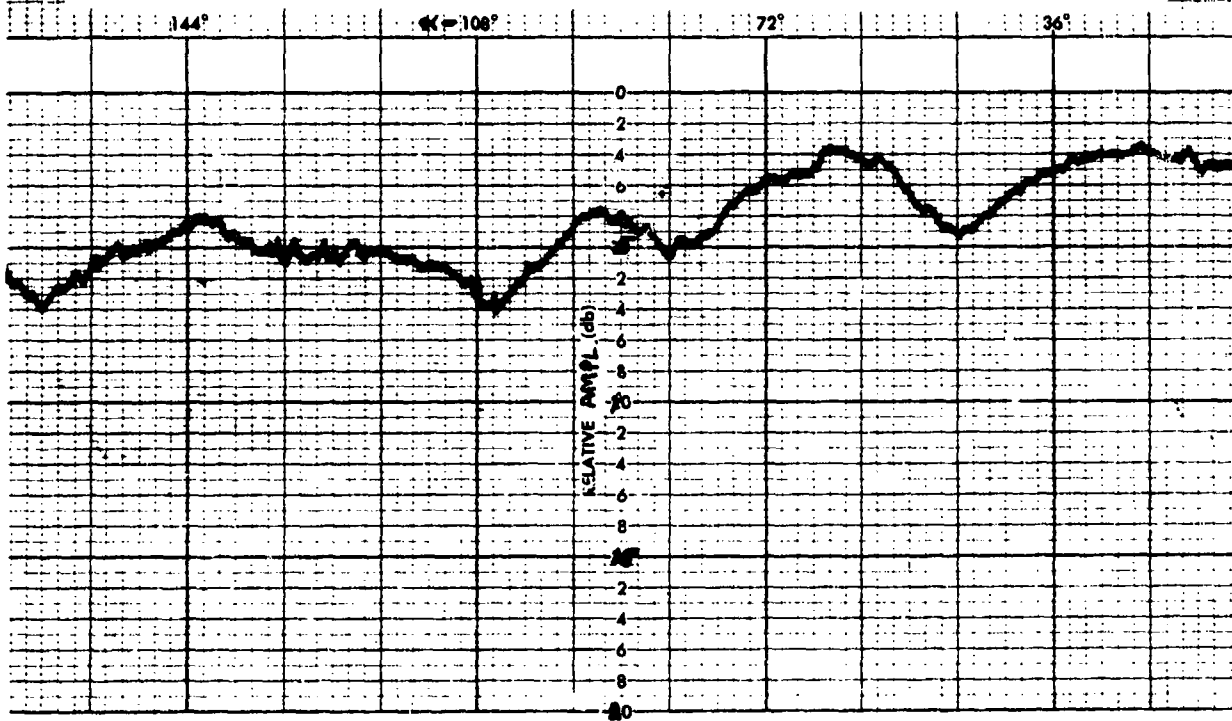


FIG. II-21. AMPLITUDE AND PHASE VARIATIONS FOR SMALL COUNTERPOISE AND HORIZONTAL POLARIZATION AT $\theta = 60^\circ$, $\phi = 180^\circ$



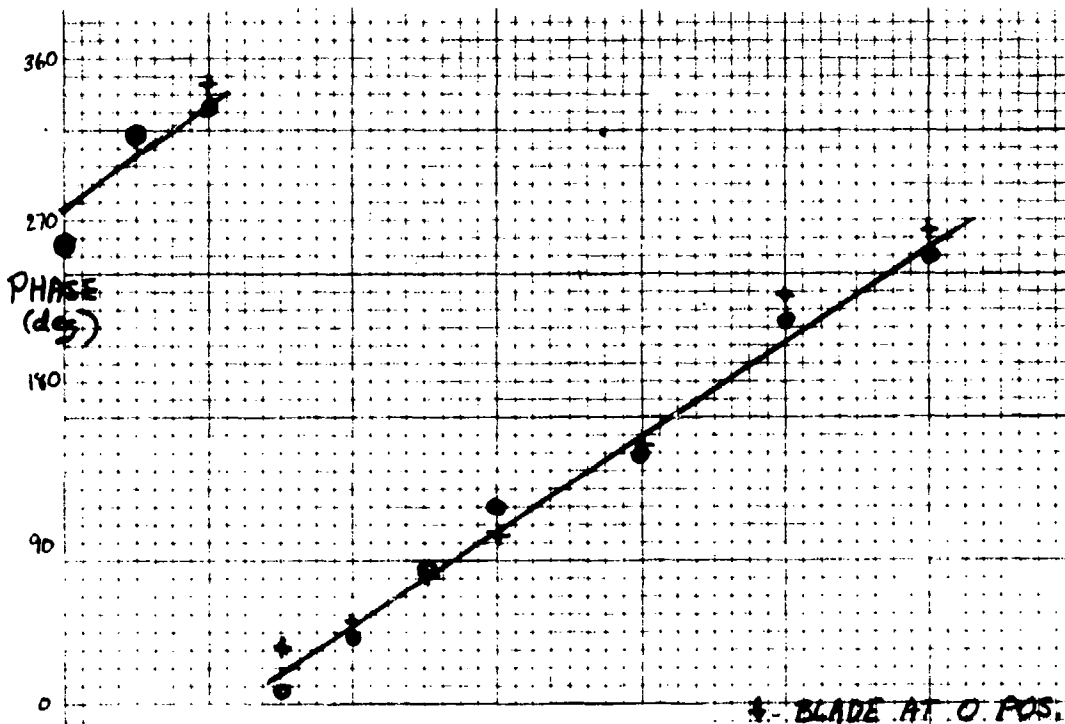
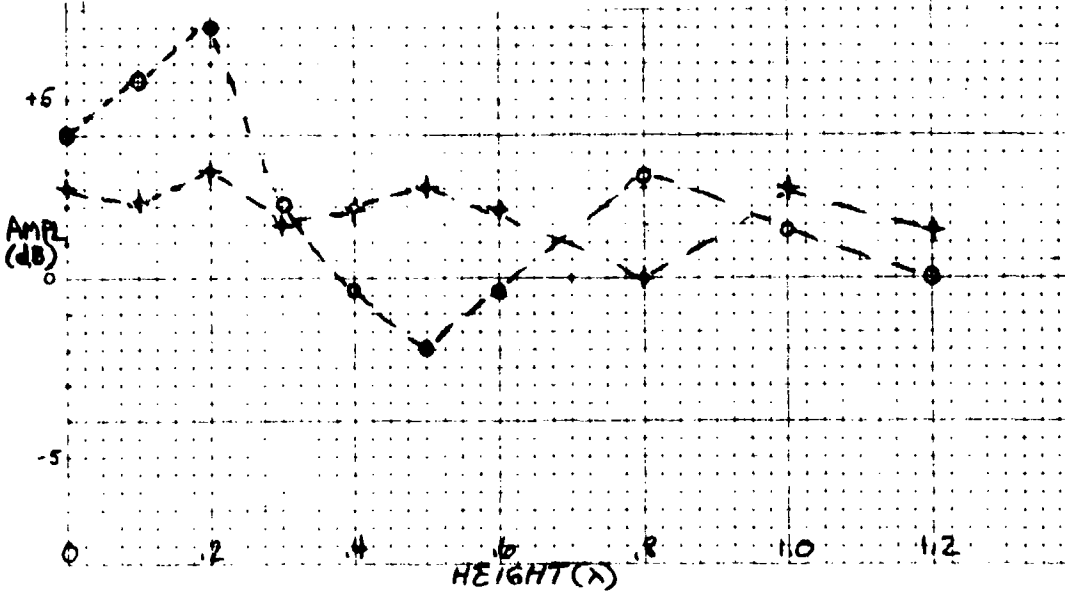


FIG. II-22. AMPLITUDE AND PHASE VARIATIONS FOR SMALL COUNTERPOISE AND HORIZONTAL POLARIZATION AT $\theta = 60^\circ$, $\phi = 180^\circ$

● - BLADE AT 0° POS.
 ★ - BLADE AT 90°



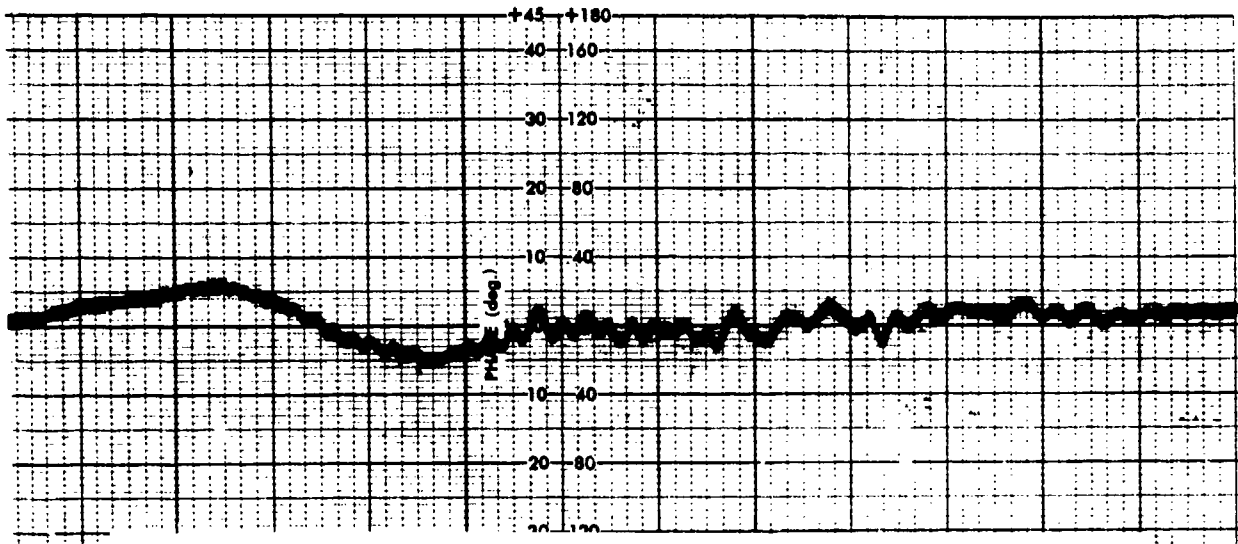
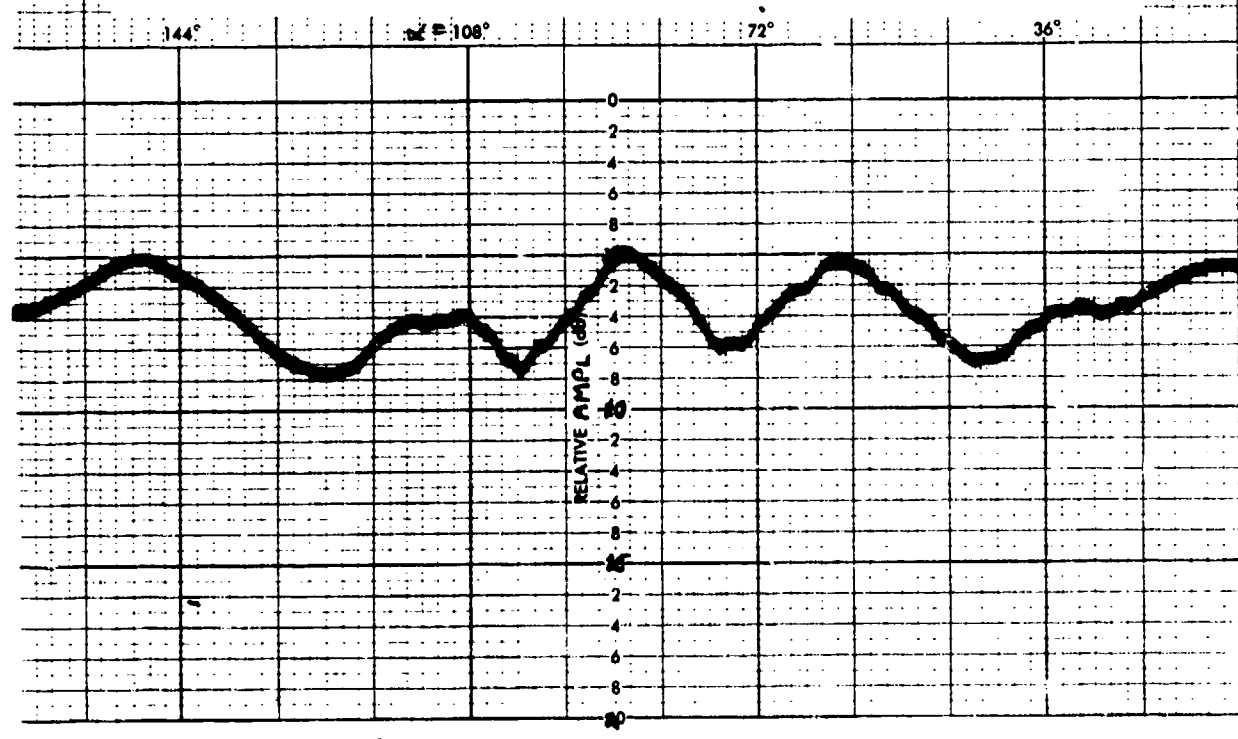
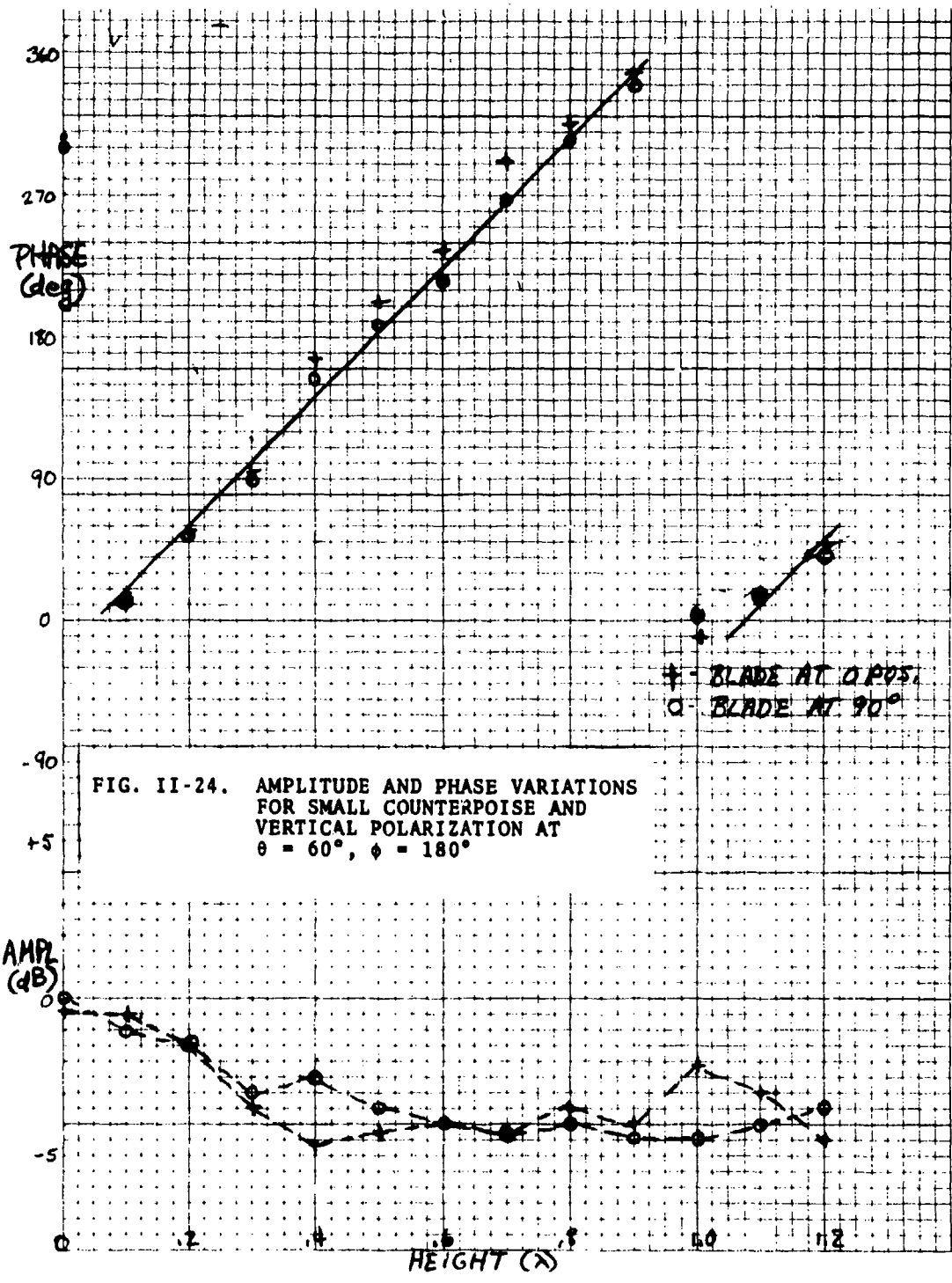


FIG. II-23. AMPLITUDE AND PHASE VARIATIONS FOR SMALL COUNTERPOISE AND VERTICAL POLARIZATION AT $\theta = 60^\circ$, $\phi = 180^\circ$





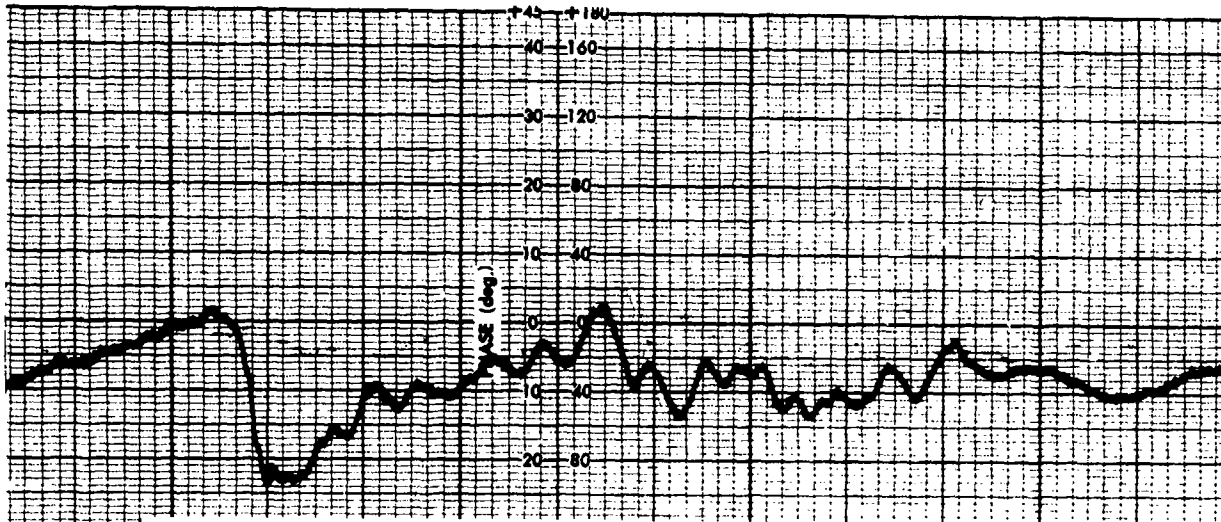
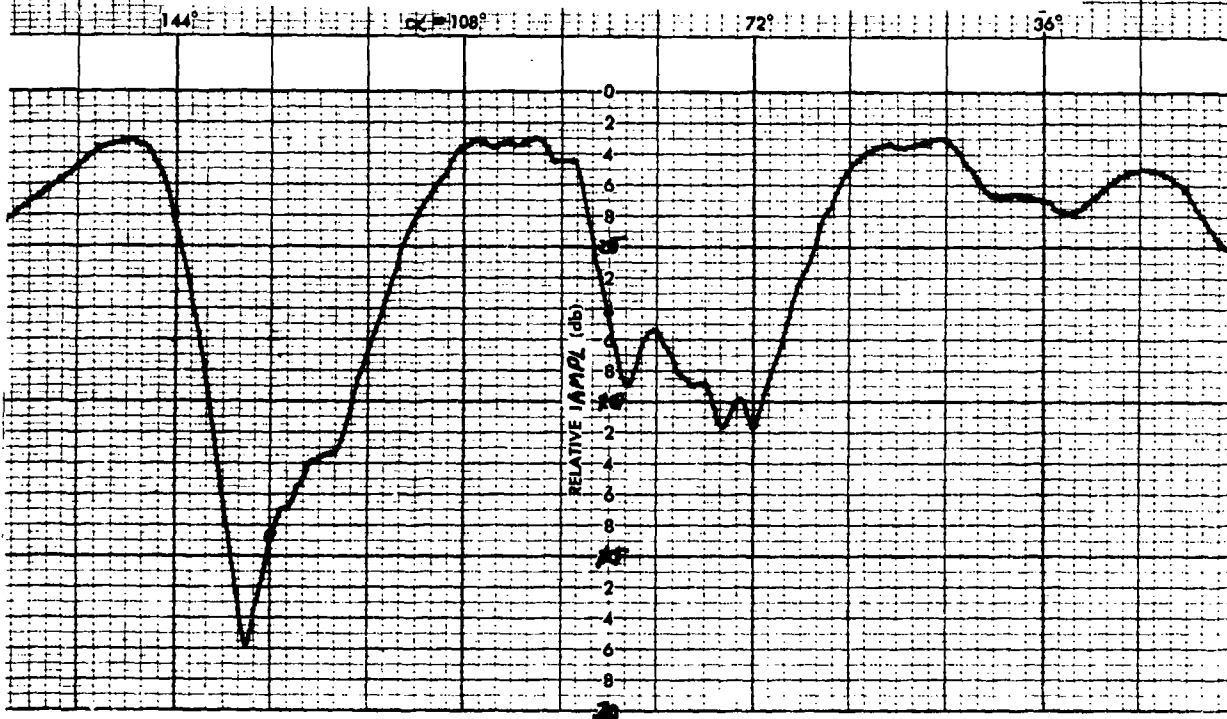
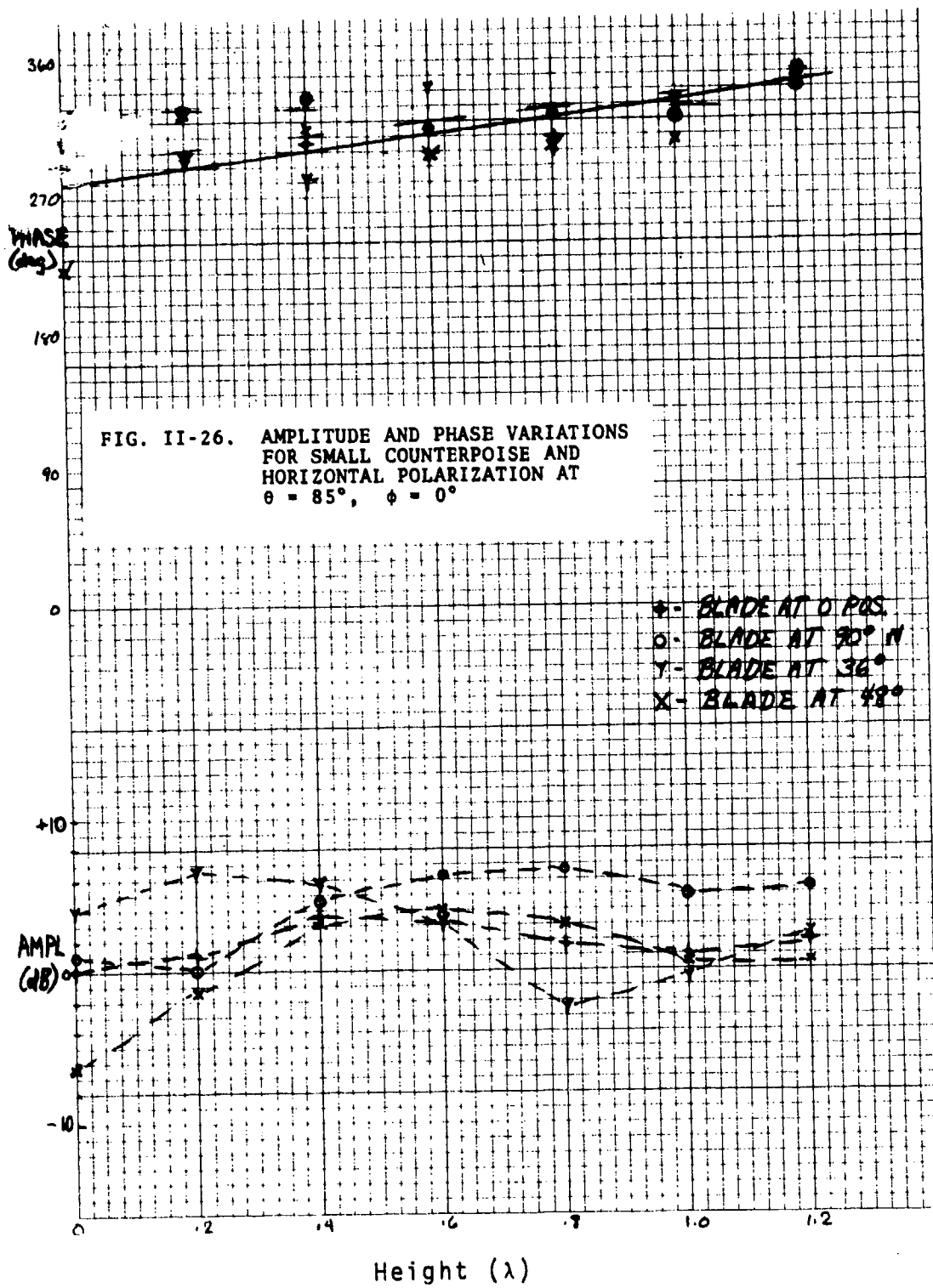


FIG. II-25. AMPLITUDE AND PHASE VARIATIONS
FOR SMALL COUNTERPOISE AND
HORIZONTAL POLARIZATION AT
 $\theta = 85^\circ$, $\phi = 0^\circ$





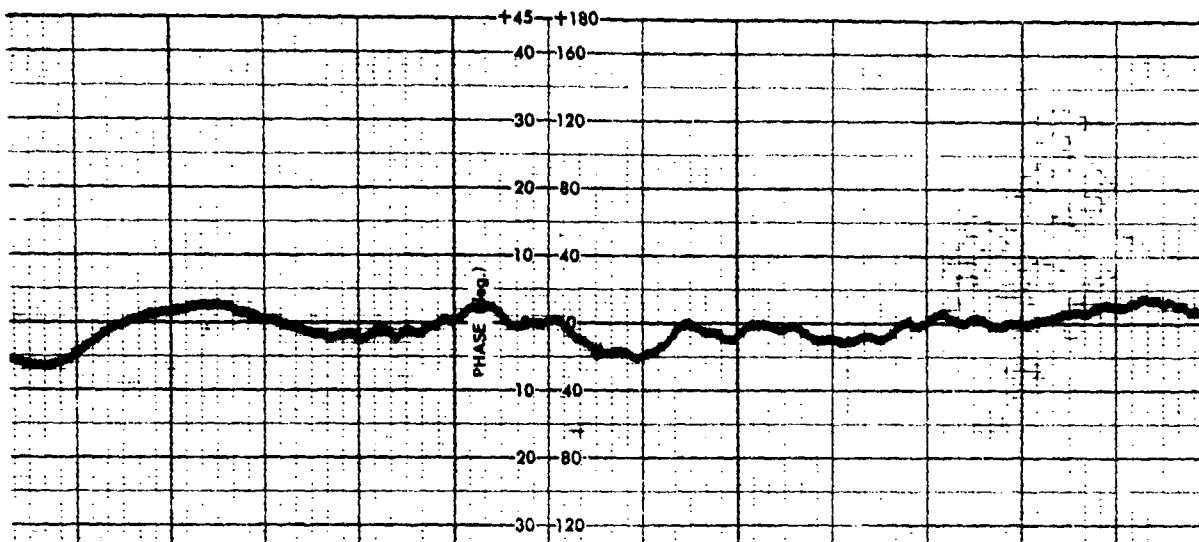
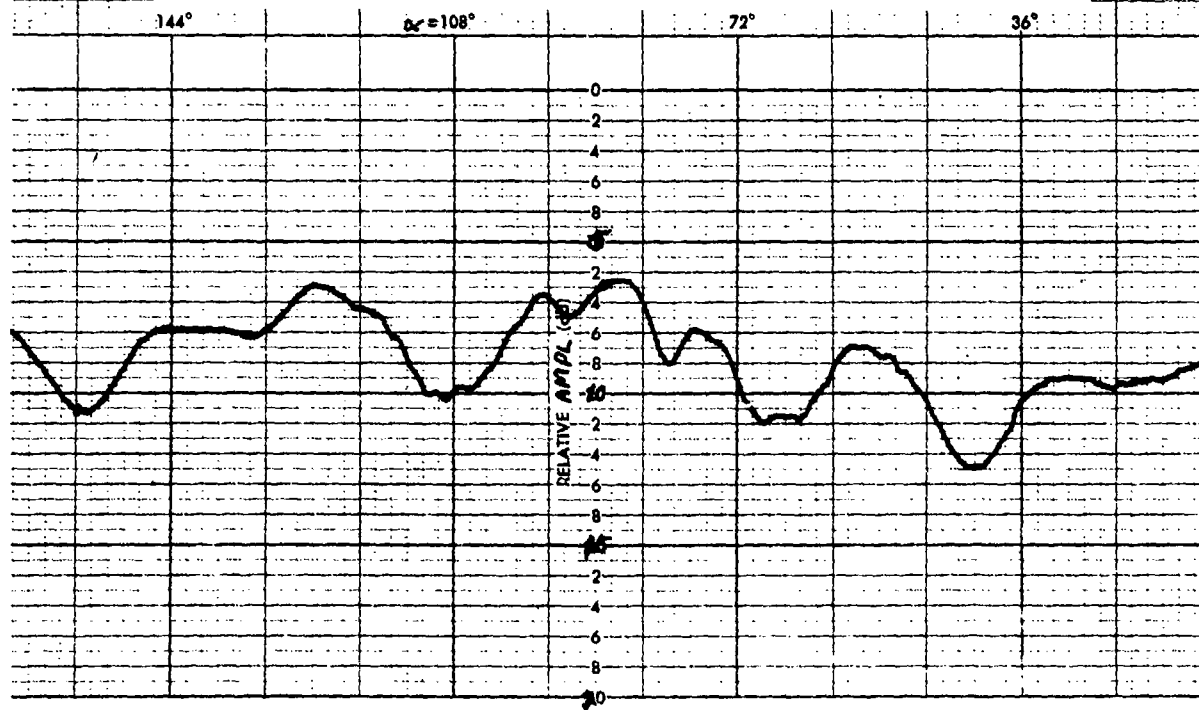


FIG. II-27. AMPLITUDE AND PHASE VARIATIONS
FOR SMALL COUNTERPOISE AND
VERTICAL POLARIZATION AT
 $\theta = 85^\circ, \phi = 0^\circ$



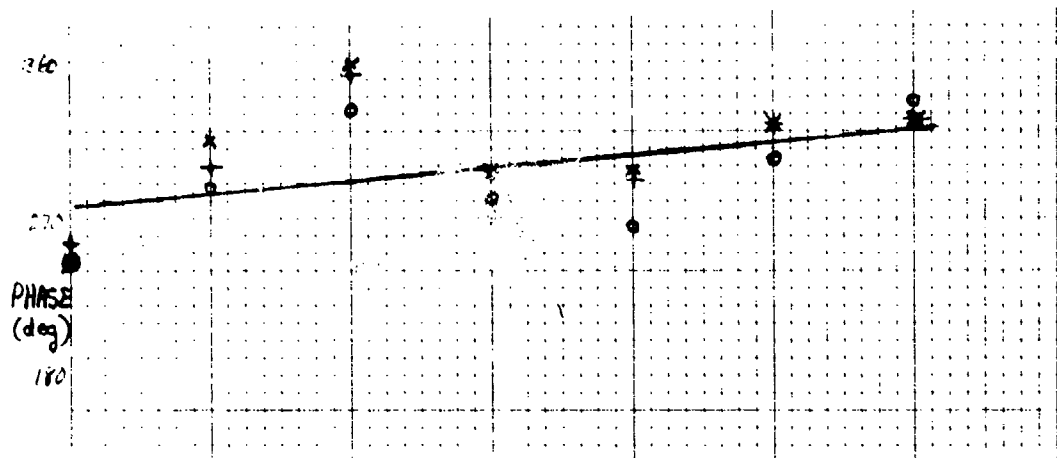
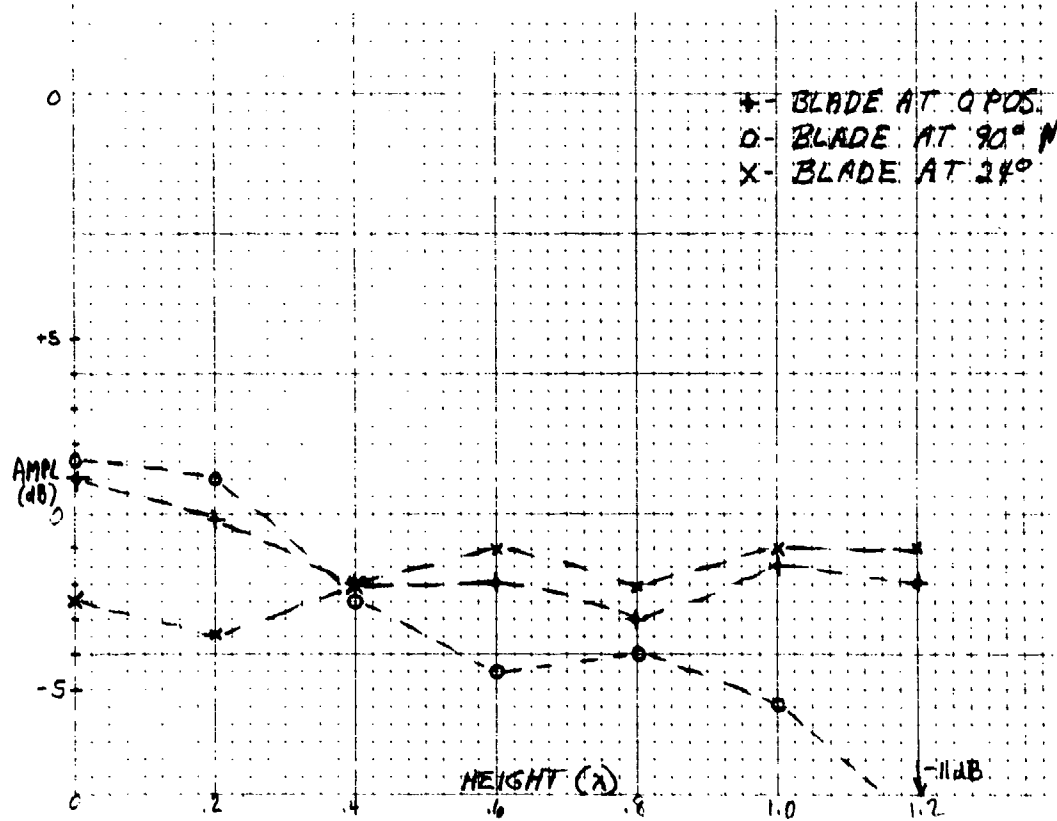


FIG. II-28. AMPLITUDE AND PHASE VARIATIONS FOR SMALL COUNTERPOISE AND VERTICAL POLARIZATION AT $\theta = 85^\circ, \phi = 0^\circ$



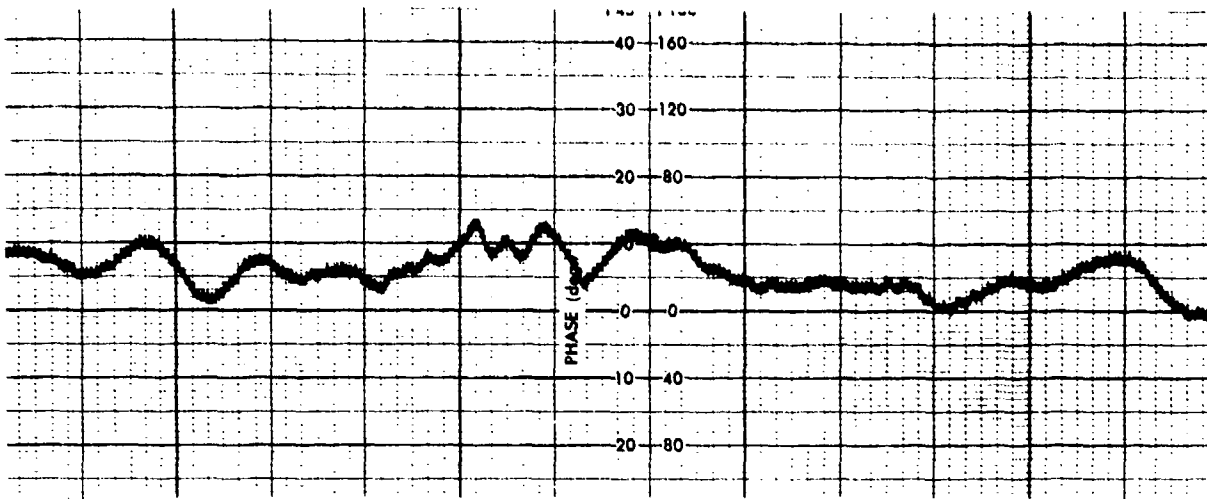
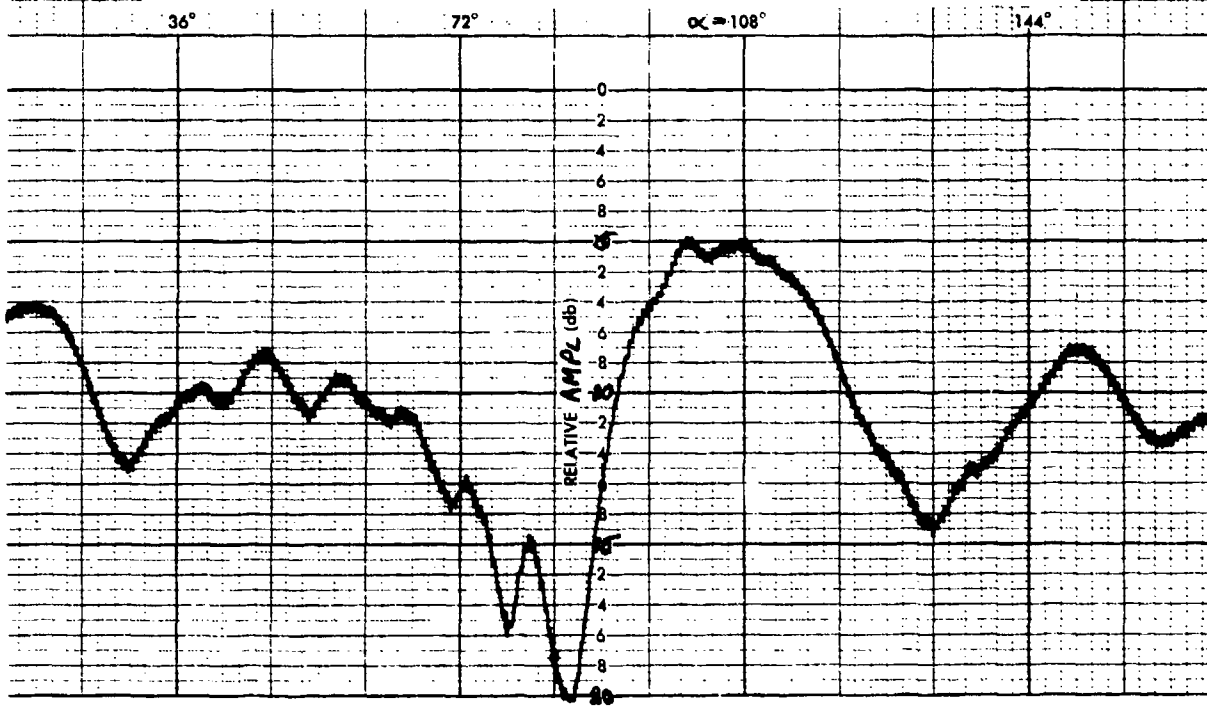


FIG. II-29. AMPLITUDE AND PHASE VARIATIONS
 FOR LARGE COUNTERPOISE AND
 HORIZONTAL POLARIZATION AT
 $\theta = 85^\circ$, $\phi = 0^\circ$



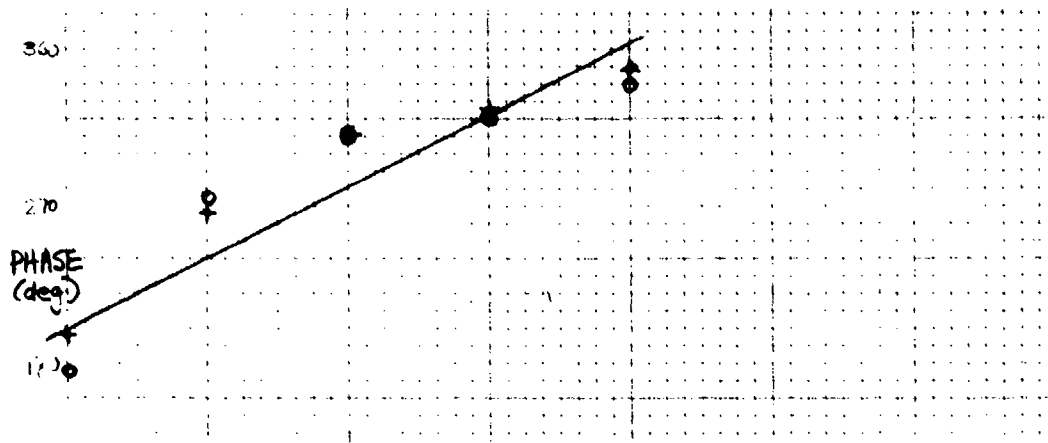
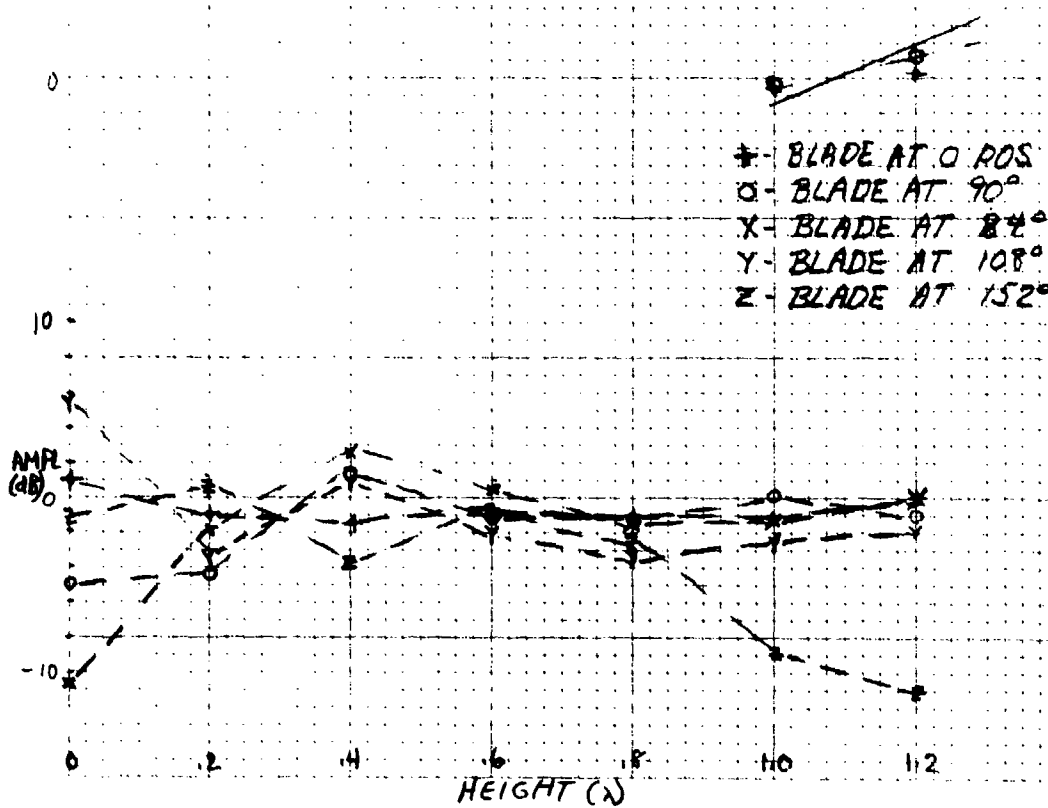


FIG. II-30. AMPLITUDE AND PHASE VARIATIONS FOR LARGE COUNTERPOISE AND HORIZONTAL POLARIZATION AT $\theta = 85^\circ$, $\phi = 0^\circ$



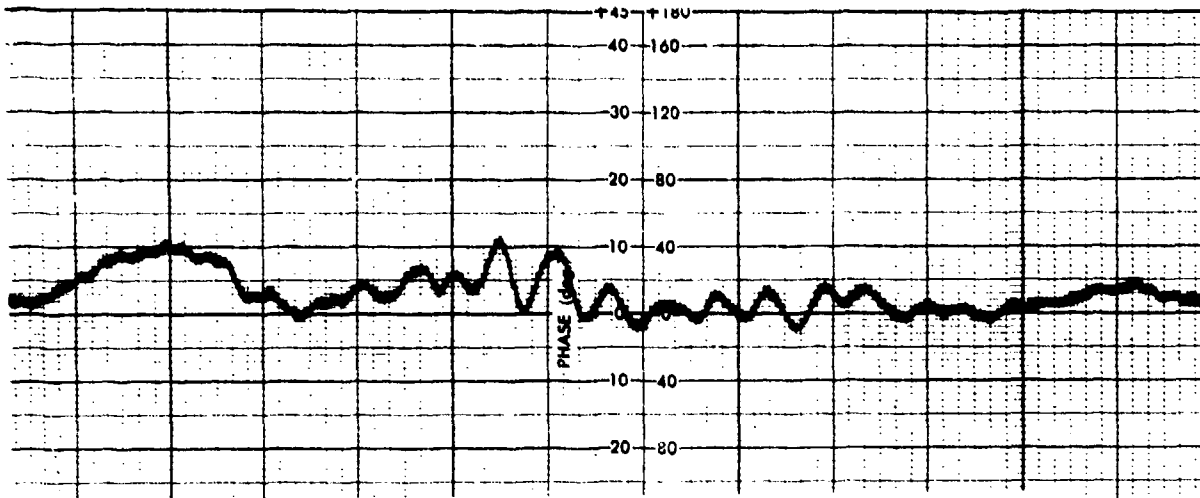
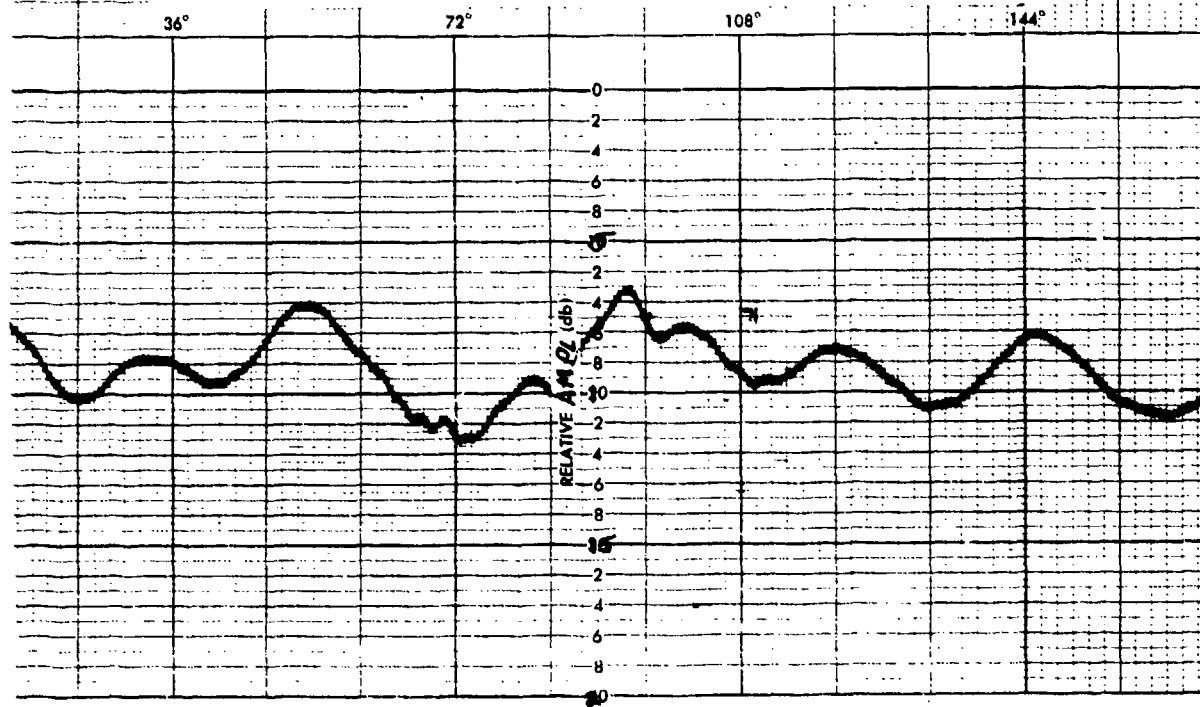


FIG. II-31. AMPLITUDE AND PHASE VARIATIONS FOR LARGE COUNTERPOISE AND VERTICAL POLARIZATION AT $\theta = 85^\circ$, $\phi = 0^\circ$



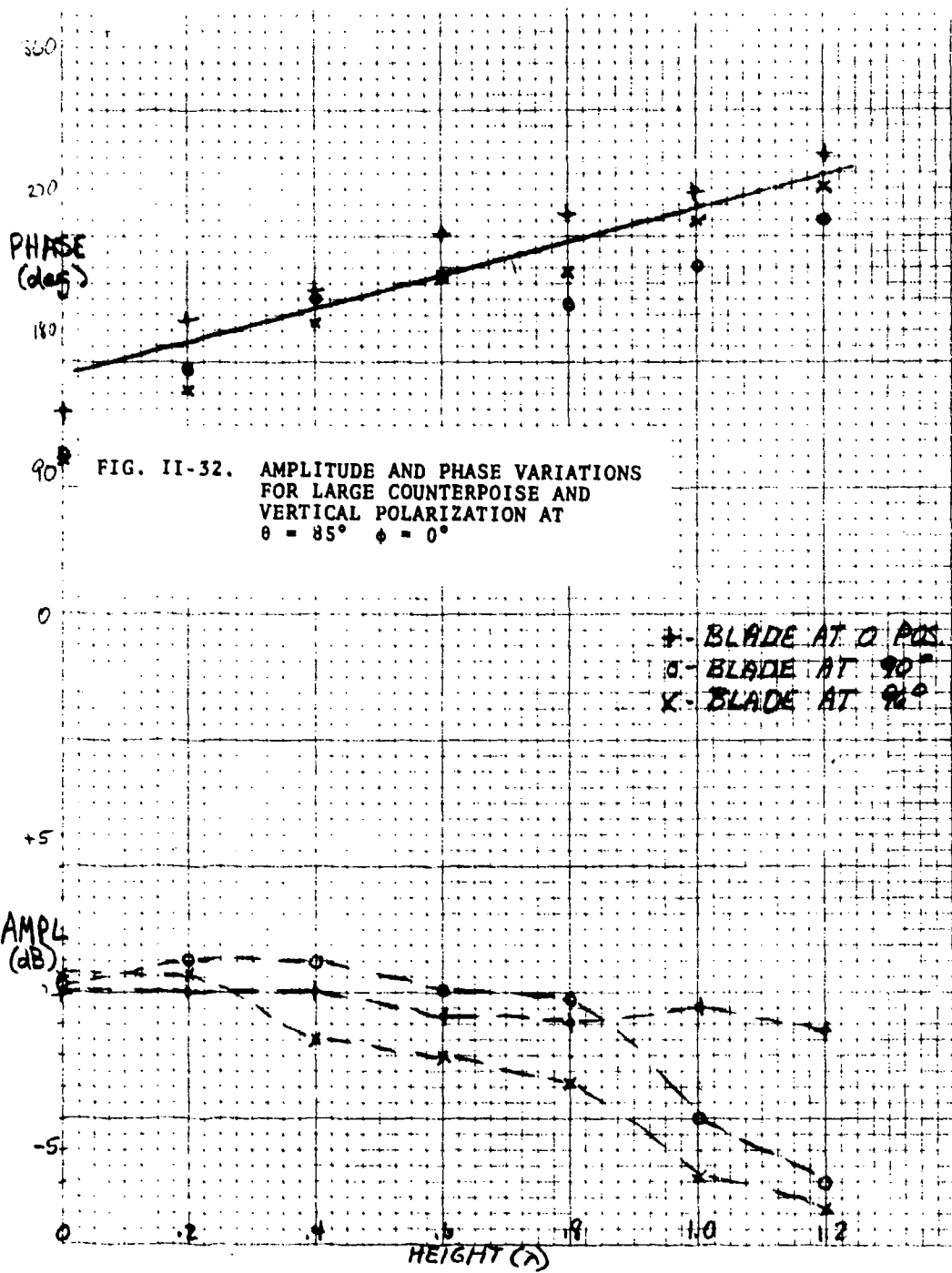


FIG. II-32. AMPLITUDE AND PHASE VARIATIONS
 FOR LARGE COUNTERPOISE AND
 VERTICAL POLARIZATION AT
 $\theta = 85^\circ \quad \phi = 0^\circ$

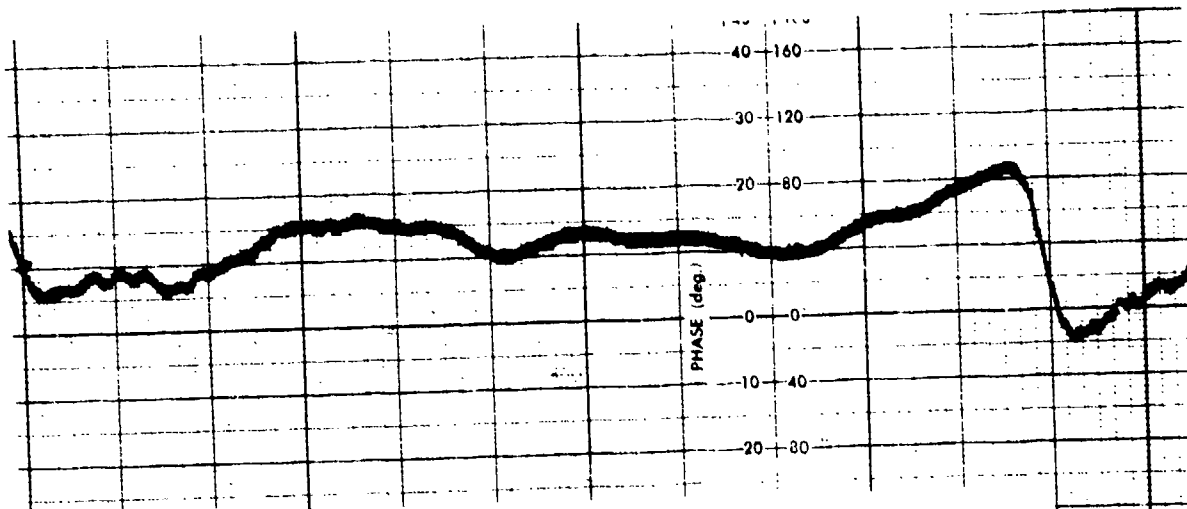
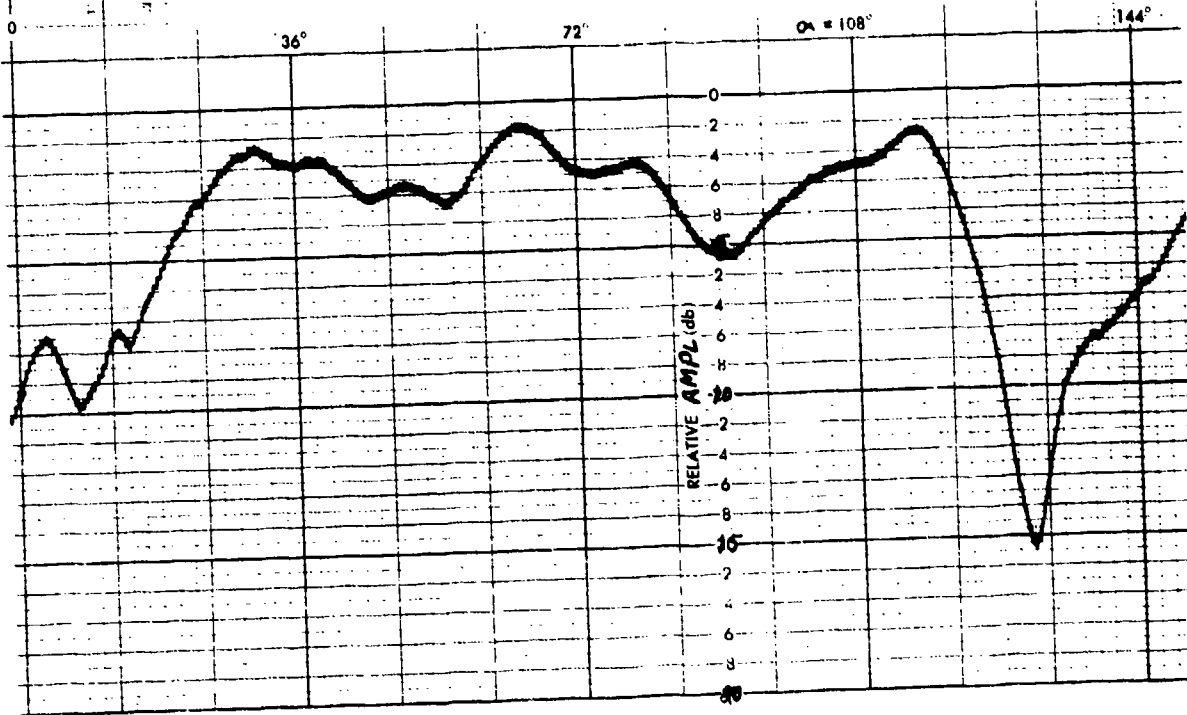


FIG. II-33. AMPLITUDE AND PHASE VARIATIONS
FOR SMALL COUNTERPOISE AND
HORIZONTAL POLARIZATION AT
 $\theta = 85^\circ$, $\phi = 90^\circ$



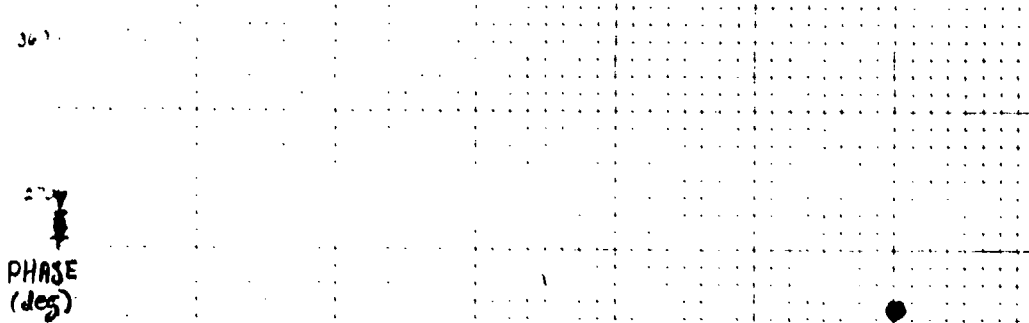
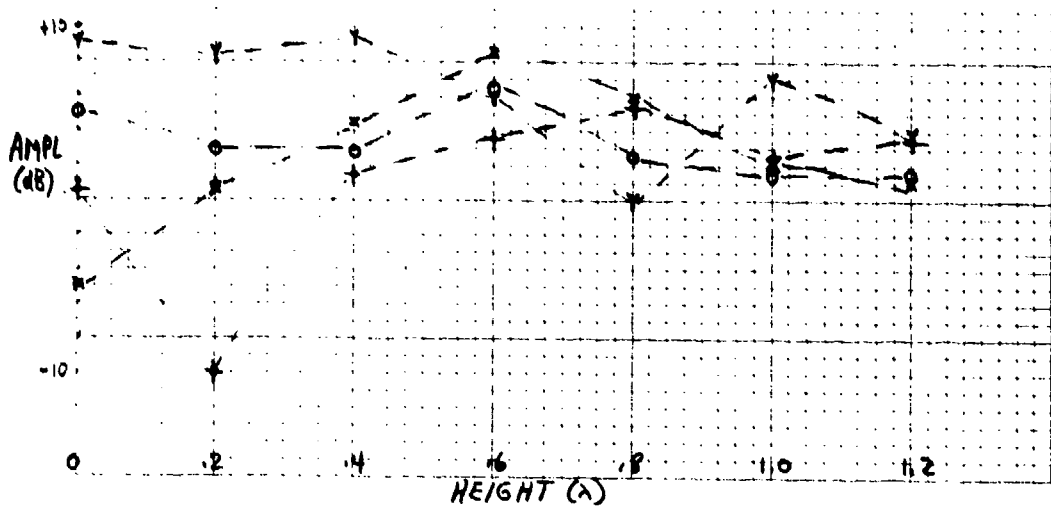


FIG. II-34. AMPLITUDE AND PHASE VARIATIONS FOR SMALL COUNTERPOISE AND HORIZONTAL POLARIZATION AT $\theta = 85^\circ$, $\phi = 90^\circ$

+ - BLADE AT 0 POS.
 O - BLADE AT 90°
 Y - BLADE AT 12°
 X - BLADE AT 18°



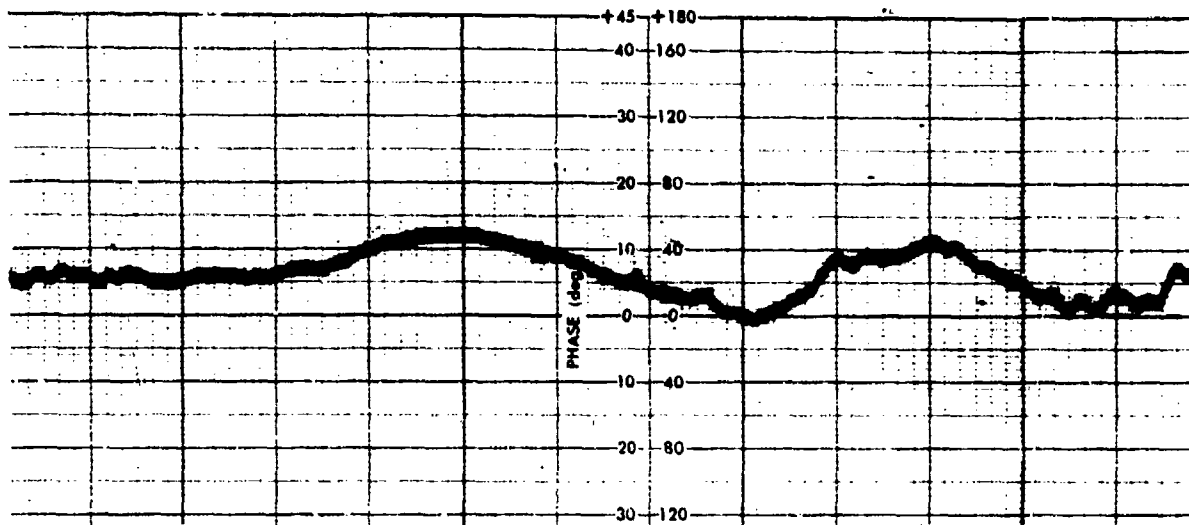
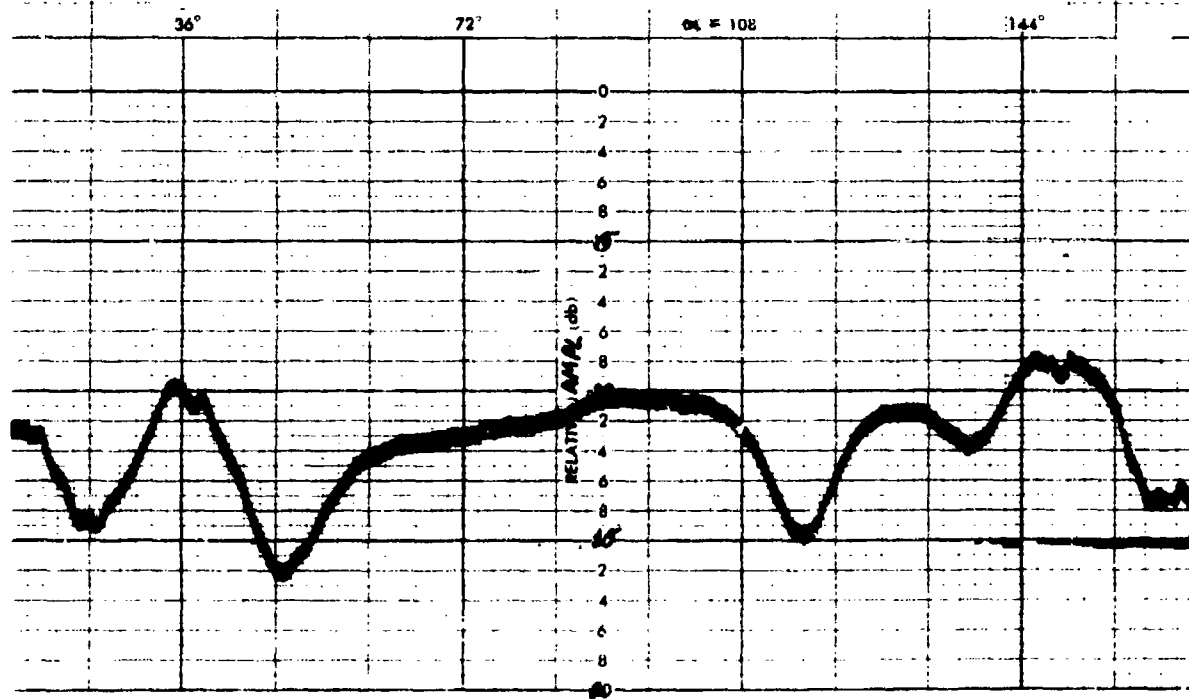
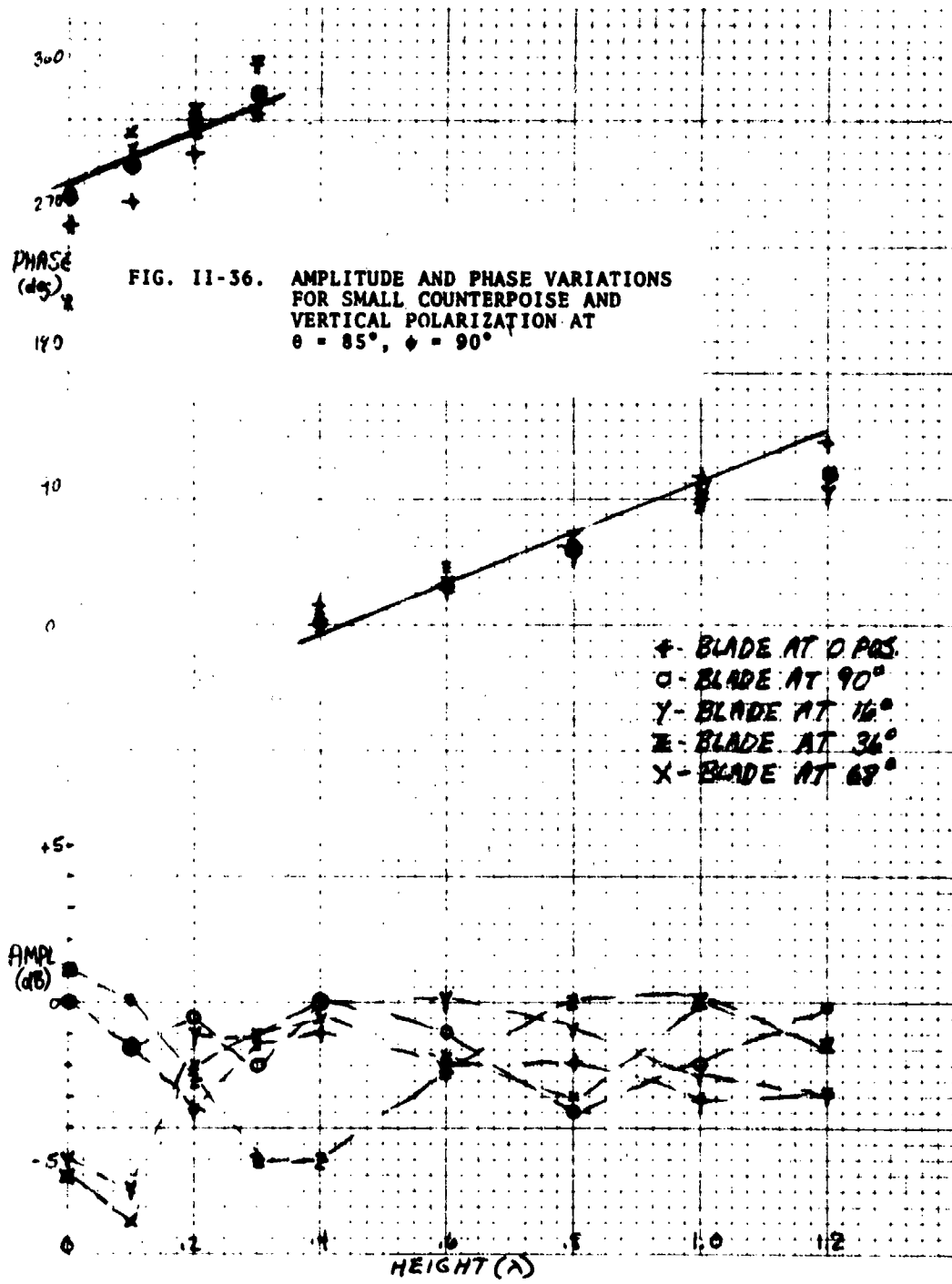


FIG. II-35. AMPLITUDE AND PHASE VARIATIONS
FOR SMALL COUNTERPOISE AND
VERTICAL POLARIZATION AT
 $\theta = 85^\circ$, $\phi = 90^\circ$





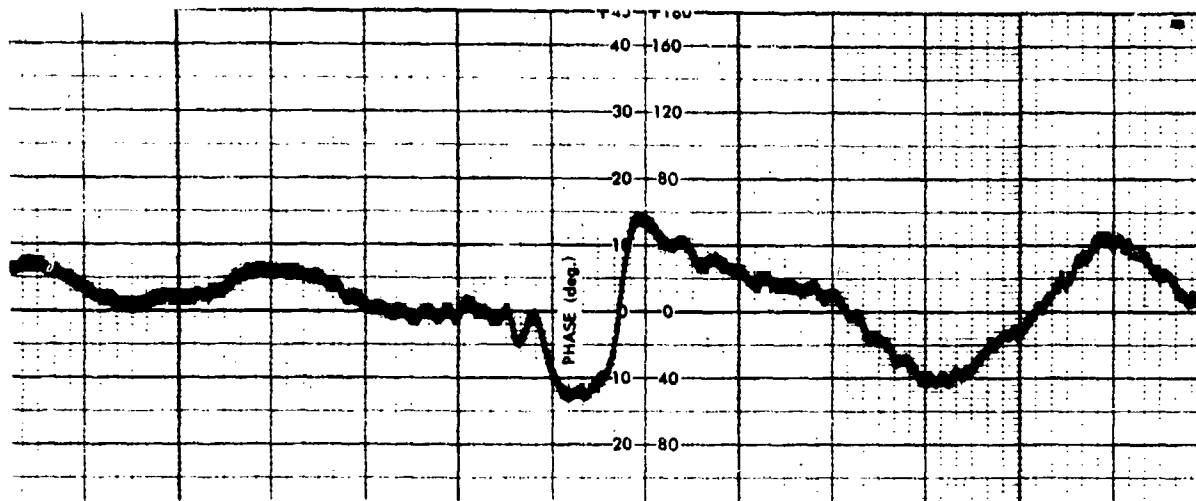
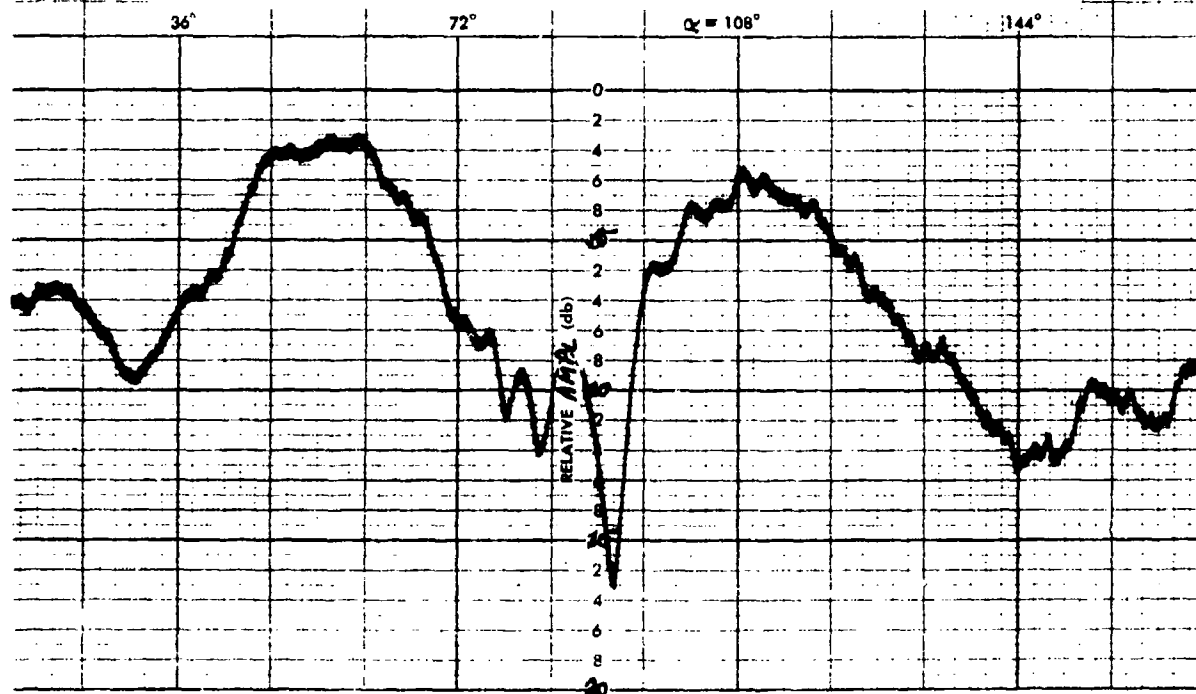
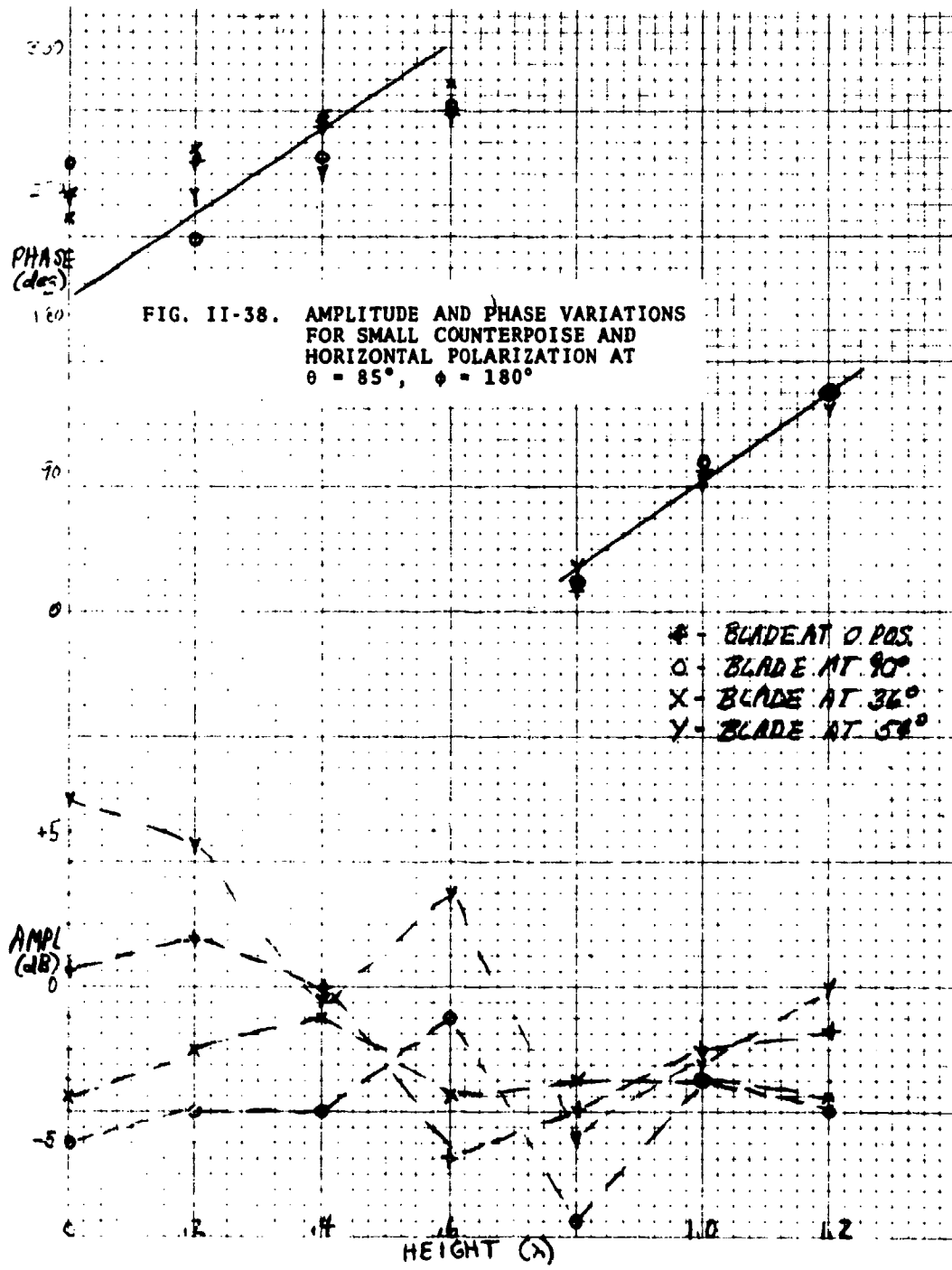


FIG. II-37. AMPLITUDE AND PHASE VARIATIONS FOR SMALL COUNTERPOISE AND HORIZONTAL POLARIZATION AT $\theta = 85^\circ$, $\phi = 180^\circ$





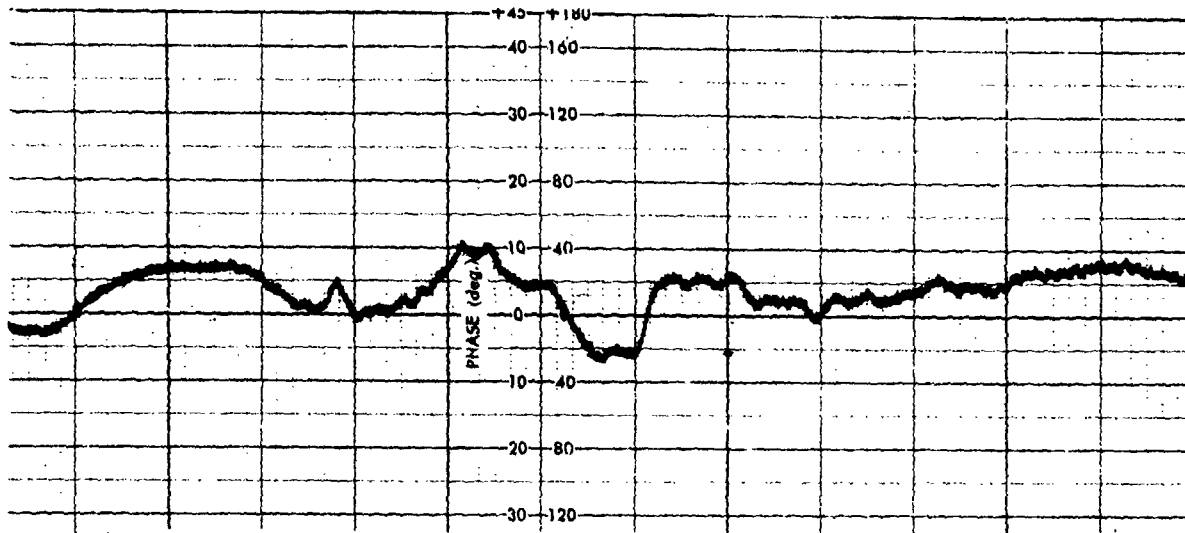
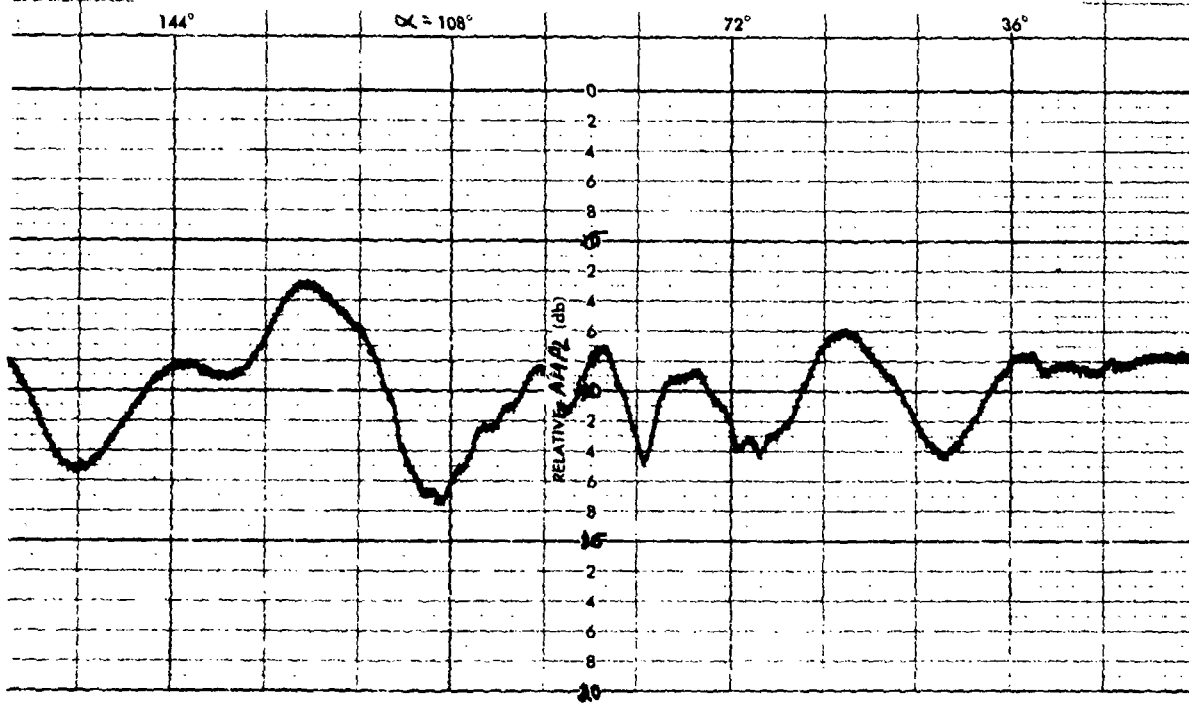
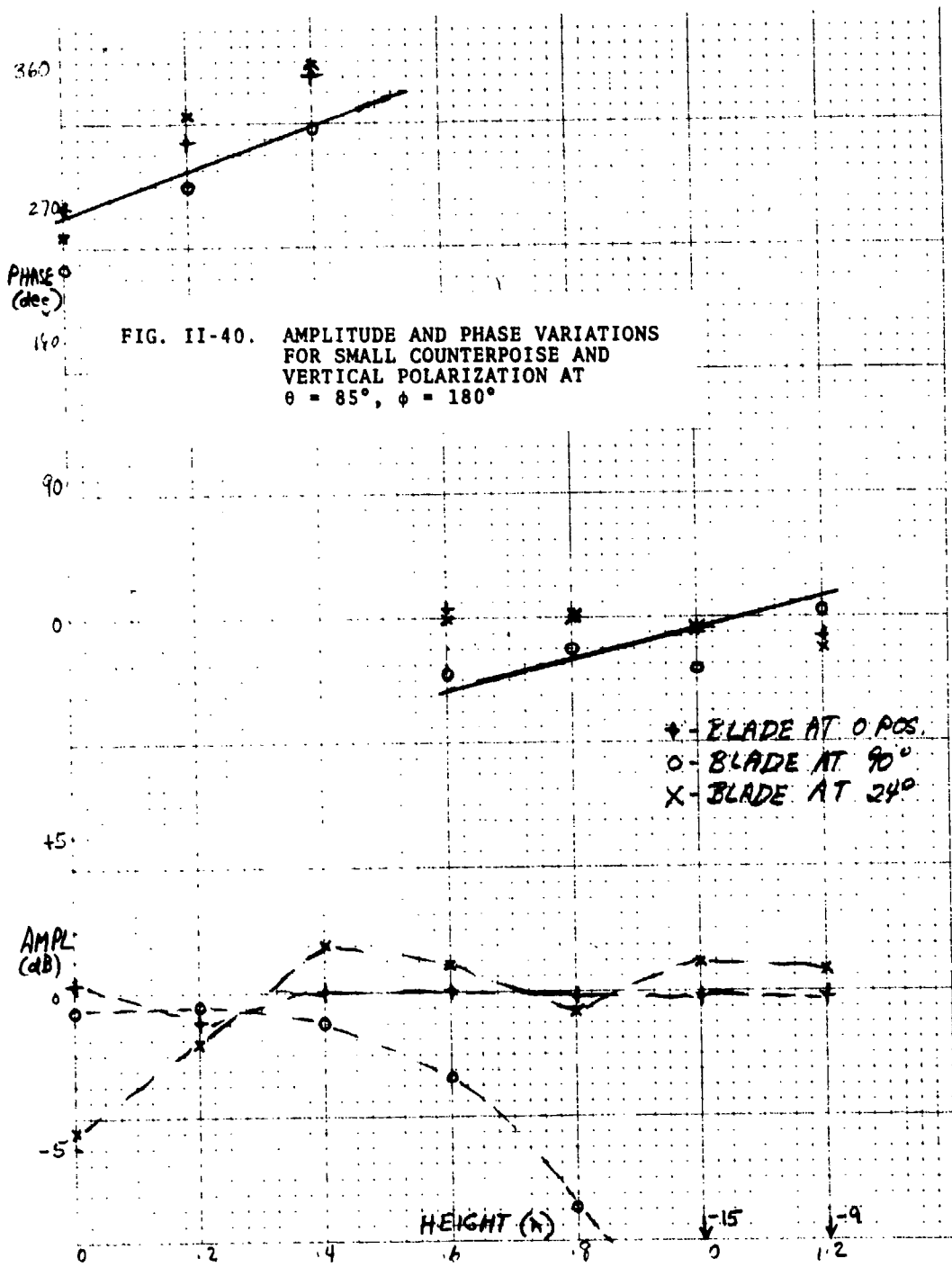


FIG. II-39. AMPLITUDE AND PHASE VARIATIONS FOR SMALL COUNTERPOISE AND VERTICAL POLARIZATION AT $\theta = 85^\circ$, $\phi = 180^\circ$





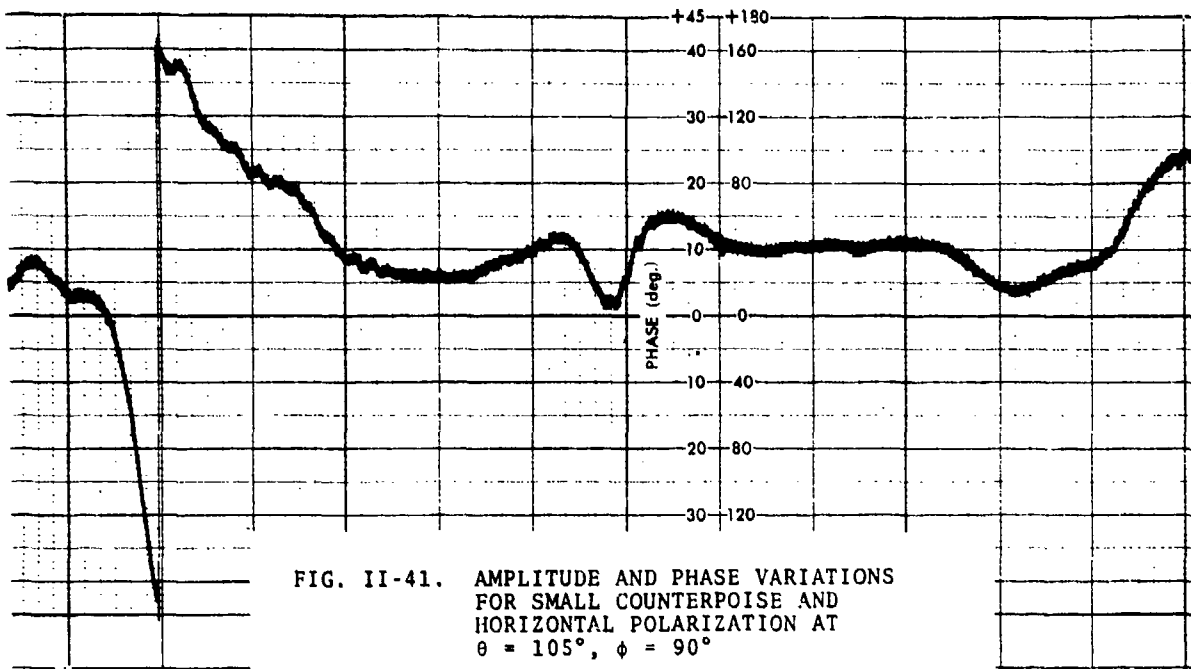
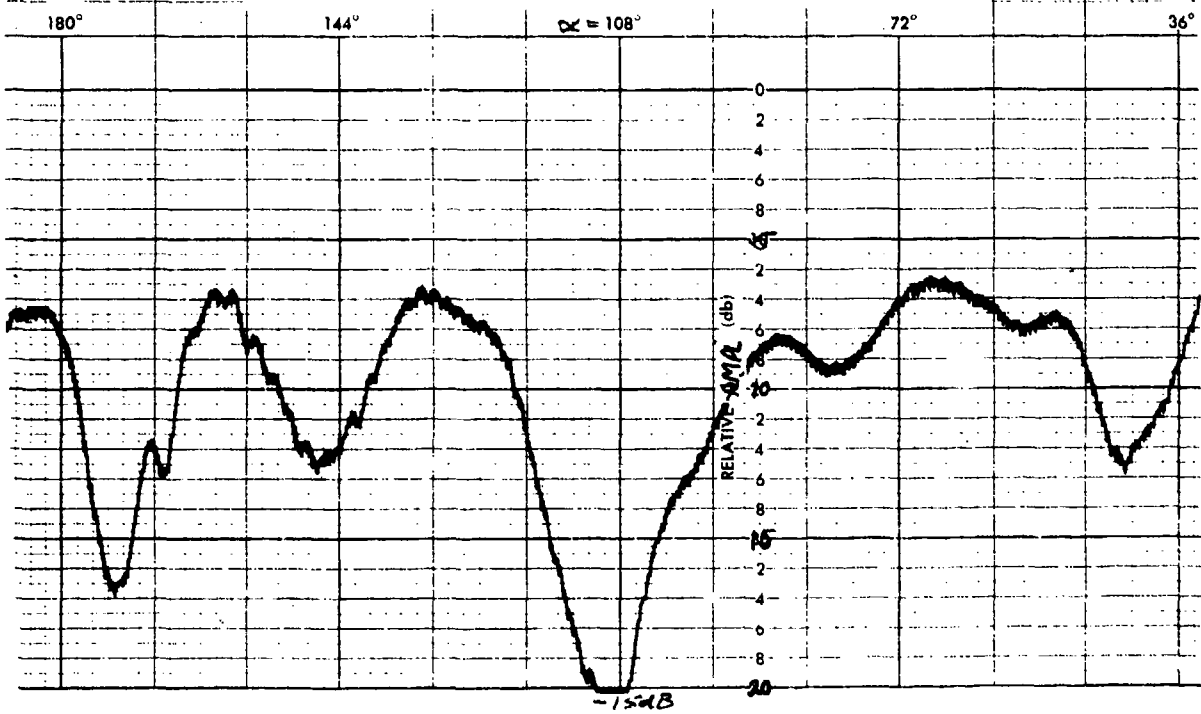
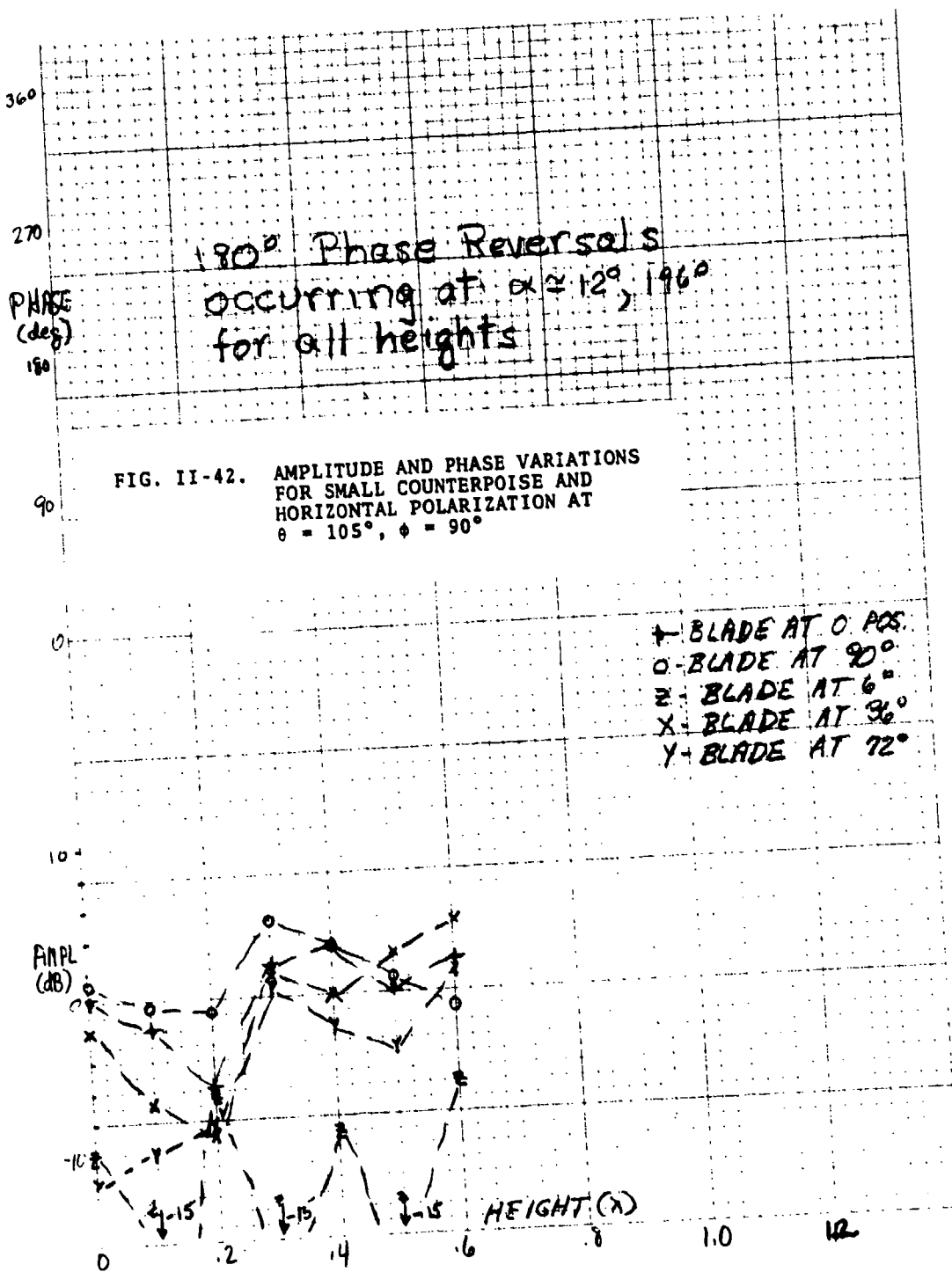


FIG. II-41. AMPLITUDE AND PHASE VARIATIONS FOR SMALL COUNTERPOISE AND HORIZONTAL POLARIZATION AT $\theta = 105^\circ$, $\phi = 90^\circ$





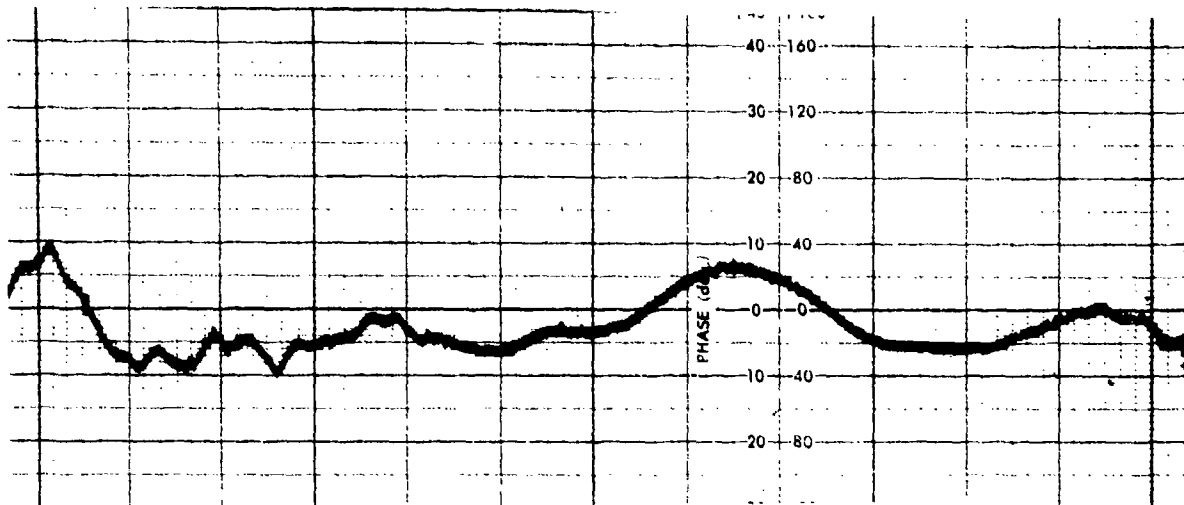
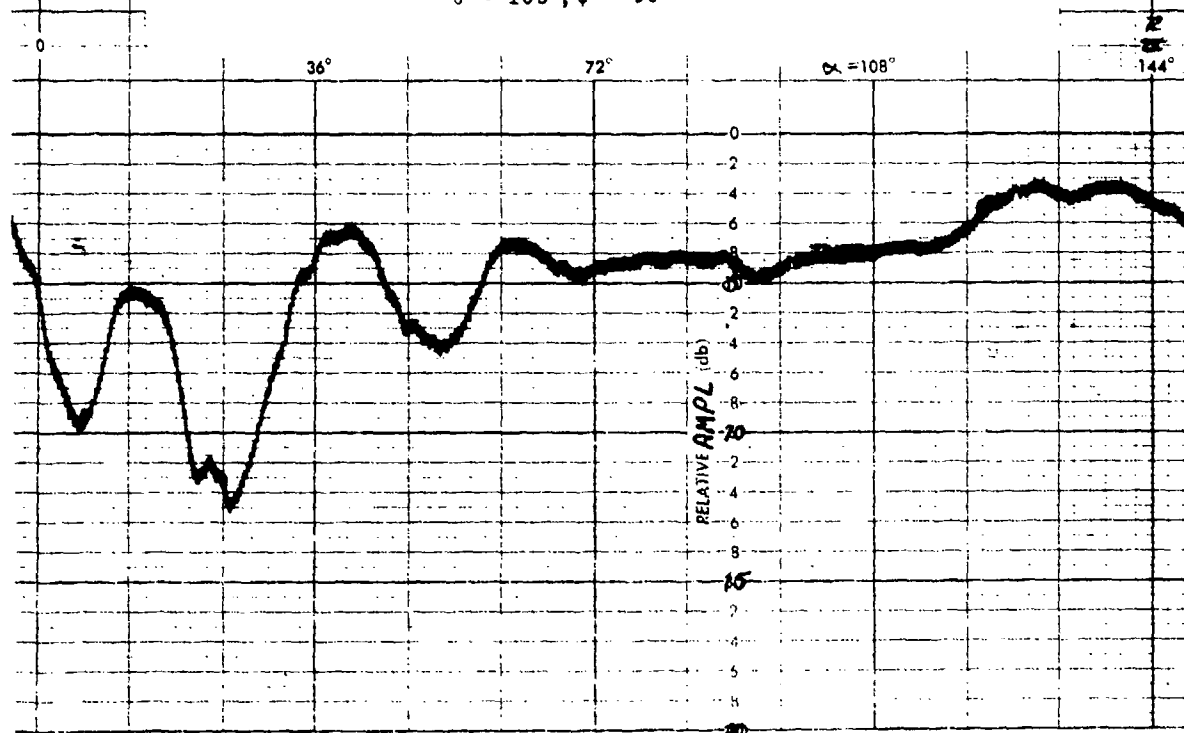
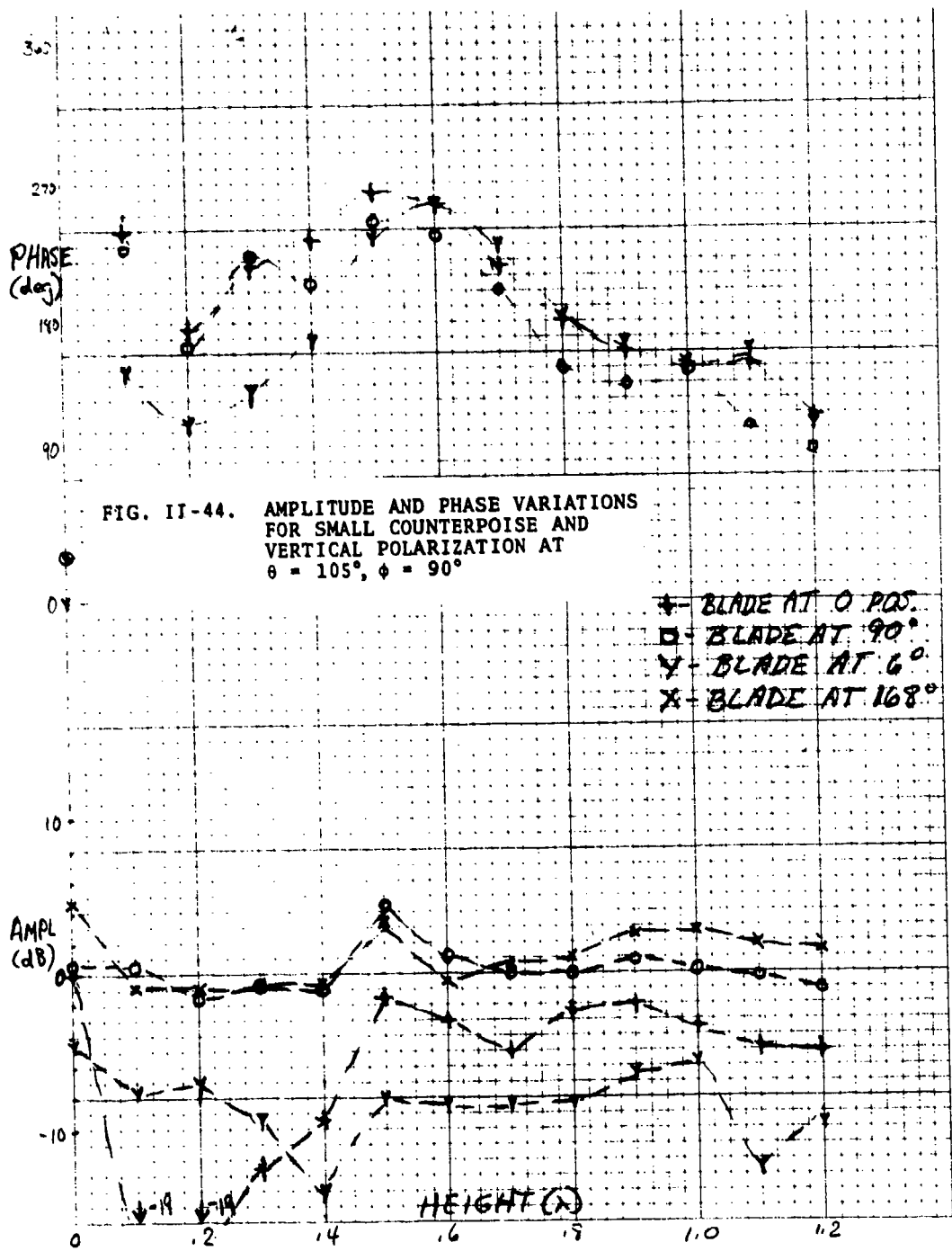


FIG. II-43. AMPLITUDE AND PHASE VARIATIONS
FOR SMALL COUNTERPOISE AND
VERTICAL POLARIZATION AT
 $\theta = 105^\circ, \phi = 90^\circ$





APPENDIX III

SELECTED EXPERIMENTAL DATA CHARACTERIZING THE SIGNAL FLUCTUATIONS AT THE TAIL ABOVE THE ROTOR

The first set of curves (Figs. III-1 to III-7) shows small counterpoise data for both polarizations at zero height. The second set of curves (Figs. III-8 to III-38) shows large counterpoise data for both polarizations. Here, however, a selection of curves from the measured data is presented to illustrate the best and worst signal reception as a function of height.

Somewhat different polar angle settings were used for the tail position measurements to compensate for the fact that the antenna-to-transmitter distance was changing with azimuth angle.

A comparison with the data of Appendix II reveals several features in the curves of Appendix III:

- (1) There is a decrease in the magnitude and duration of the amplitude variations as a function of rotor position;
- (2) Differences in response to horizontal and vertical polarization still occur. However, for some directions of incidence, the vertically polarized signal is received virtually undisturbed;
- (3) The phase deviations for all directions of incidence were smaller and no 180° phase reversals occurred.

Some curves are also presented to show the effect of tail rotor proximity. In general, the tail rotor does not interfere except at banking angles. However, there may still be other directions of incidence not investigated during this study where a strong reflection from this blade can occur. In such a case, the counterpoise should provide adequate shielding. The shielding effectiveness of the different-sized counterpoises is more apparent in the curves of Appendix III due to the narrower range over which the disturbances occur. As expected, the large counterpoise provided better shielding. However, the counterpoise size had little or no effect on vertically polarized signals while notable changes occurred for horizontally polarized signals. This is due to the fact that the tangential electric field must be zero at the surface of the metal disk, and that the electric field component in the horizontally polarized signal is always greater than or equal to that in the vertically polarized signal. Hence the vertically polarized signal is influenced to a lesser degree by the counterpoise.

The test results show that the small counterpoise should provide effective shielding at the tail location.

The following notes discuss details of the individual curves:

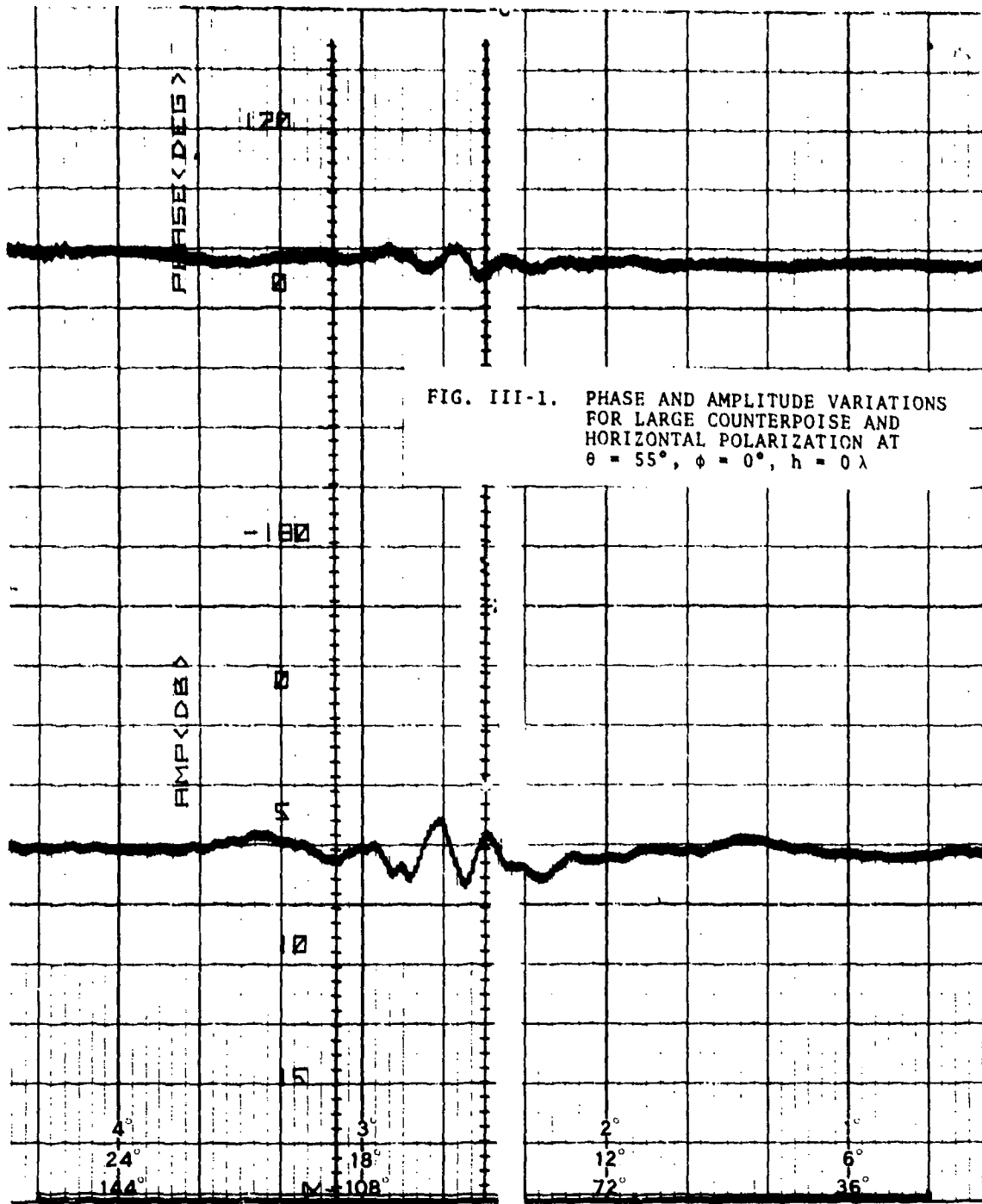
(1) Curves for $\theta = 55^\circ$ and $\phi = 0^\circ, 90^\circ, 180^\circ$ are shown for the 1λ diameter counterpoise in Figs. III-1 and III-2 and for the 2λ counterpoise in Figs. III-8 to III-15. This data shows peak-to-peak amplitude variations ≤ 7 dB in the worst case with no significant phase variations;

(2) Curves for the set $\theta = 70^\circ$ and $\phi = 0^\circ, 90^\circ$ are shown in Fig. III-3 and in Figs. III-16 to III-21 according to counterpoise size. Compared

to case (1), somewhat greater amplitude and phase variations occurred for this direction of incidence. Signal reception was not affected by movement of the tail rotor;

(3) Curves for the set $\theta = 85^\circ$ and $\phi = 0^\circ, 45^\circ, 90^\circ, 180^\circ$ are shown in Figs. III-4 and III-5 and in Figs. III-22 to III-28. In general, significant differences occurred for the two polarizations. However, for some directions of incidence in this set, only one curve is presented since no best/worst case could be distinguished. At $\phi = 90^\circ$ and horizontal polarization, scattering from the tail rotor occurred;

(4) Curves for the set $\theta = 105^\circ$ and $\phi = 0^\circ, 45^\circ, 90^\circ, 110^\circ$ are shown in Figs. III-6 and III-7, and in Figs. III-29 to III-38. Severe signal distortions can occur during banking and turning maneuvers since there is a marked difference between polarizations and there may be some blockage due to the rotor shaft at $\phi = 0^\circ$. For horizontal polarization, a strong tail rotor effect occurs at $\phi = 45^\circ$ and $h = 1.2\lambda$.



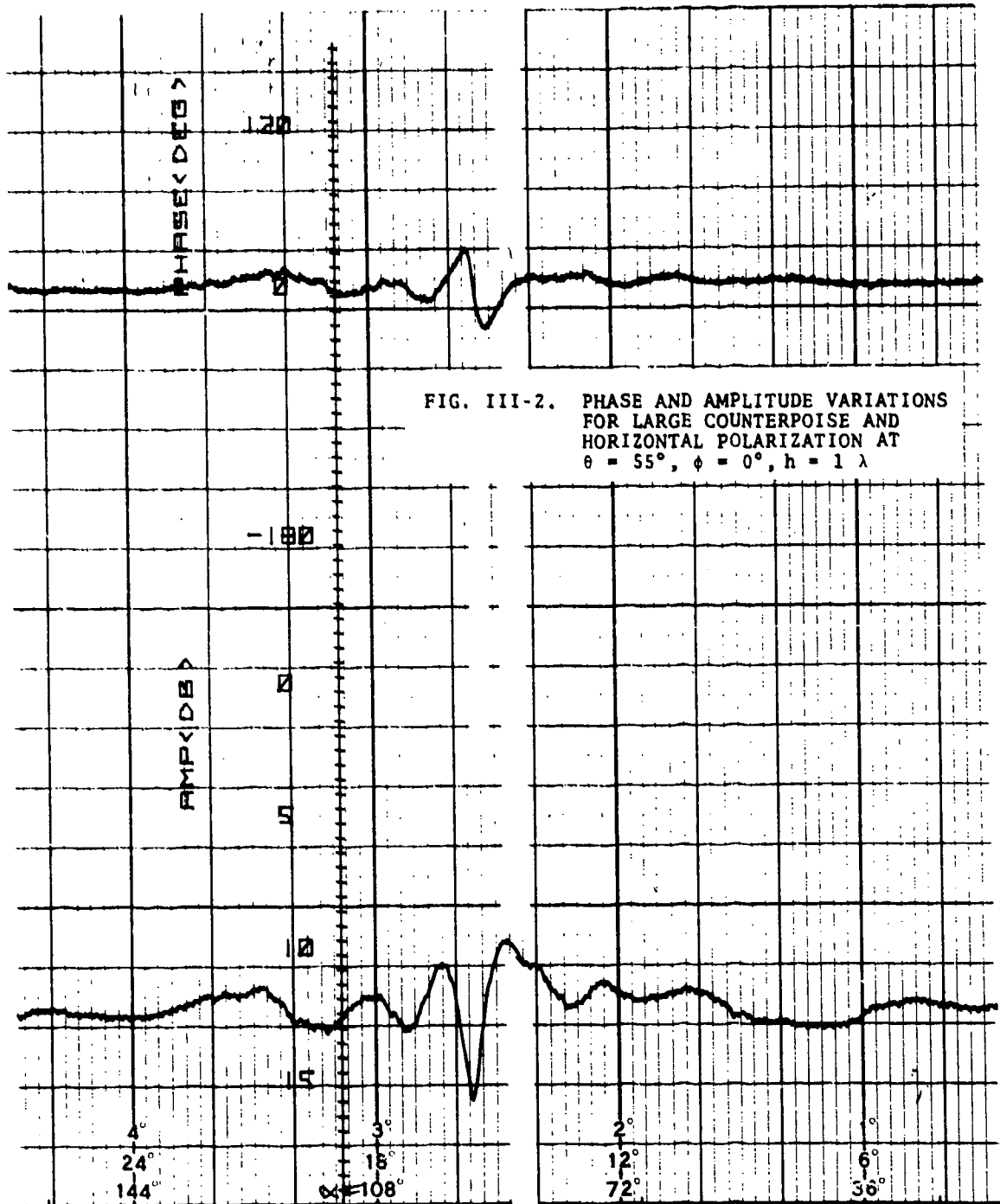
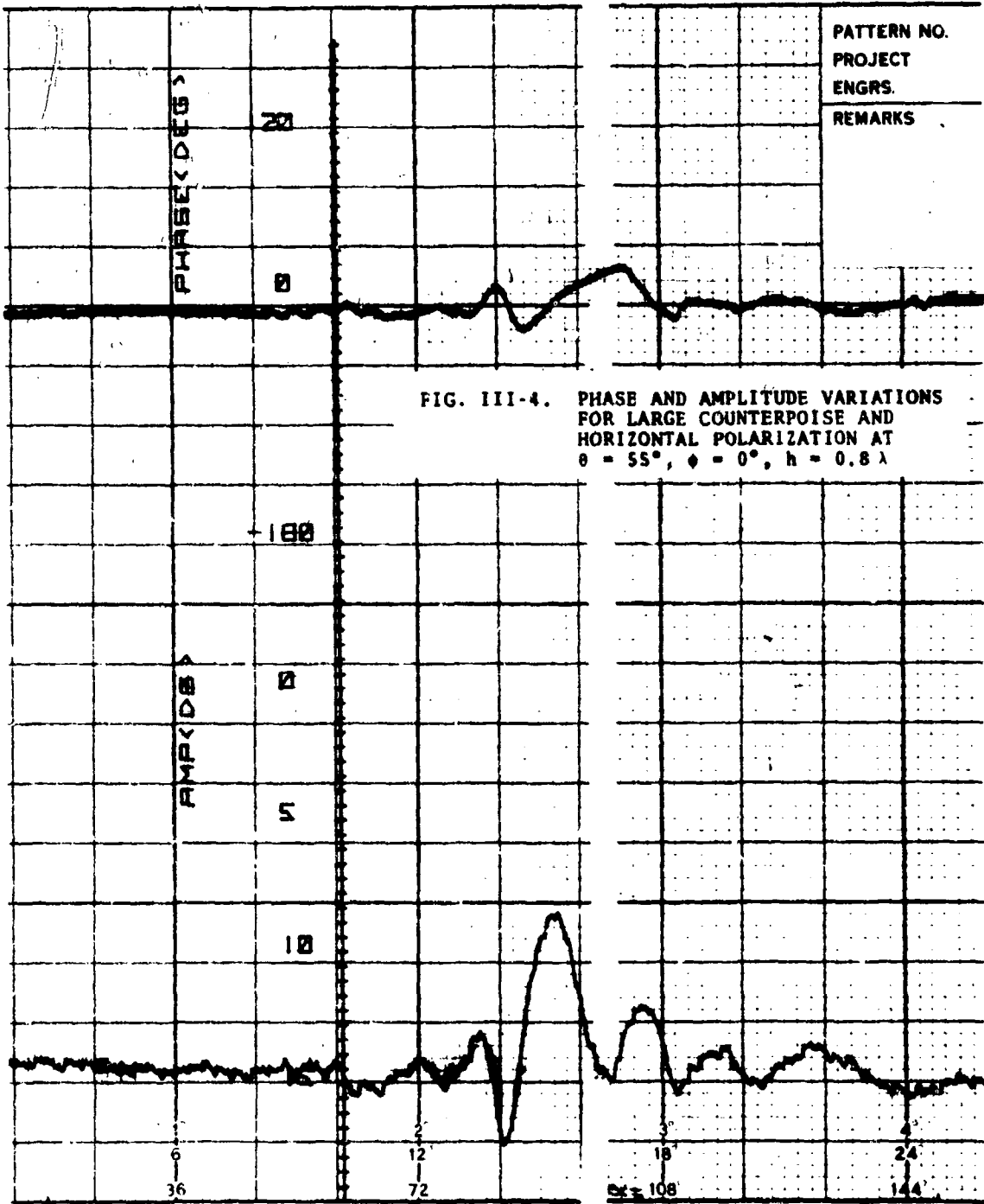
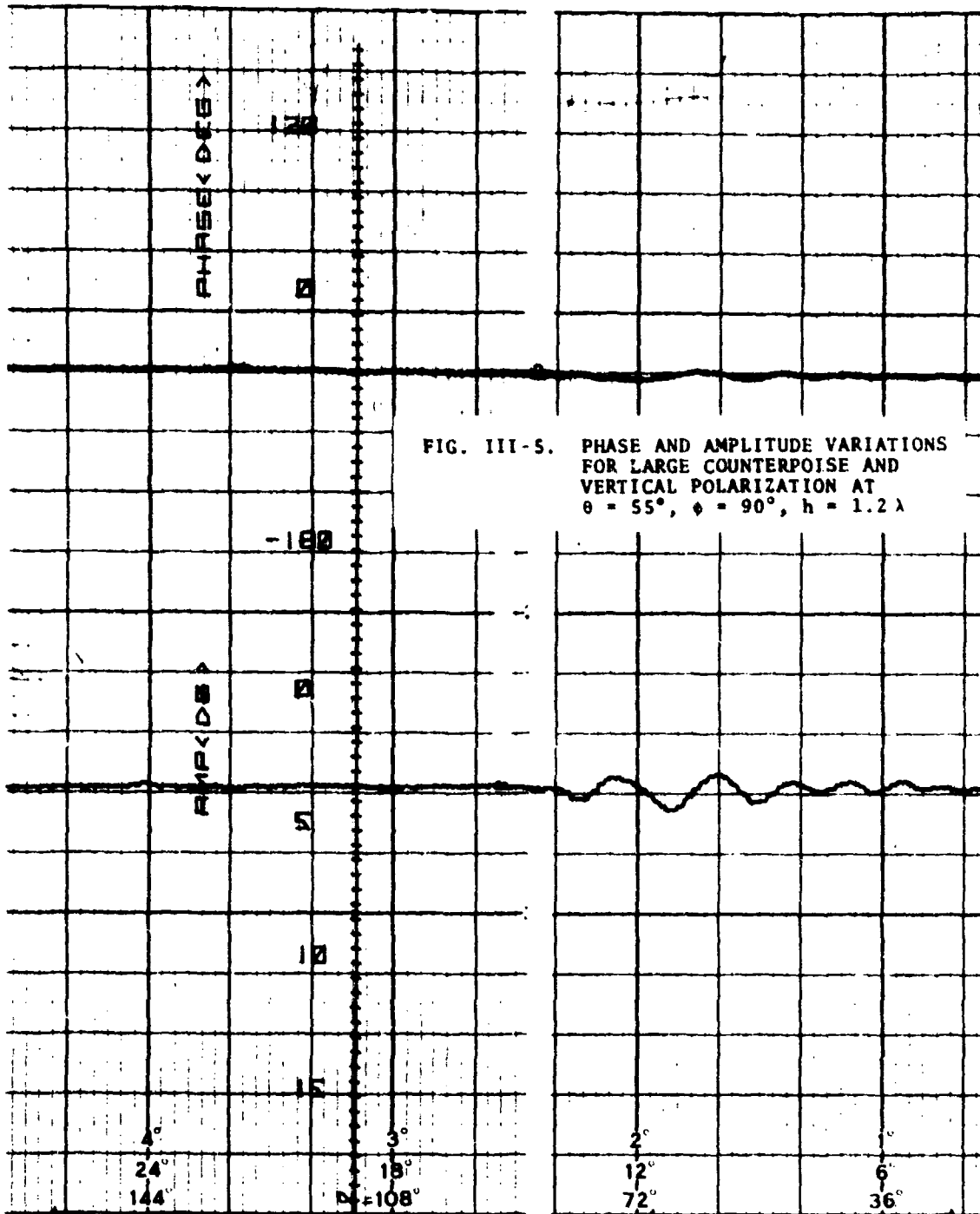
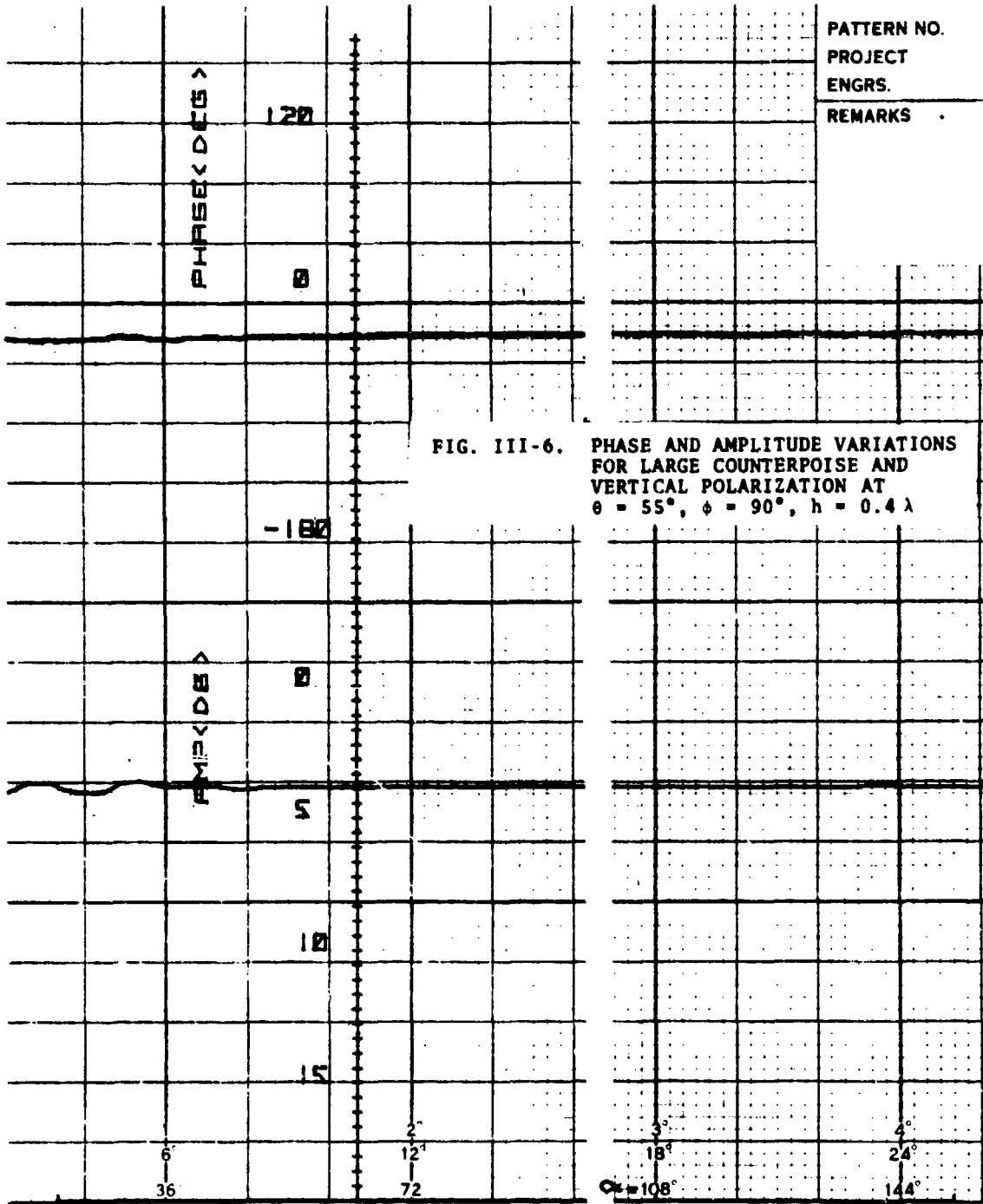
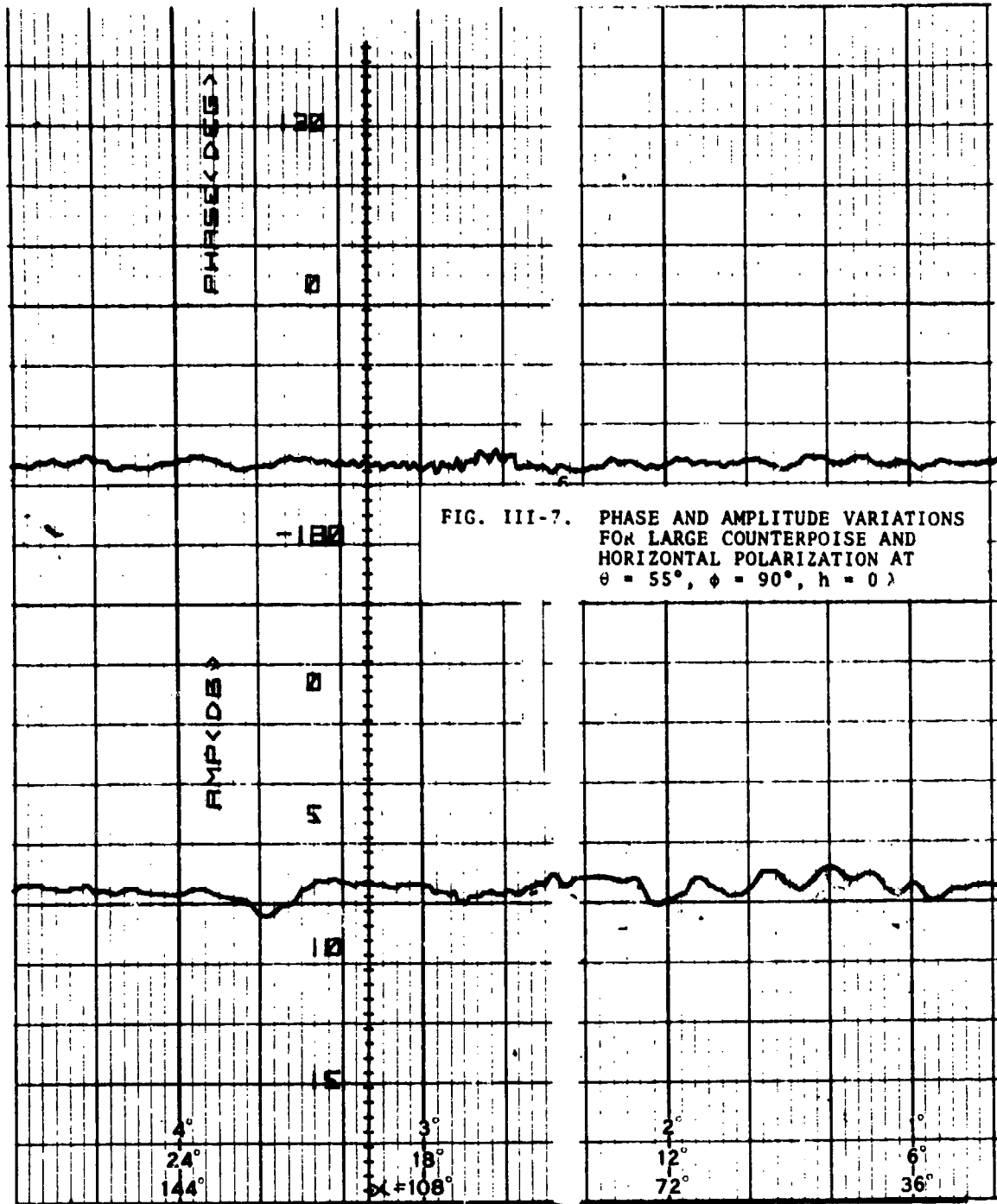


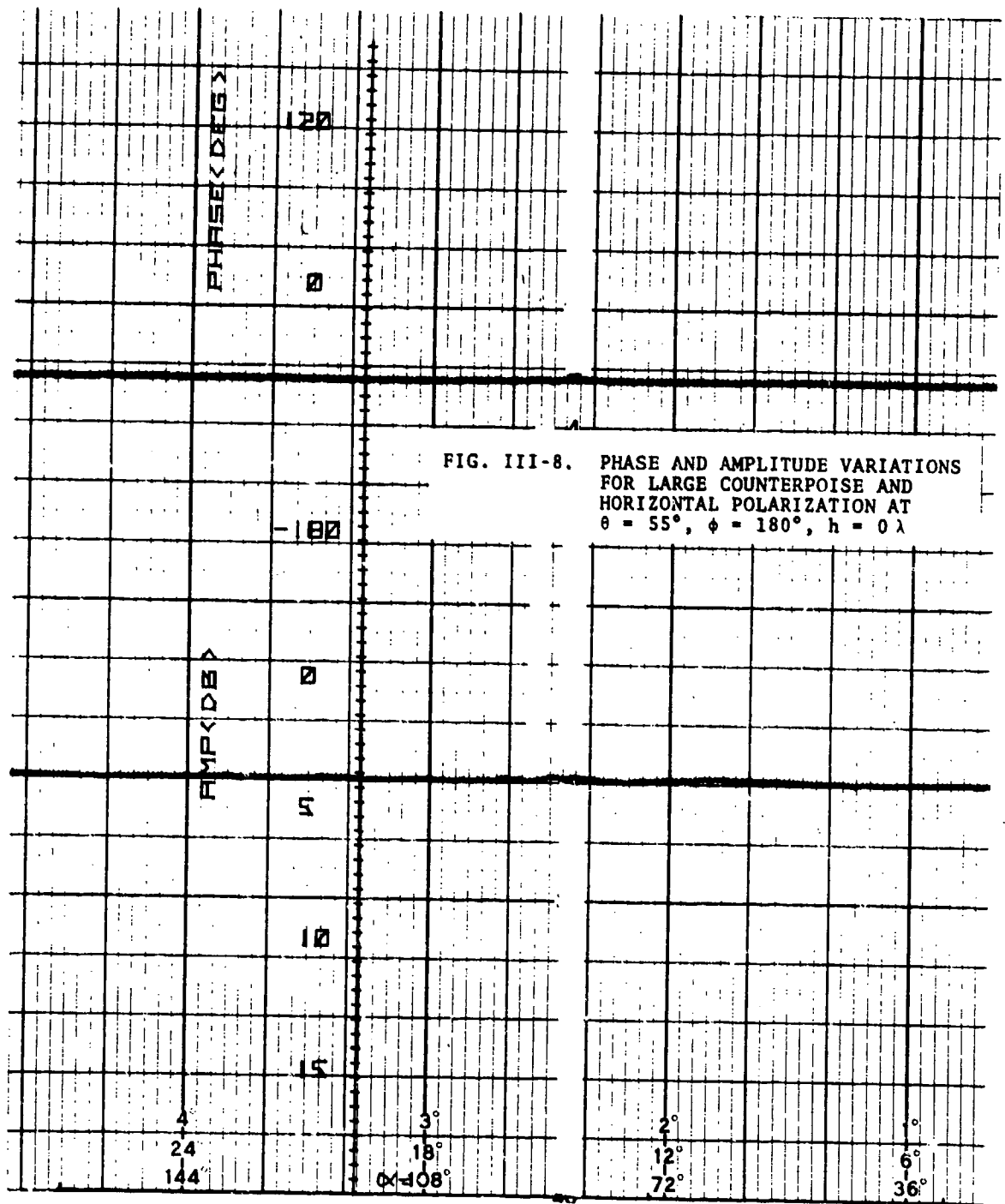
FIG. III-2. PHASE AND AMPLITUDE VARIATIONS FOR LARGE COUNTERPOISE AND HORIZONTAL POLARIZATION AT $\theta = 55^\circ$, $\phi = 0^\circ$, $h = 1 \lambda$

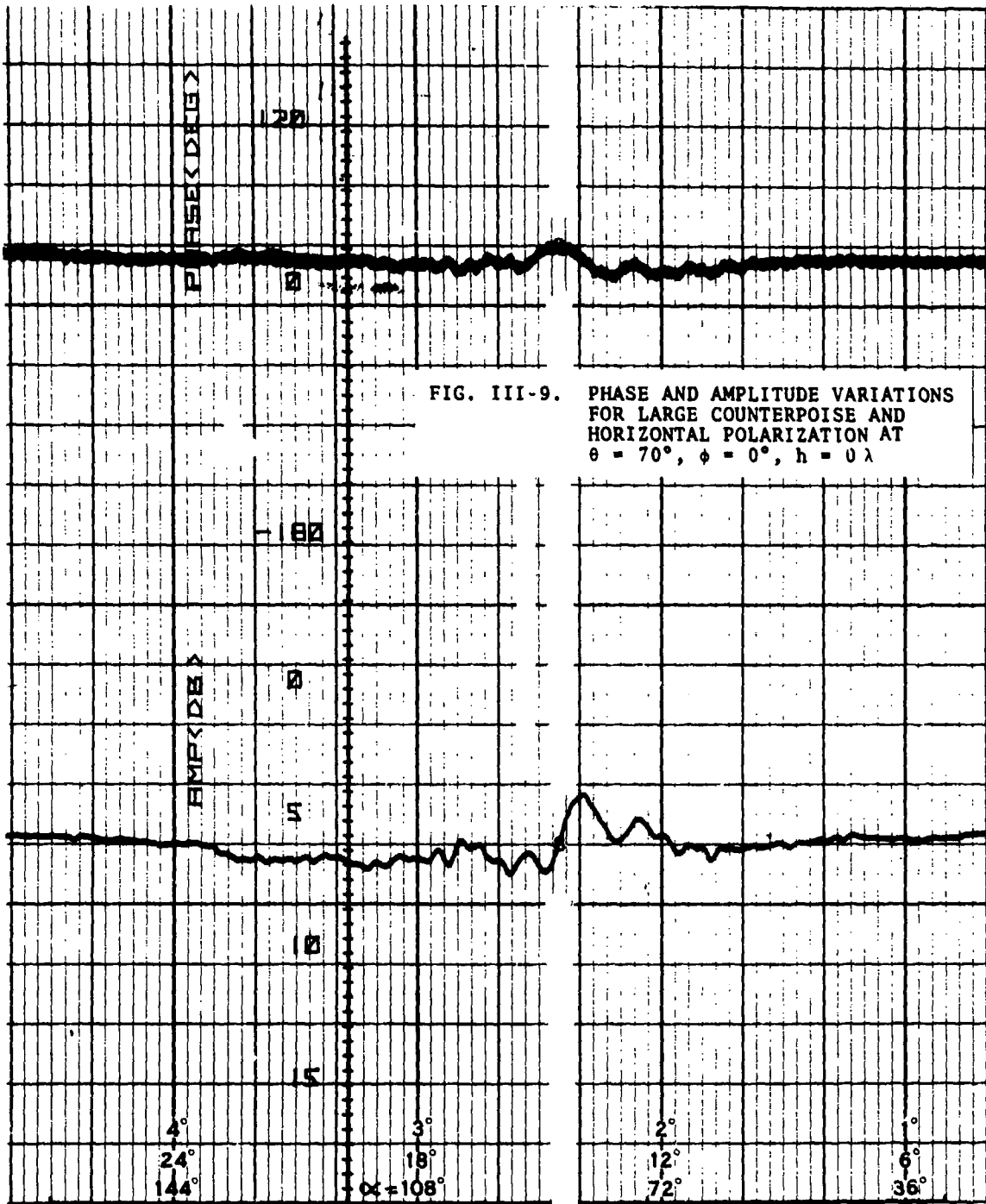


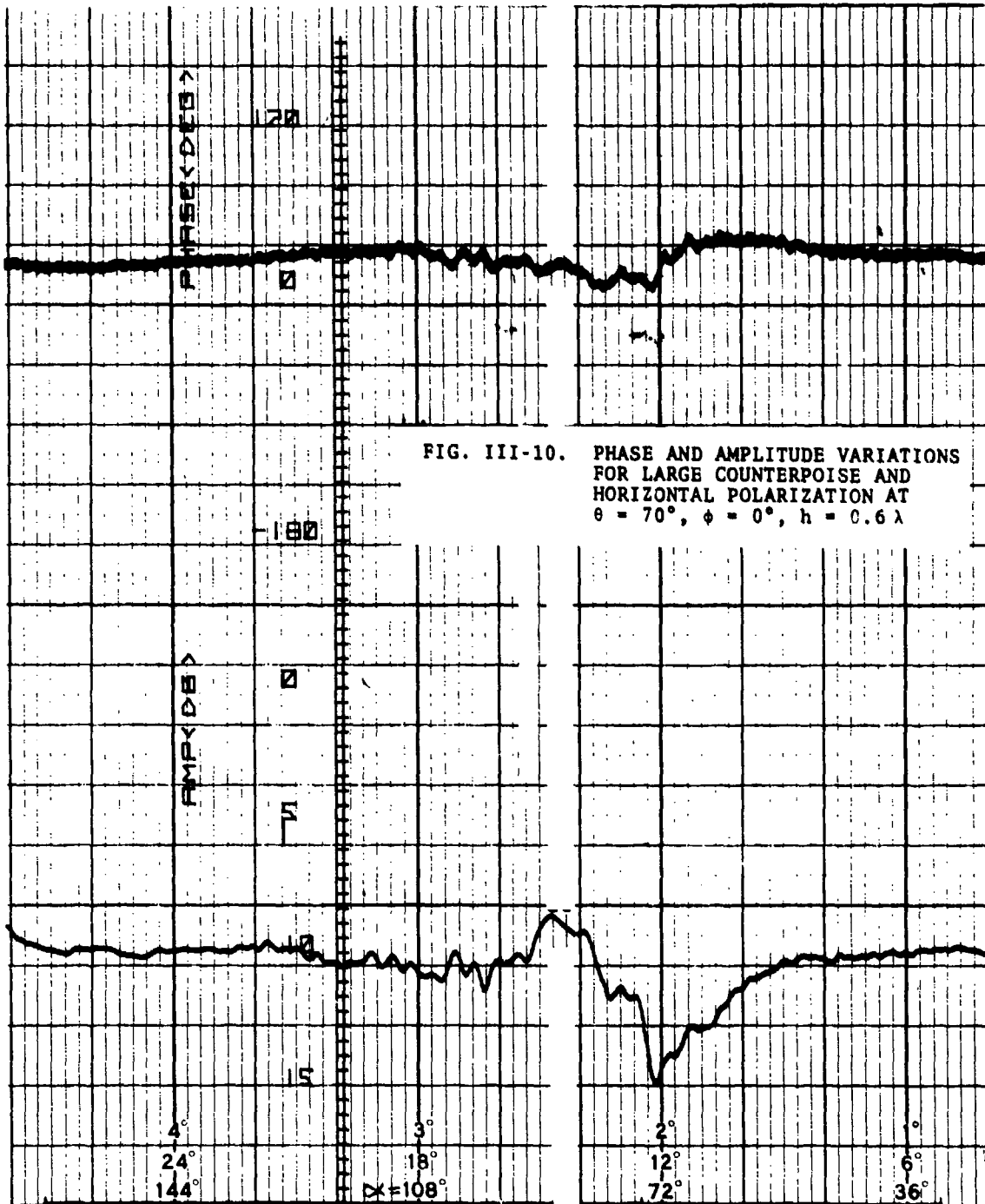


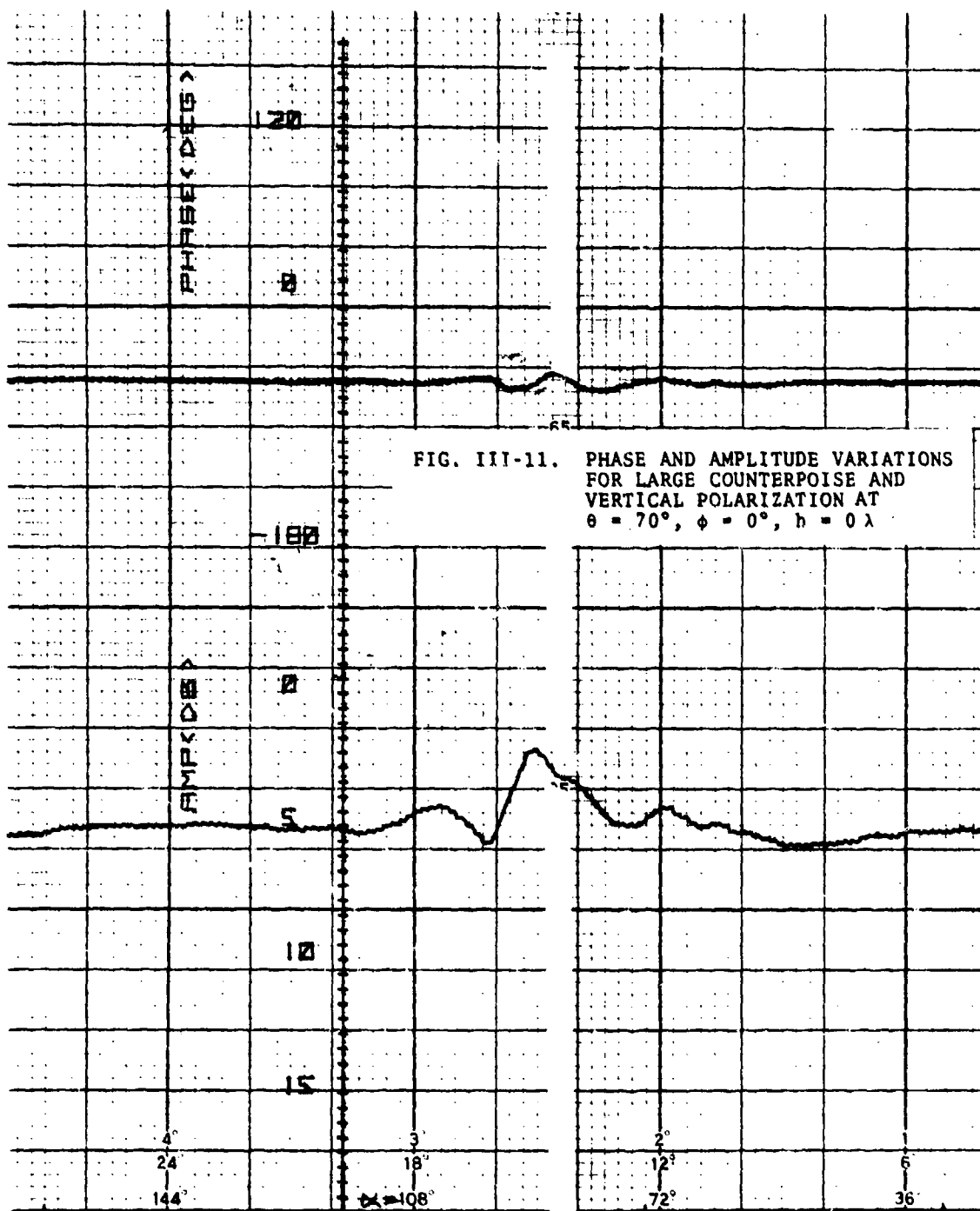












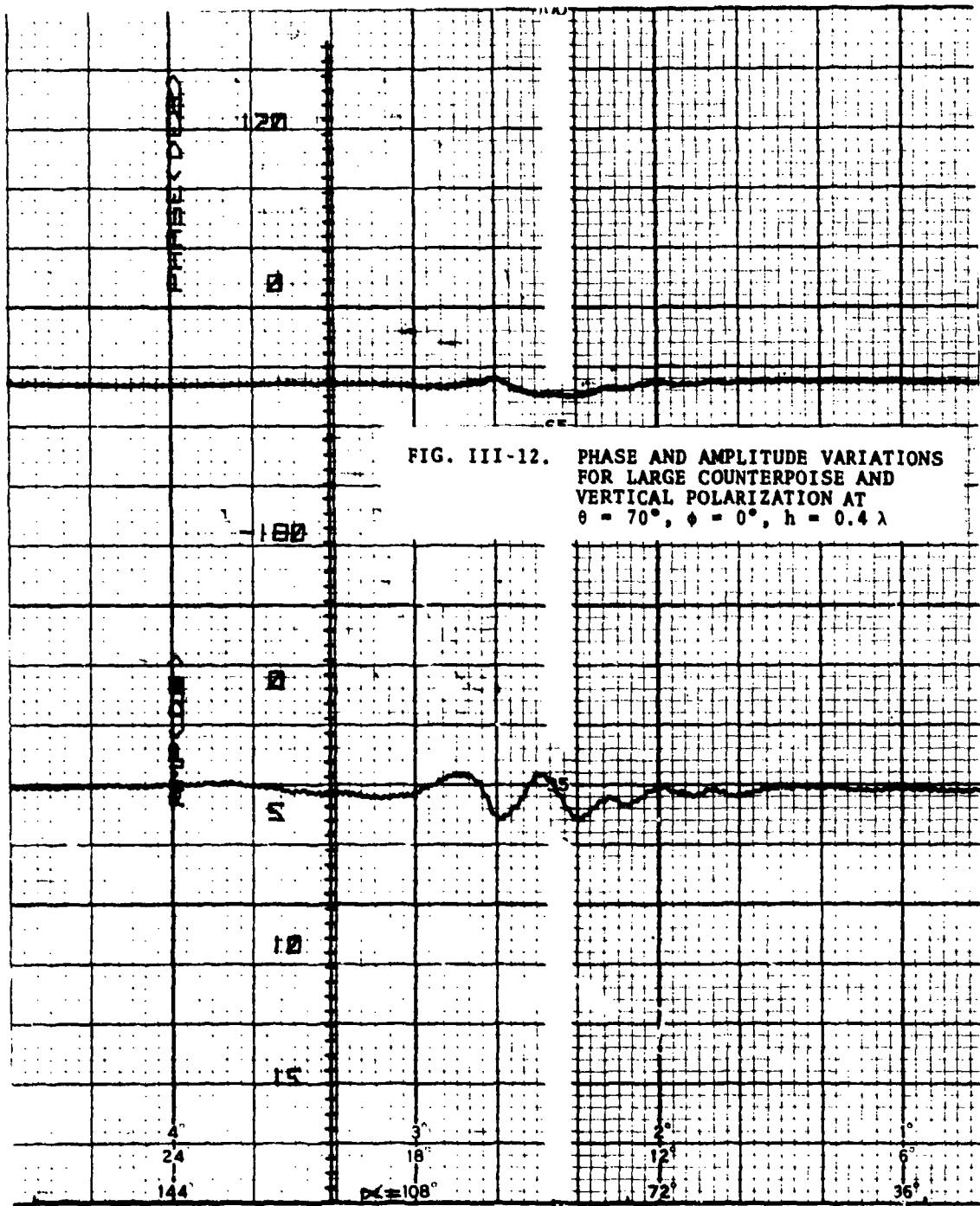
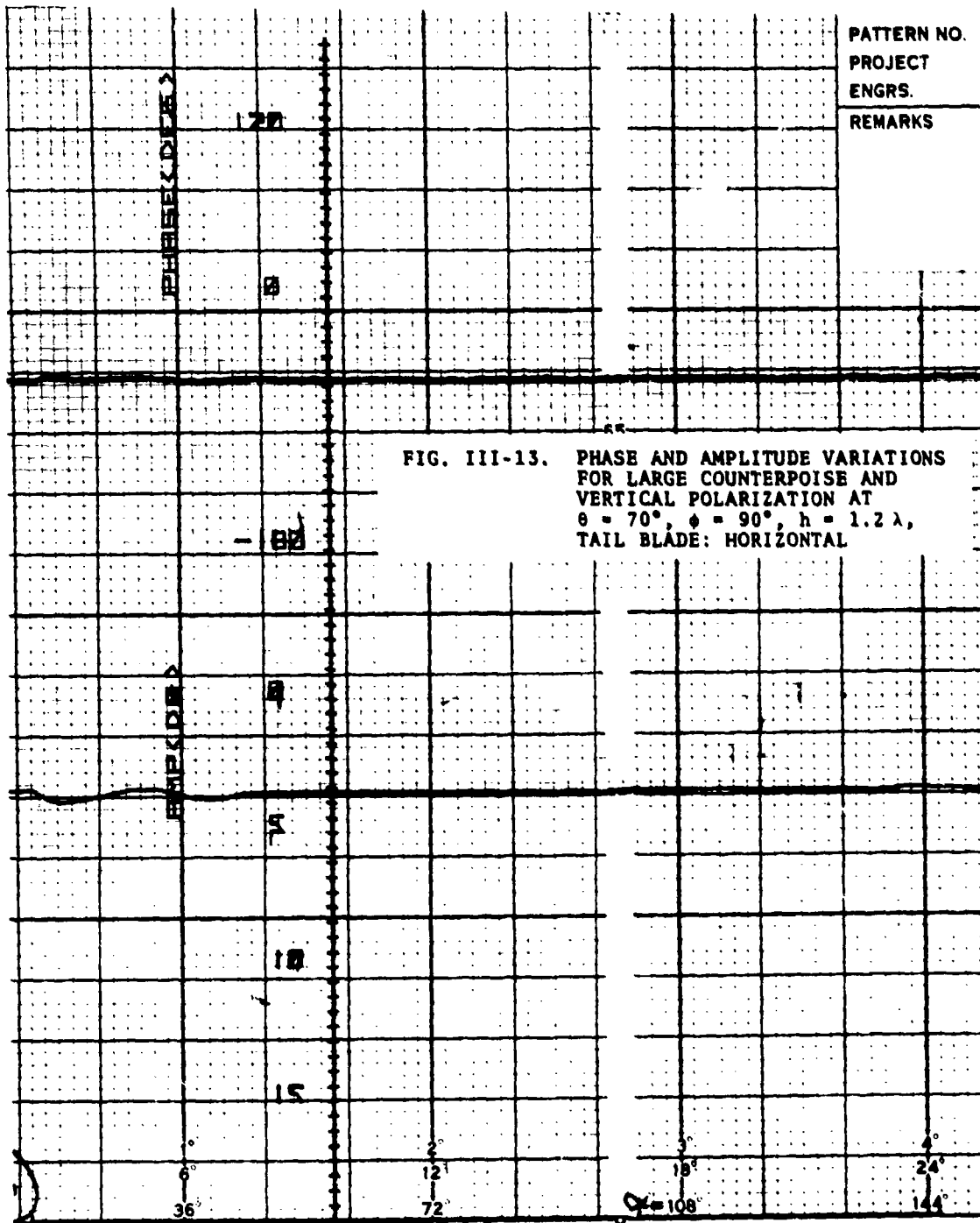
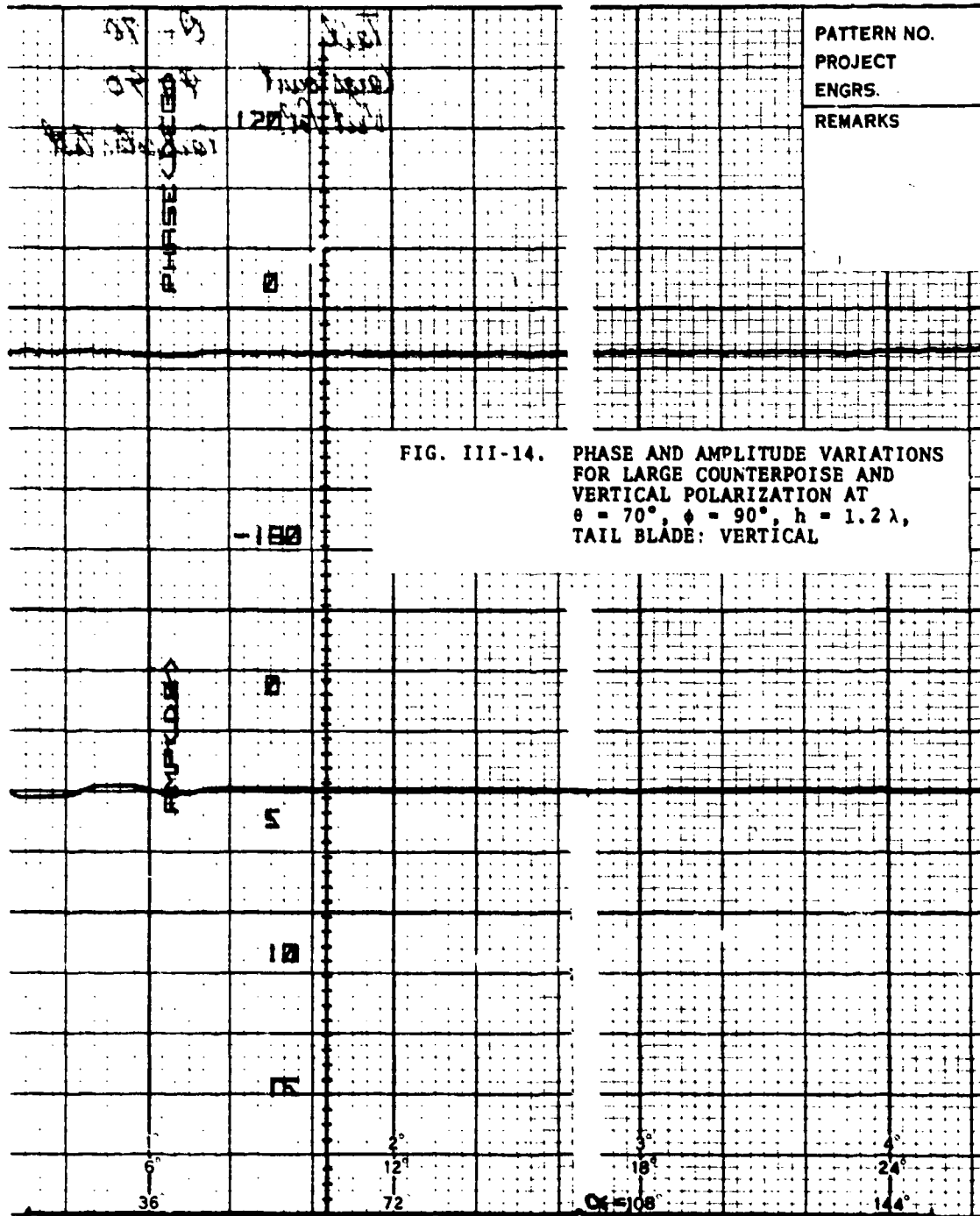
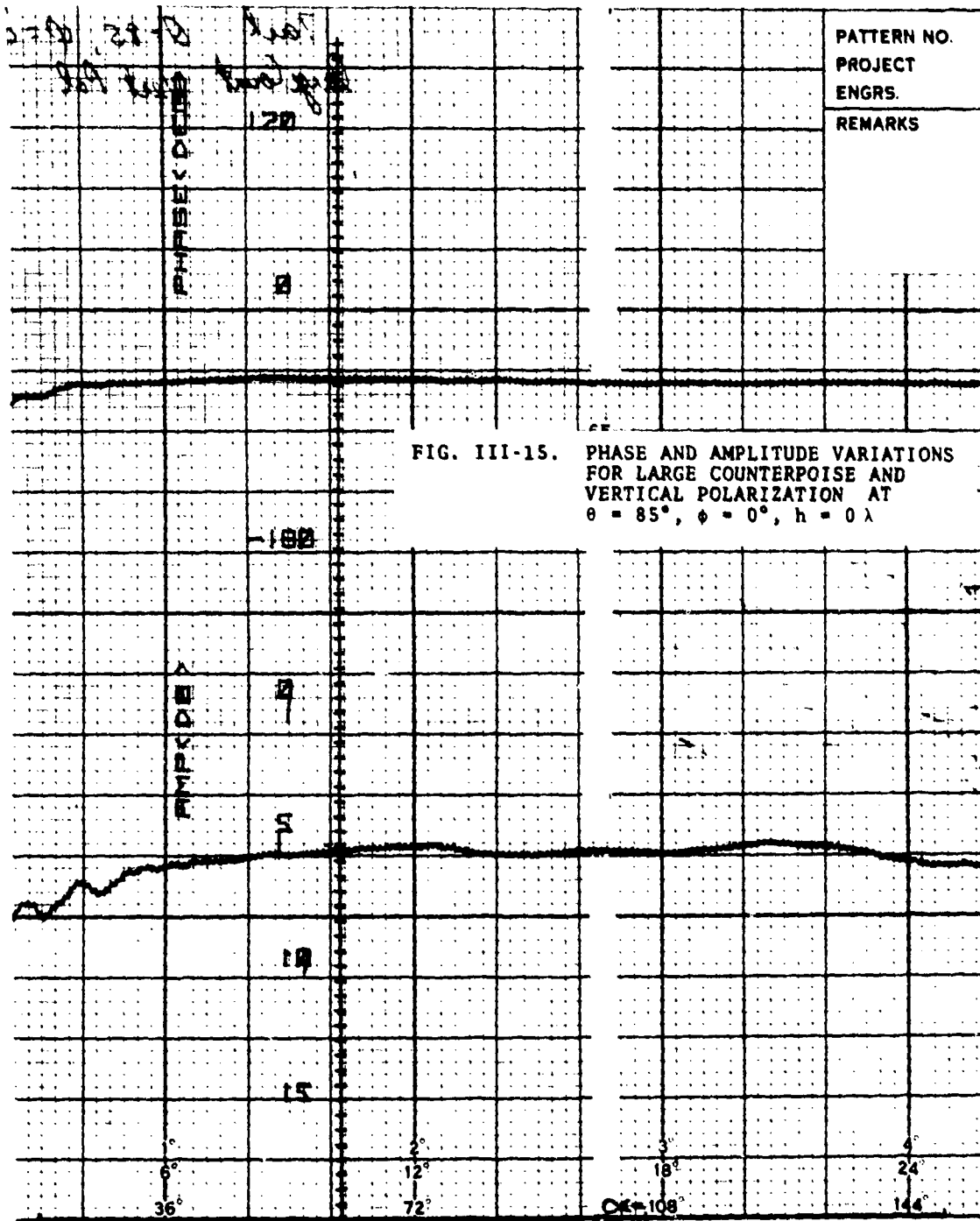
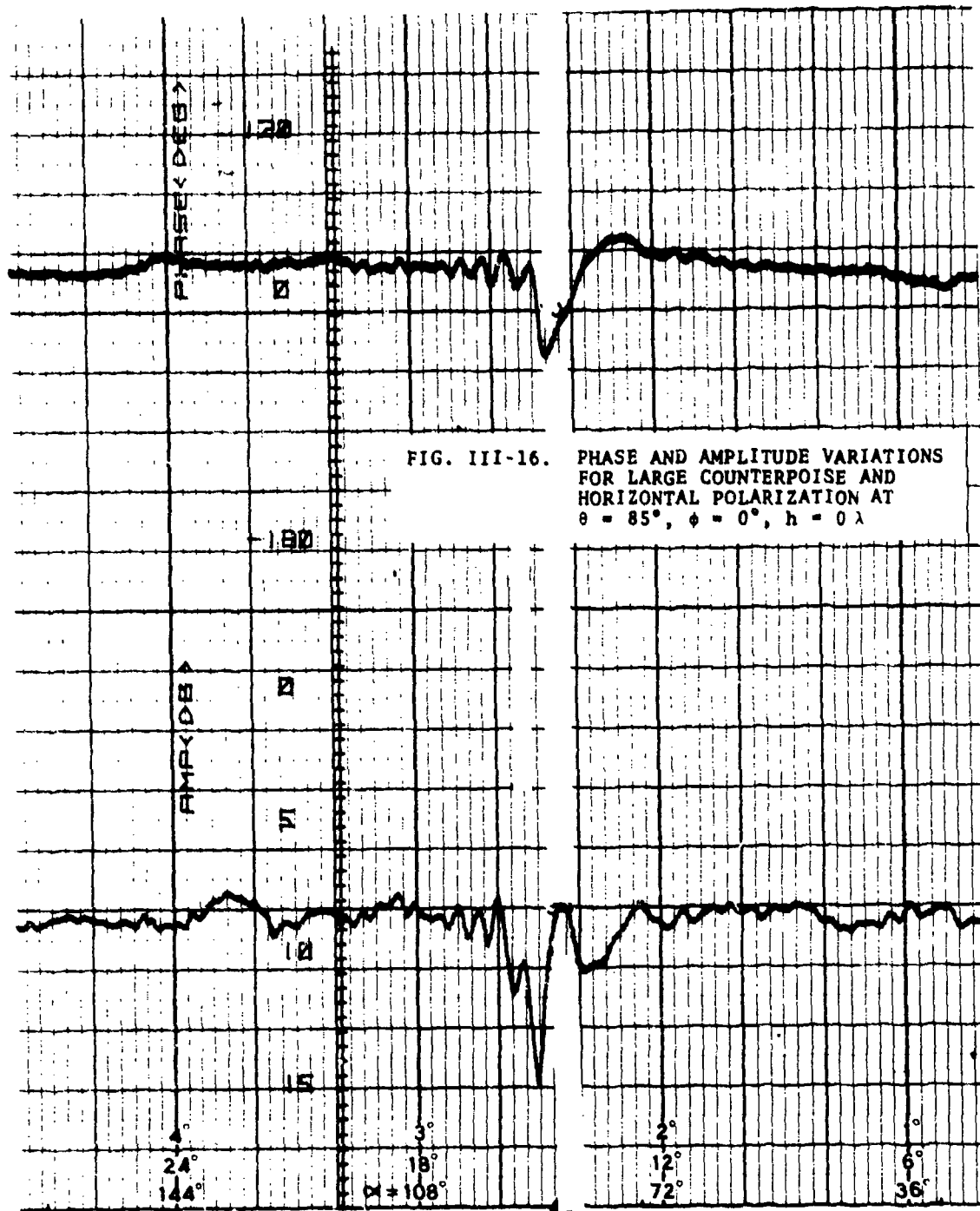


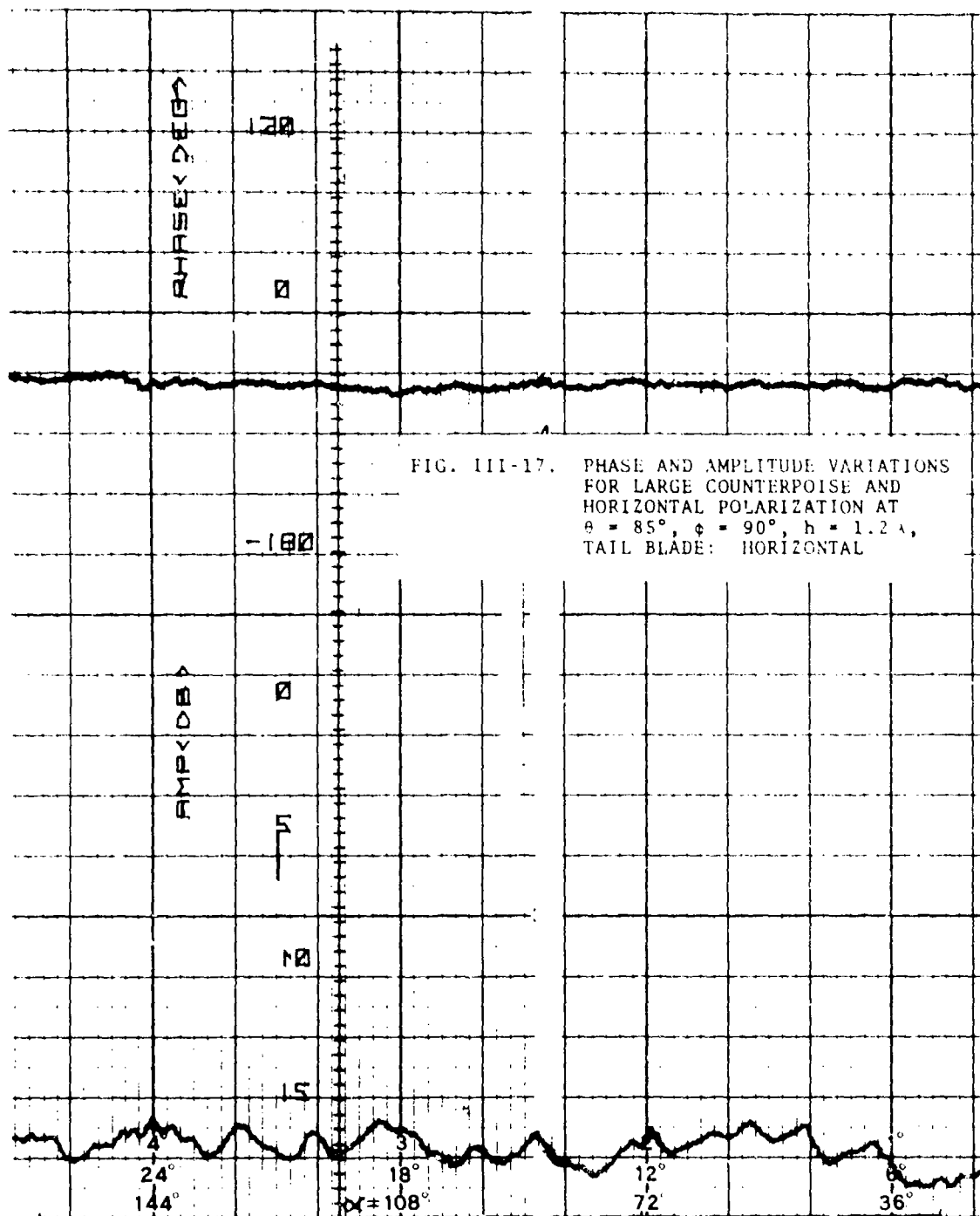
FIG. III-12. PHASE AND AMPLITUDE VARIATIONS FOR LARGE COUNTERPOISE AND VERTICAL POLARIZATION AT $\theta = 70^\circ$, $\phi = 0^\circ$, $h = 0.4 \lambda$











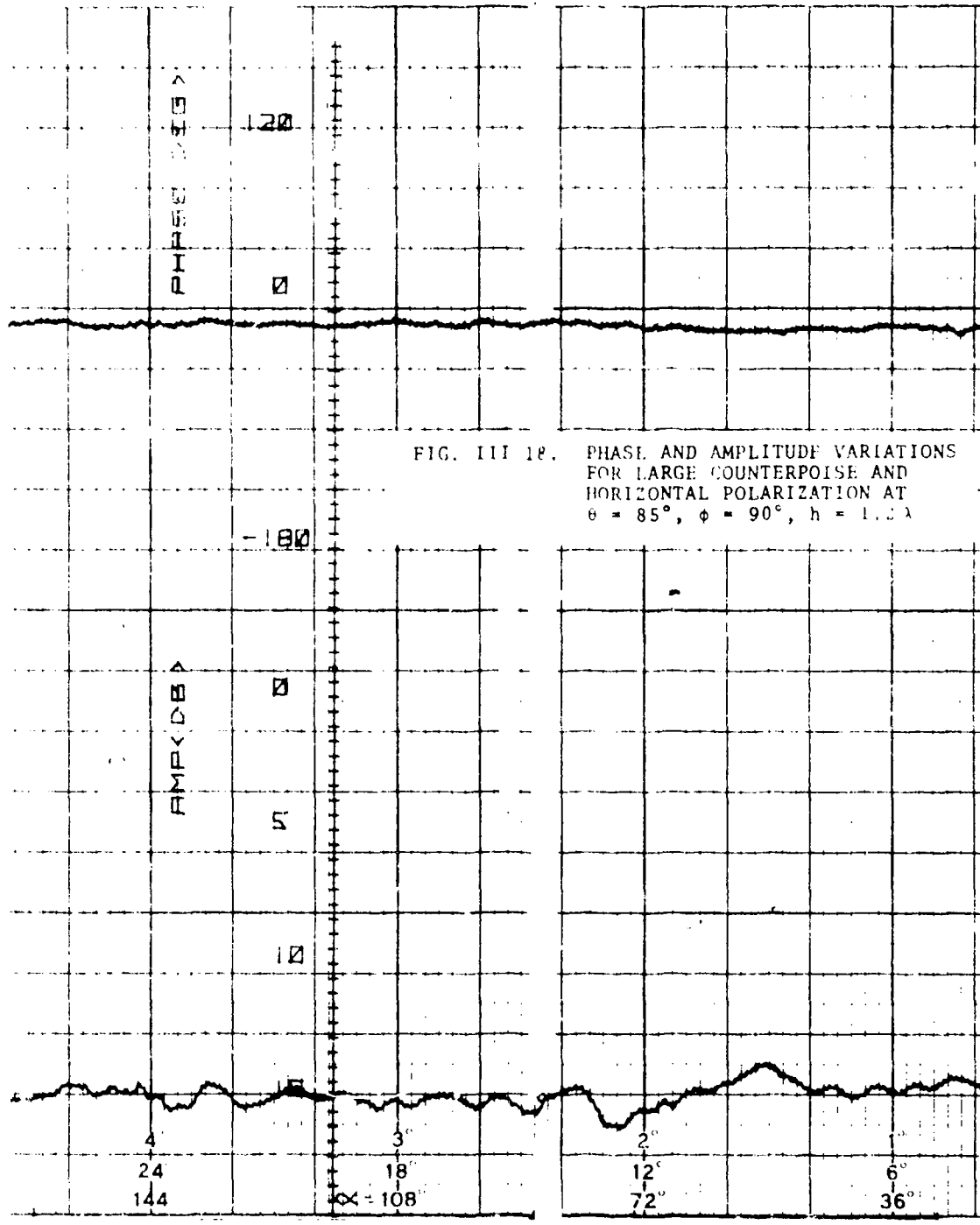
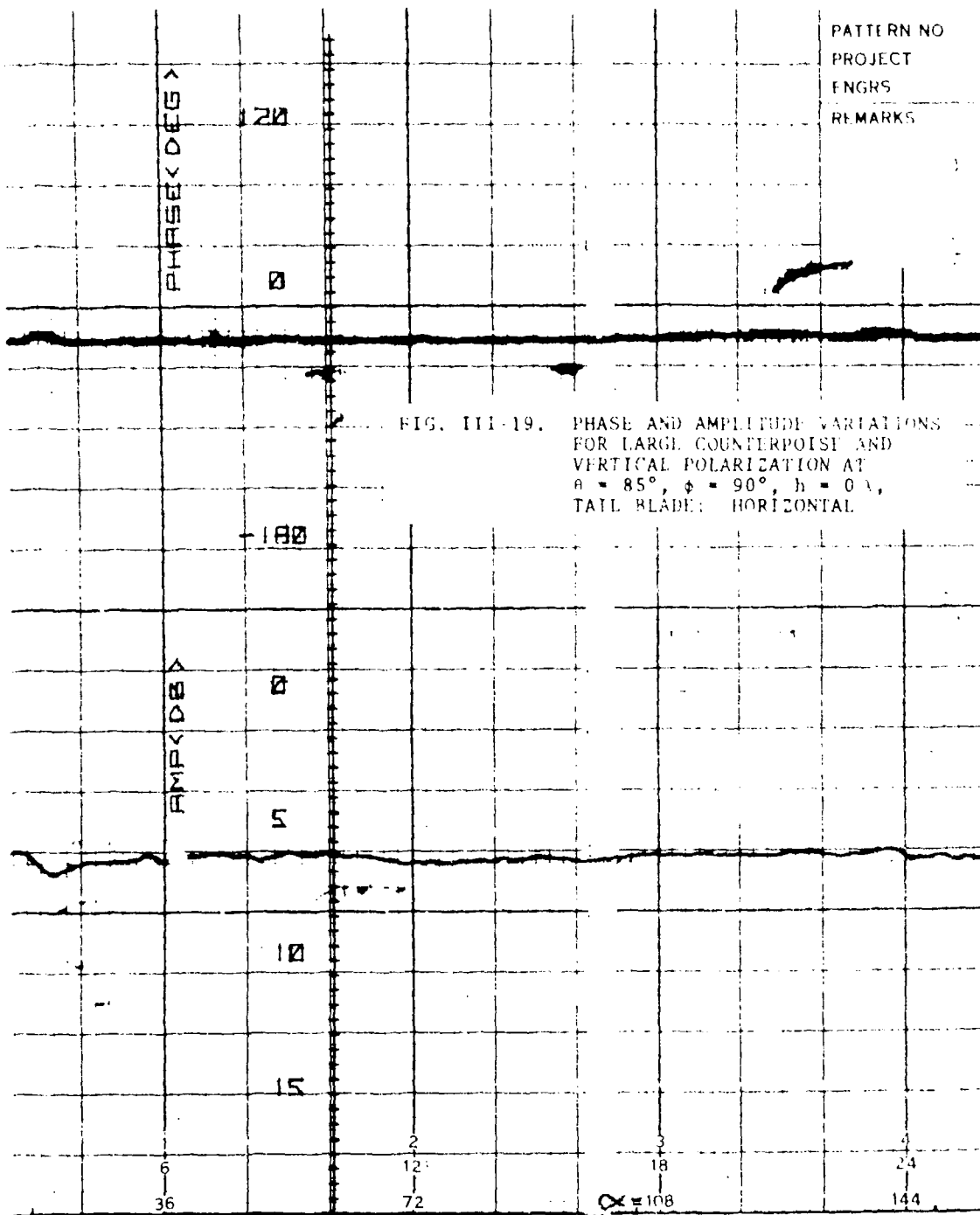
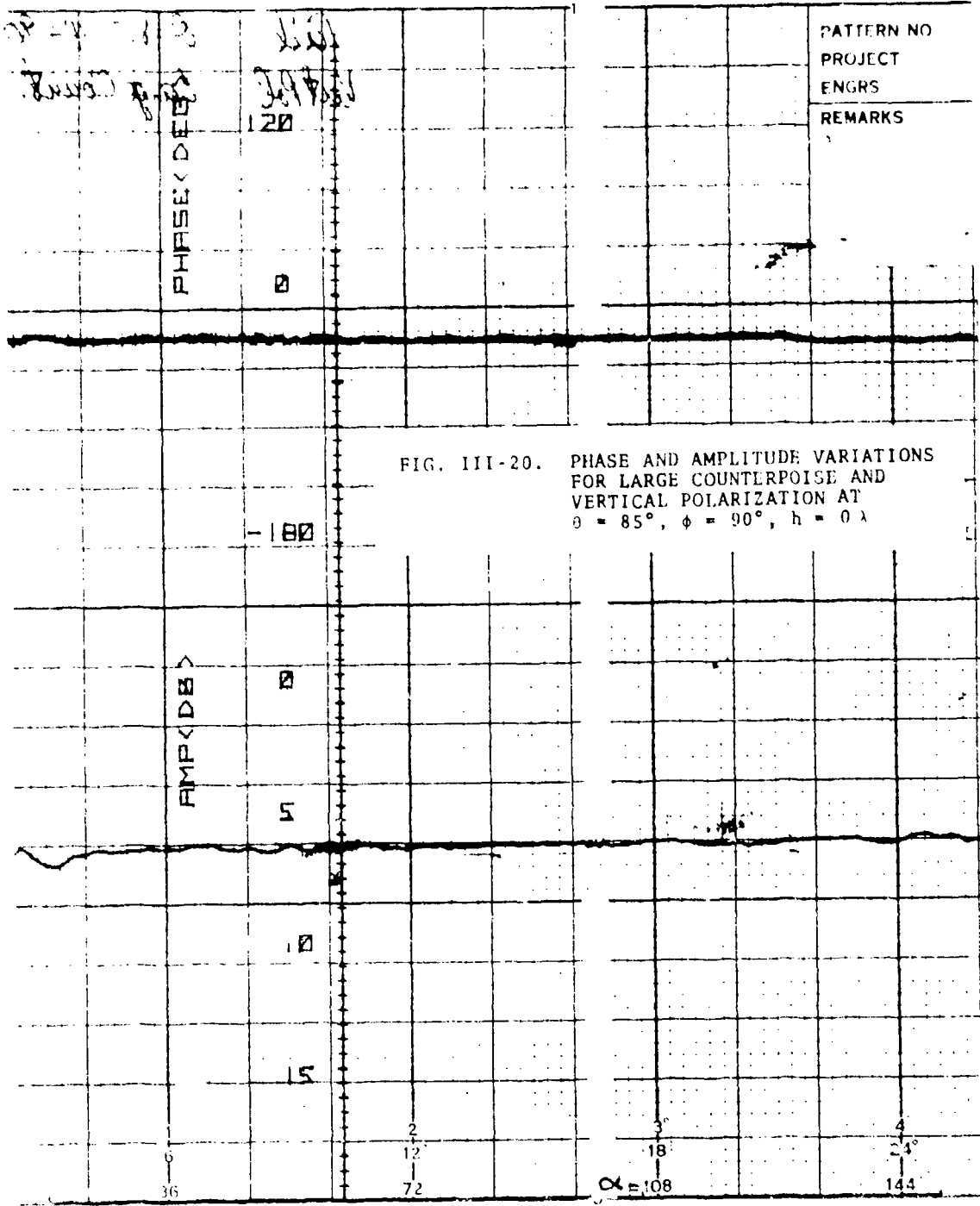
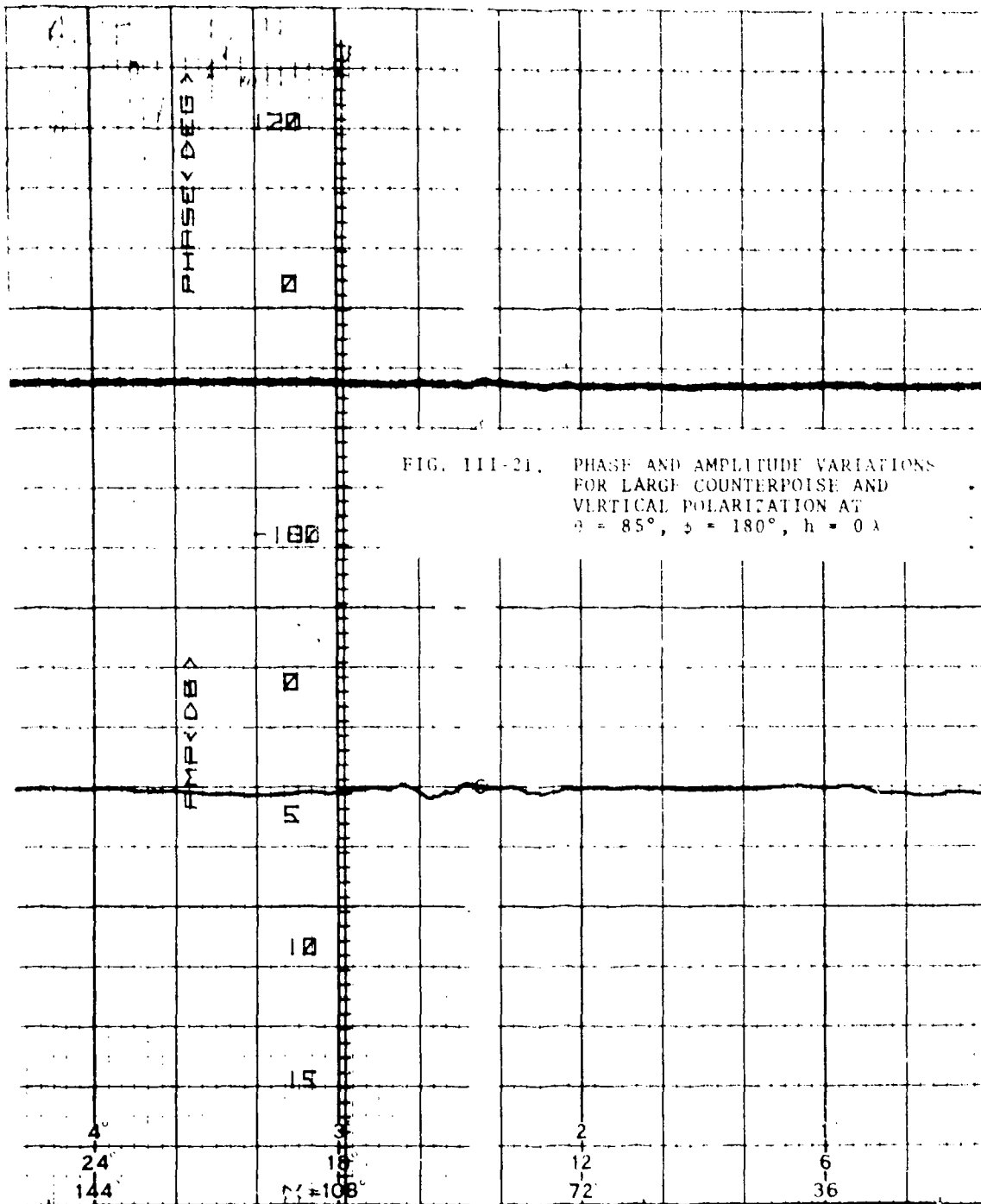


FIG. III 12. PHASE AND AMPLITUDE VARIATIONS FOR LARGE COUNTERPOISE AND HORIZONTAL POLARIZATION AT $\theta = 85^\circ$, $\phi = 90^\circ$, $h = 1.0 \lambda$







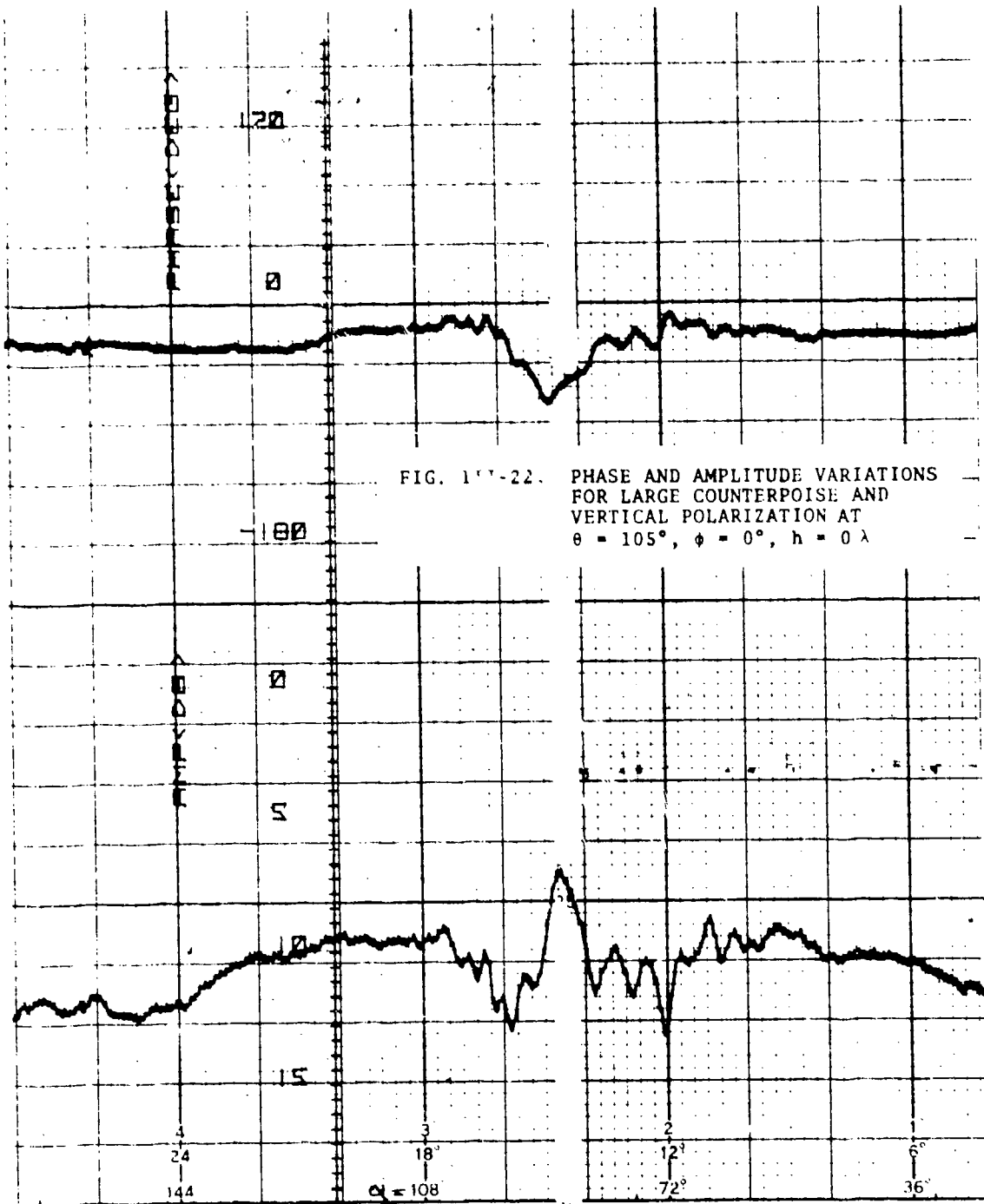
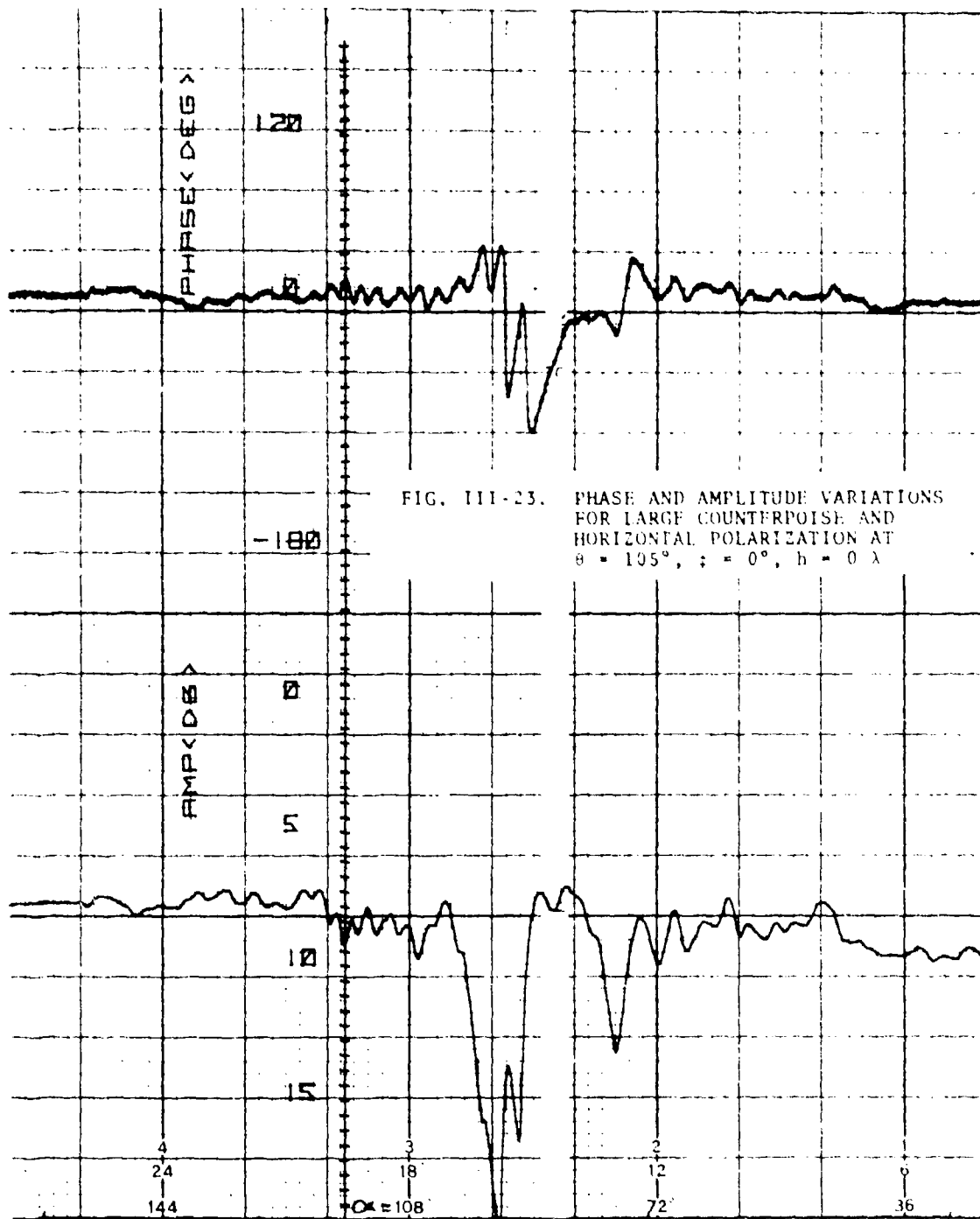
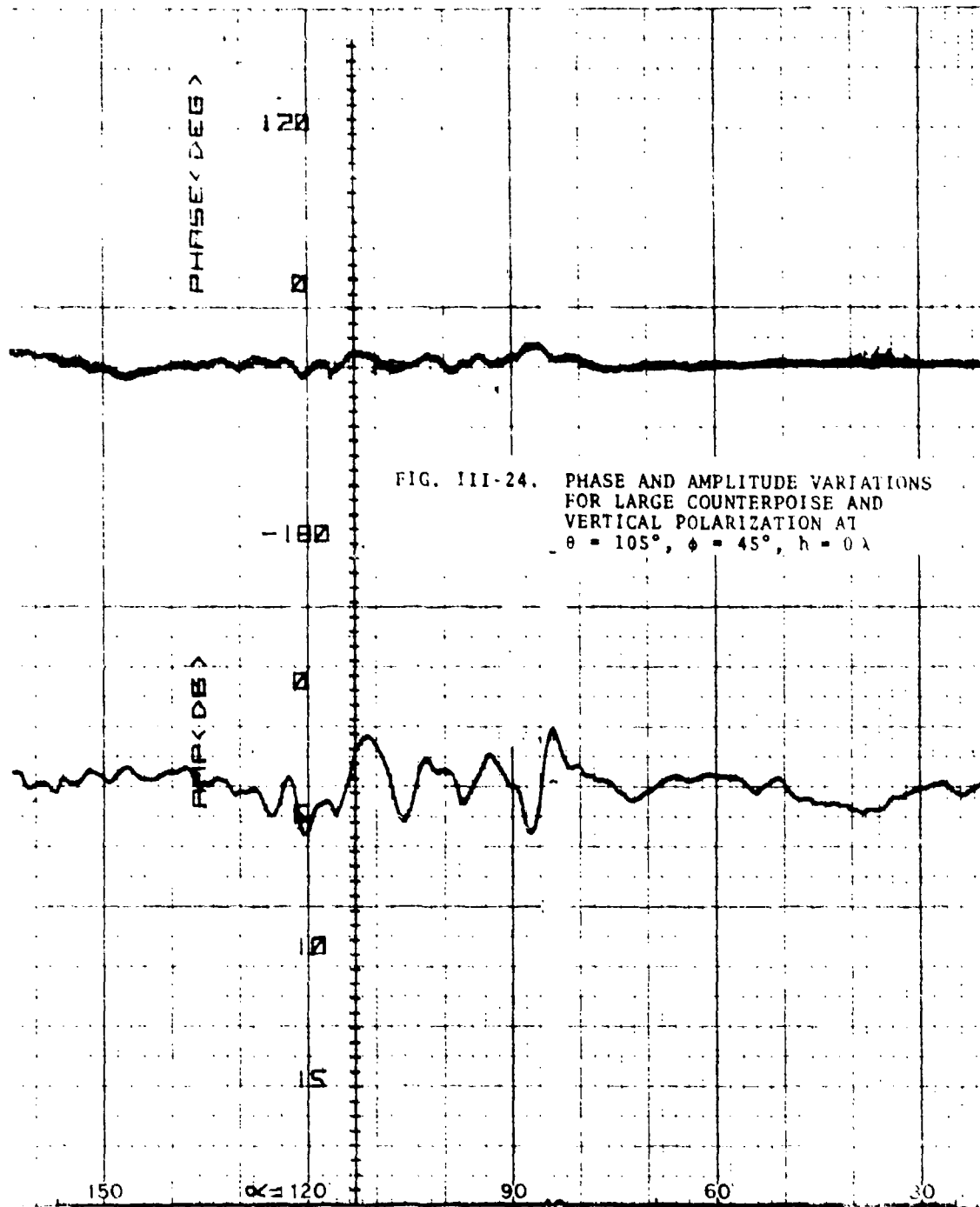


FIG. 1¹¹-22. PHASE AND AMPLITUDE VARIATIONS FOR LARGE COUNTERPOISE AND VERTICAL POLARIZATION AT $\theta = 105^\circ$, $\phi = 0^\circ$, $h = 0\lambda$





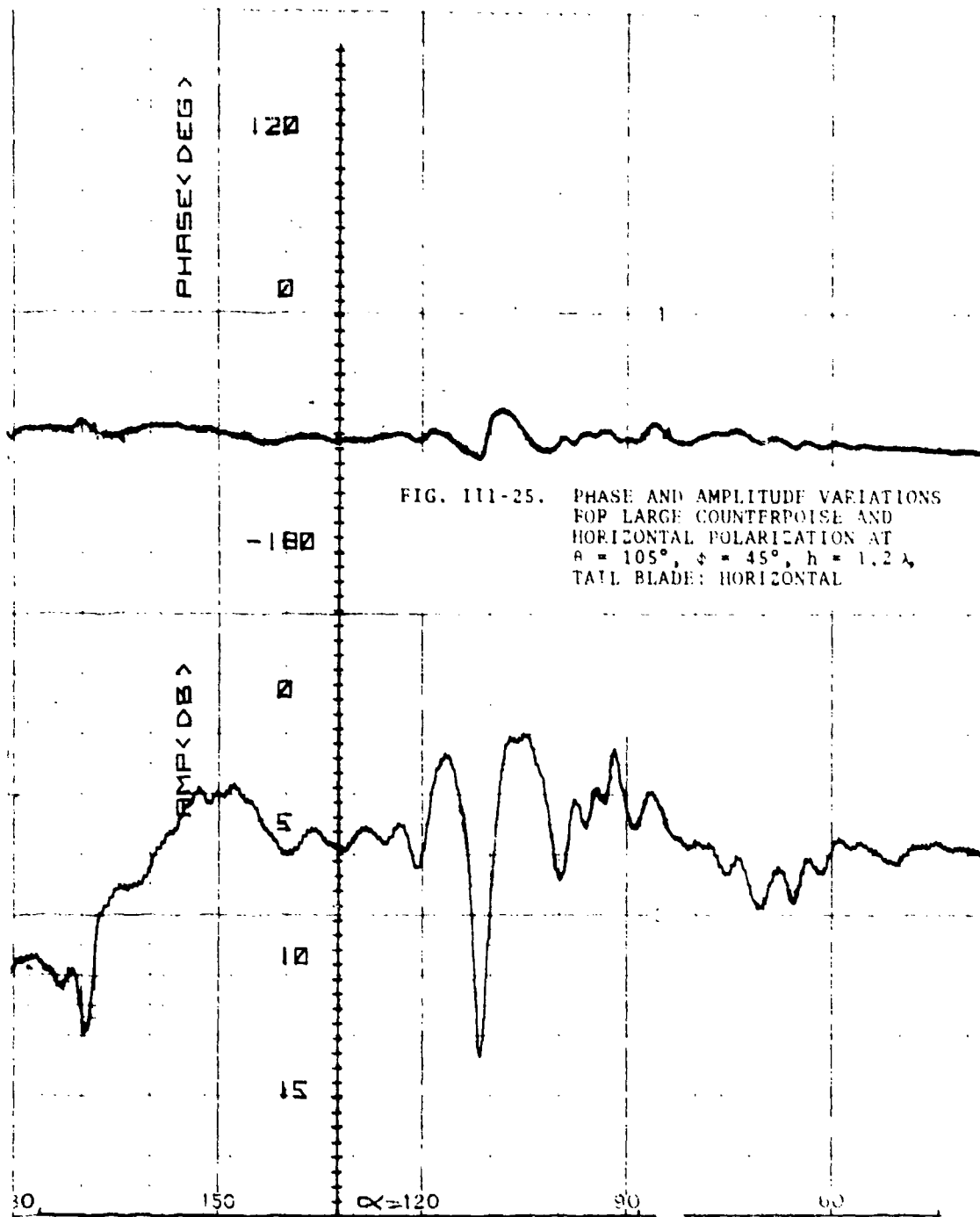
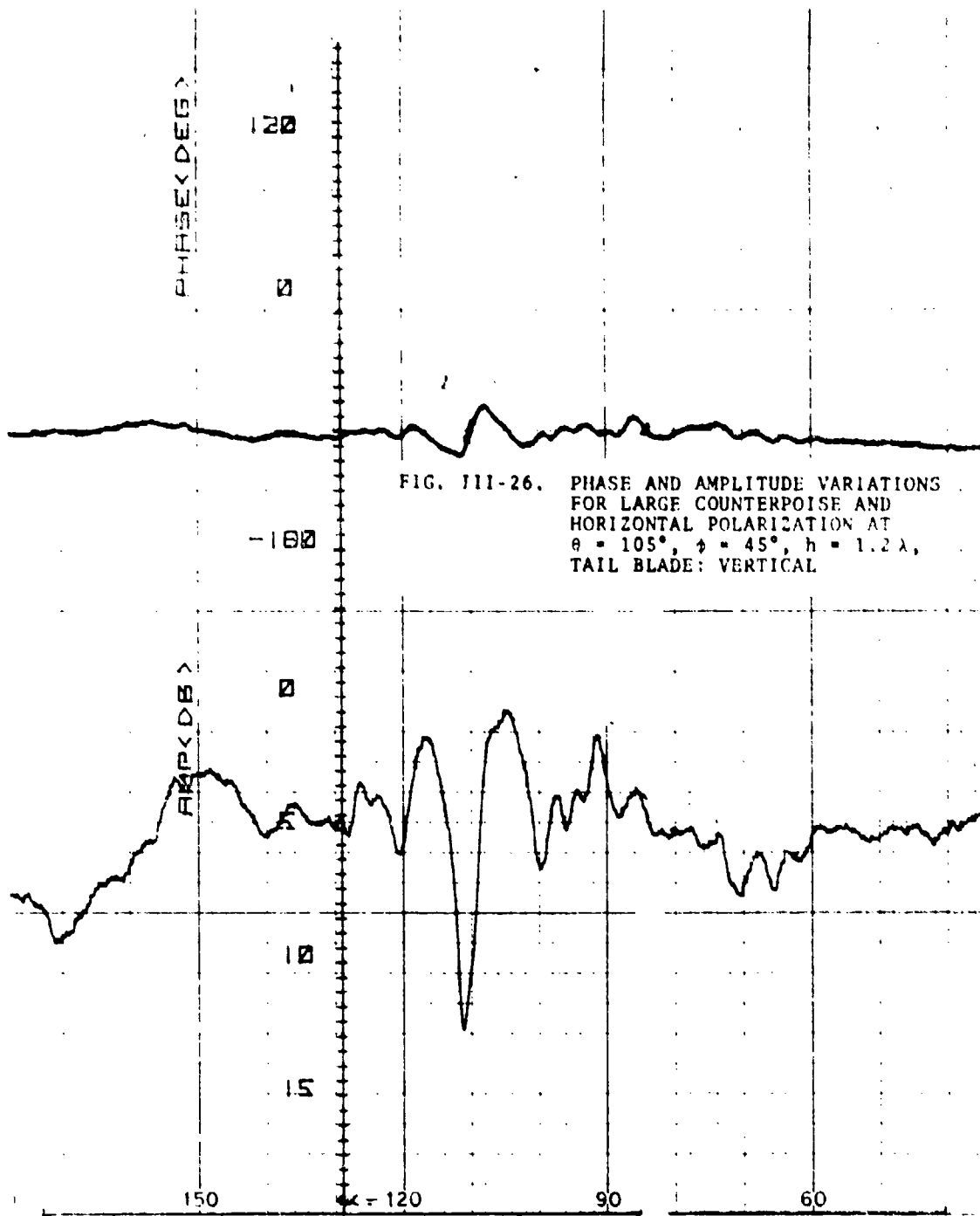
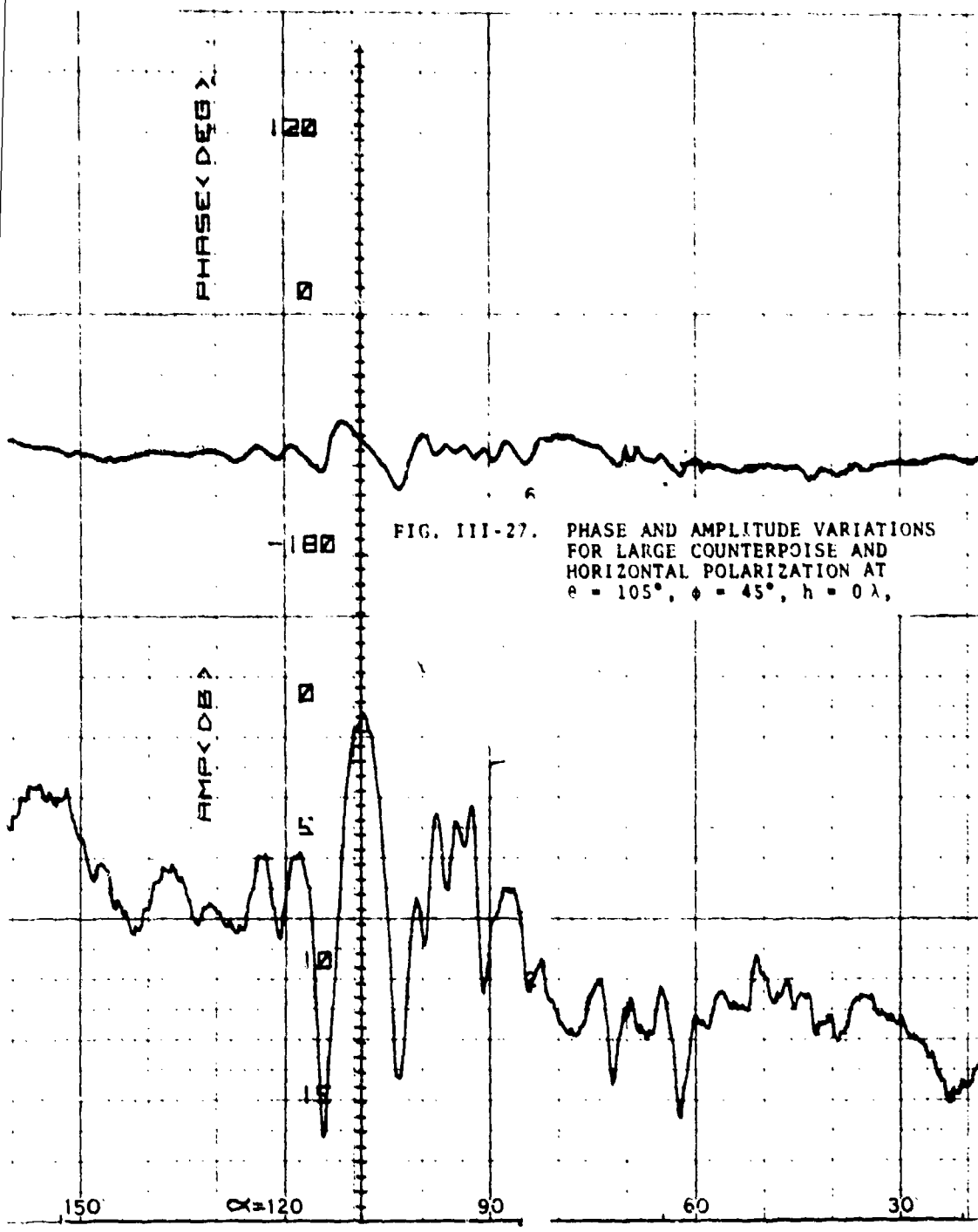


FIG. III-25. PHASE AND AMPLITUDE VARIATIONS FOR LARGE COUNTERPOISE AND HORIZONTAL POLARIZATION AT $\alpha = 105^\circ$, $\phi = 45^\circ$, $h = 1.2 \lambda$, TAIL BLADE: HORIZONTAL





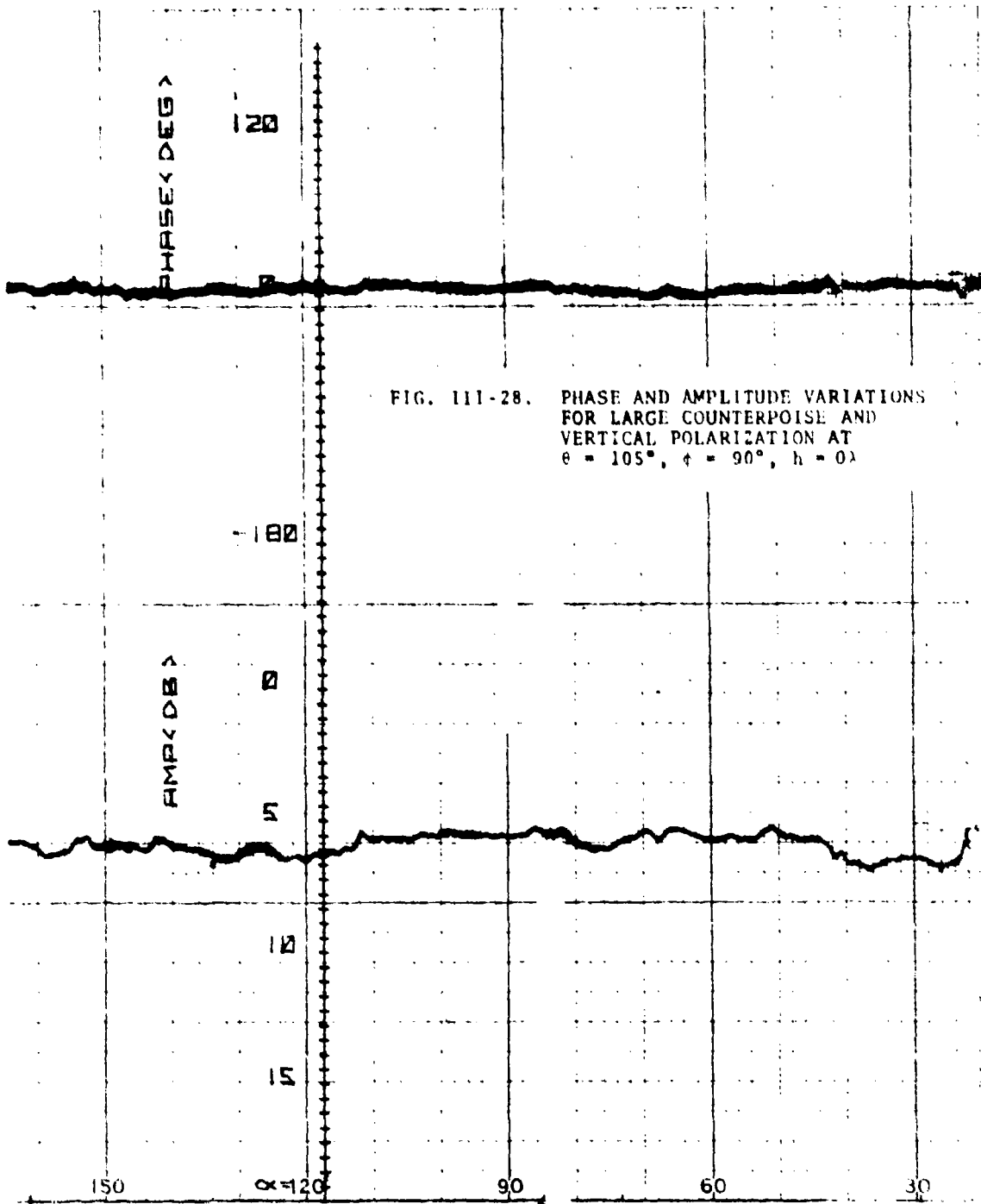
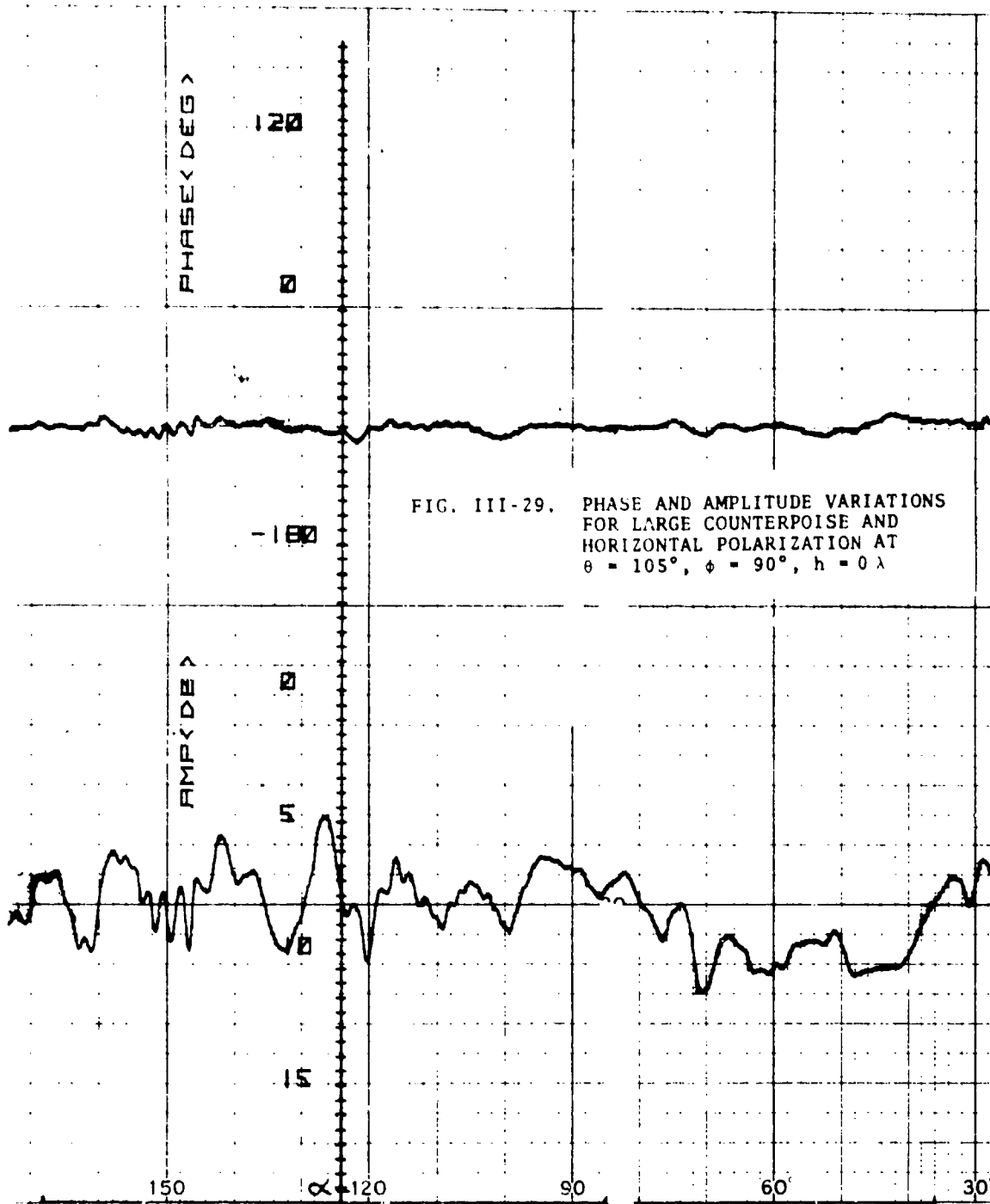
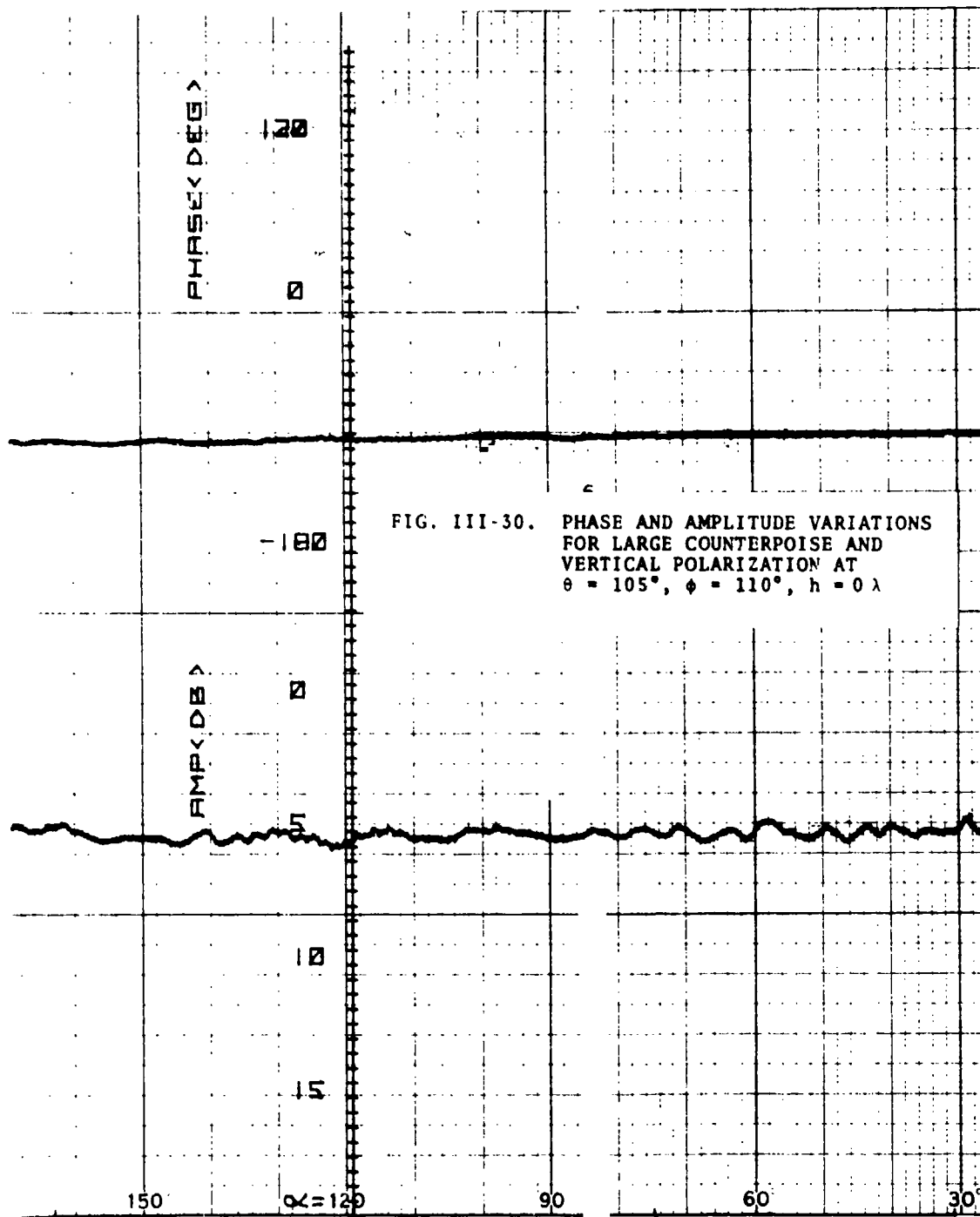
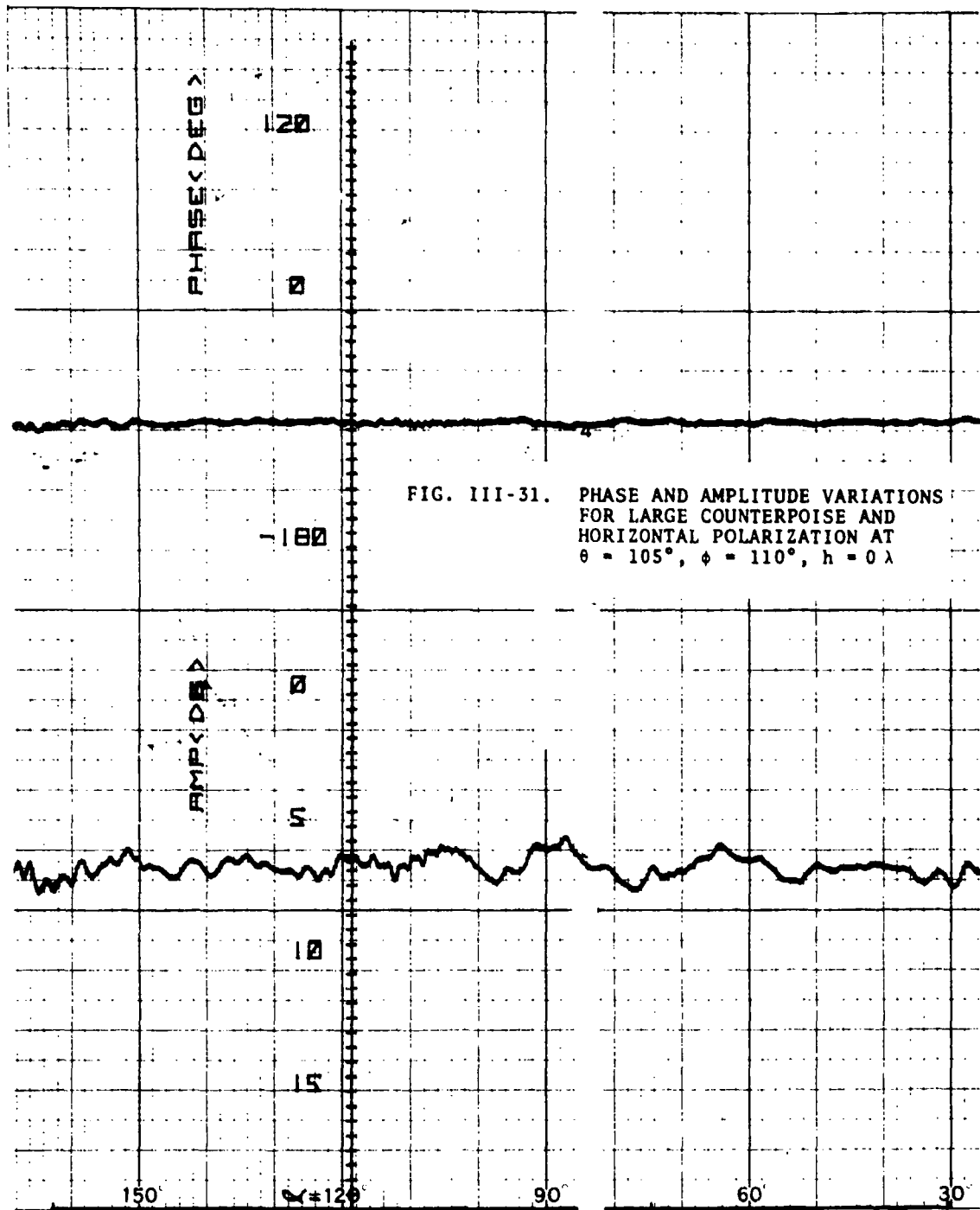


FIG. 111-28. PHASE AND AMPLITUDE VARIATIONS FOR LARGE COUNTERPOISE AND VERTICAL POLARIZATION AT $e = 105^{\circ}$, $\phi = 90^{\circ}$, $h = 0.1$







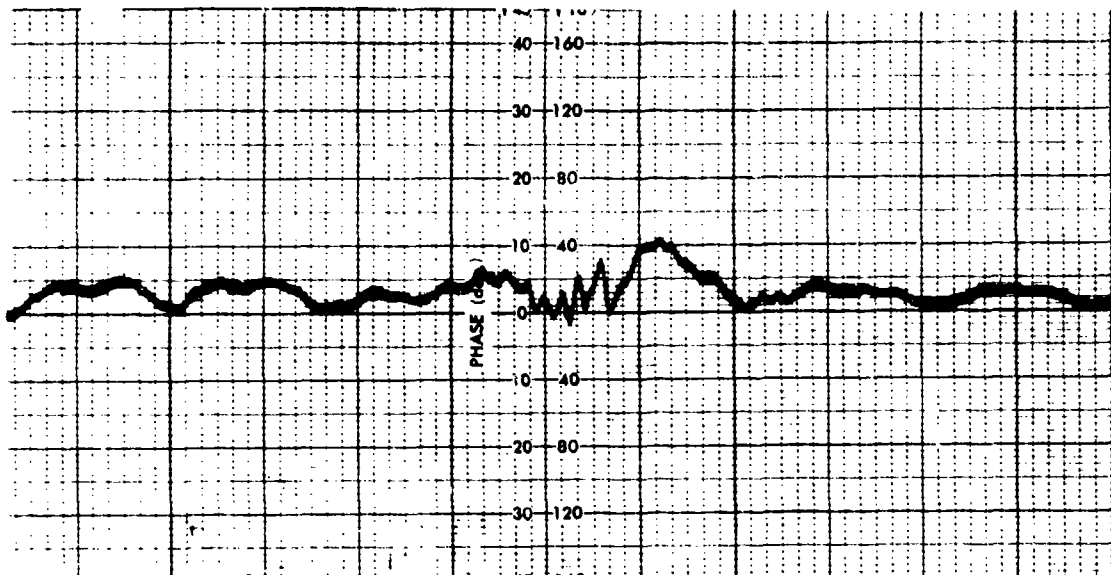
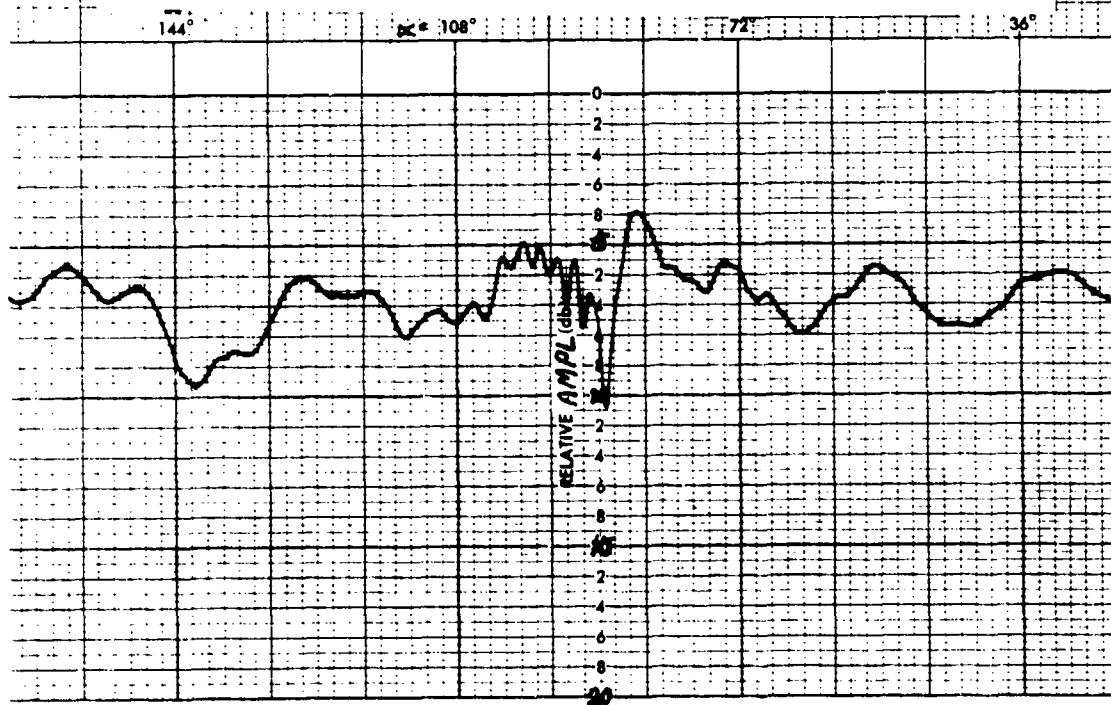


FIG. III-32. PHASE AND AMPLITUDE VARIATIONS
FOR SMALL COUNTERPOISE AND
HORIZONTAL POLARIZATION AT
 $\theta = 55^\circ$, $\phi = 45^\circ$, $h = 0 \lambda$



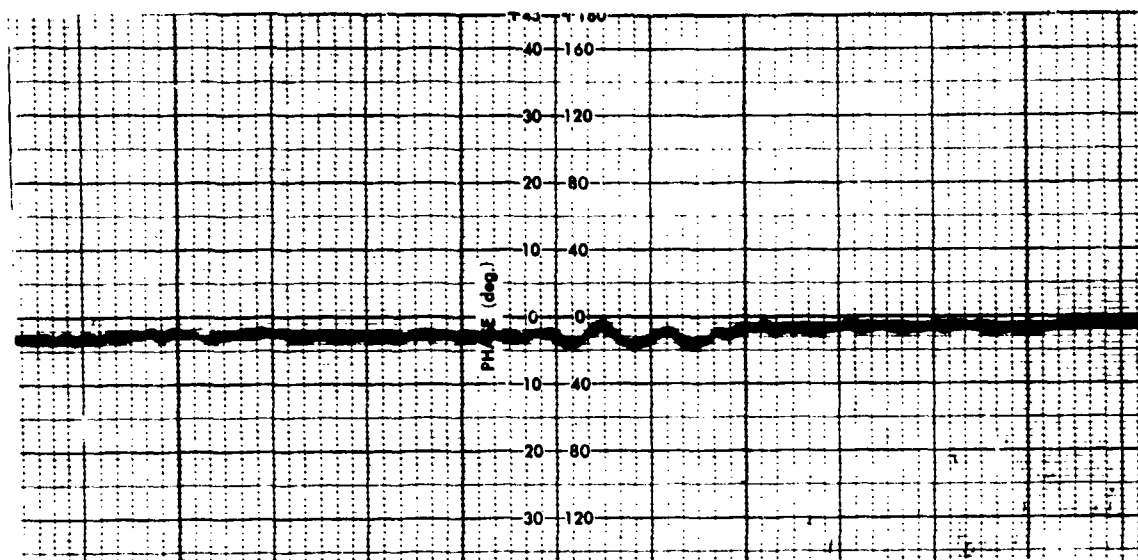
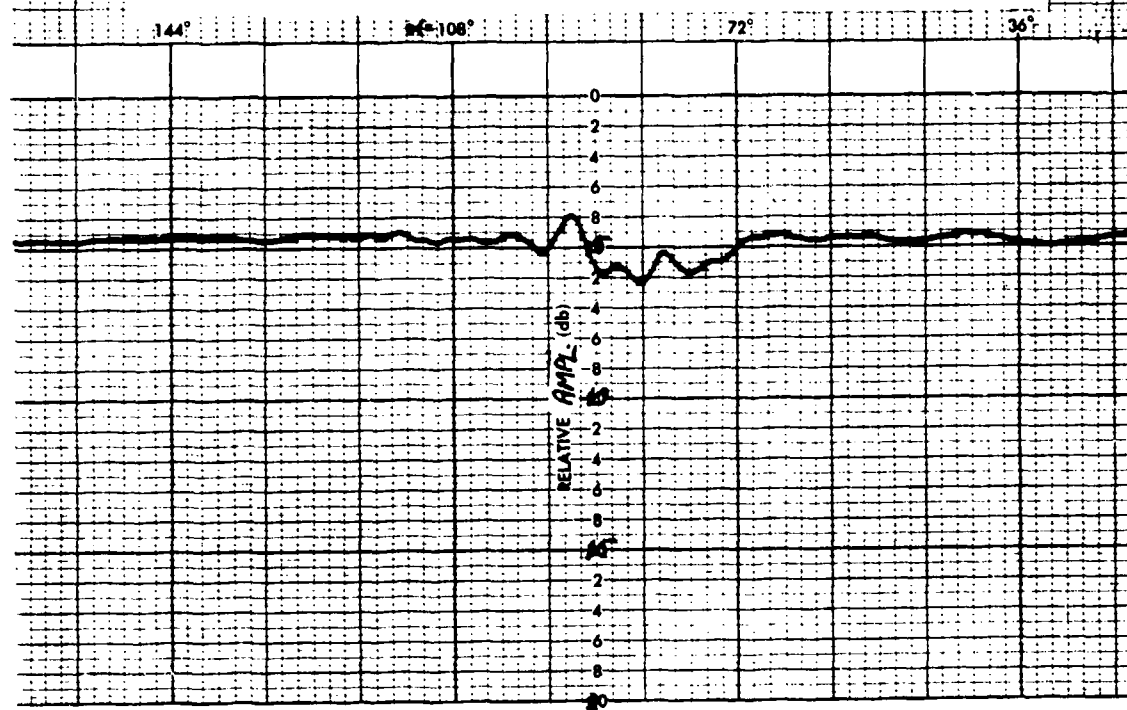


FIG. III-33. PHASE AND AMPLITUDE VARIATIONS FOR SMALL COUNTERPOISE AND VERTICAL POLARIZATION AT $\theta = 55^\circ$, $\phi = 0^\circ$, $h = 0 \lambda$



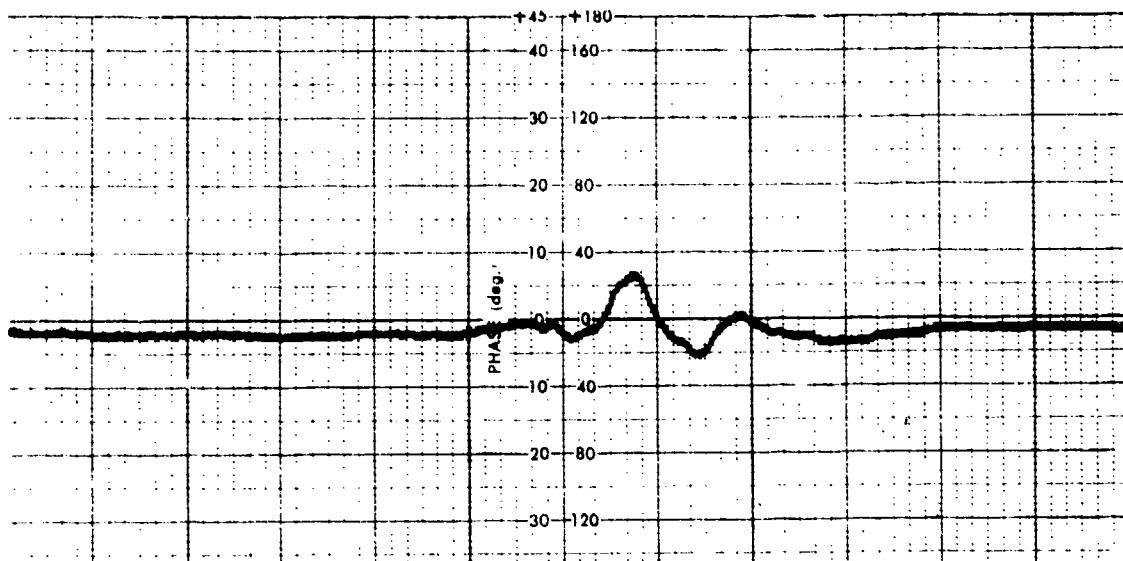
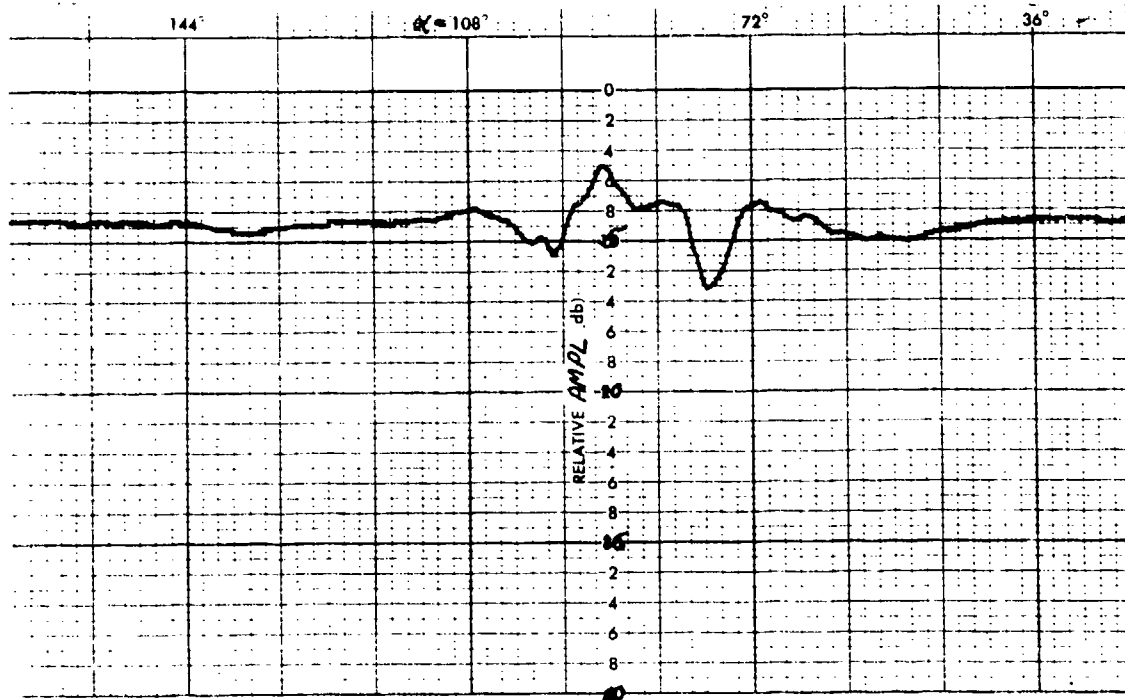


FIG. III-34. PHASE AND AMPLITUDE VARIATIONS
FOR SMALL COUNTERPOISE AND
VERTICAL POLARIZATION AT
 $\theta = 70^\circ$, $\phi = 0^\circ$, $h = 0 \lambda$



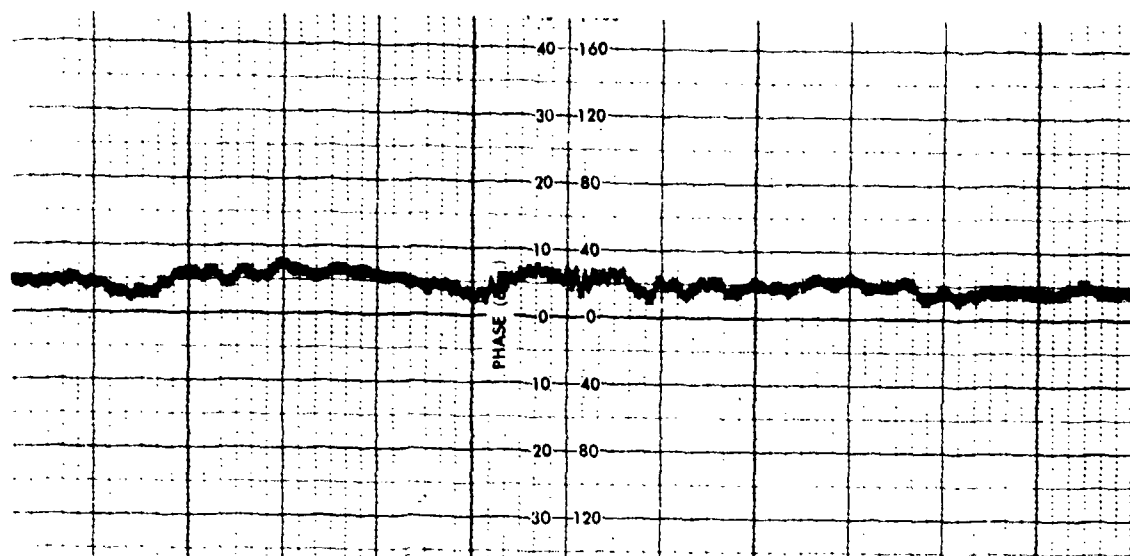
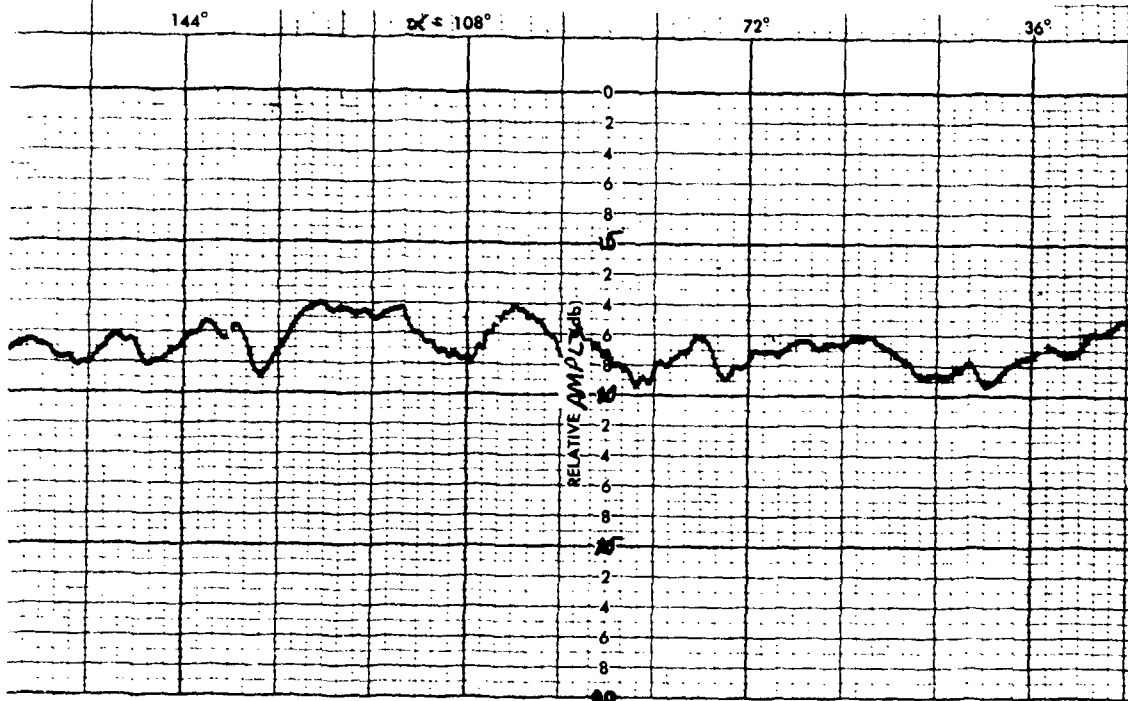


FIG. III-35. PHASE AND AMPLITUDE VARIATIONS
 FOR SMALL COUNTERPOISE AND
 VERTICAL POLARIZATION AT
 $\theta = 85^\circ$, $\phi = 90^\circ$, $h = 0 \lambda$



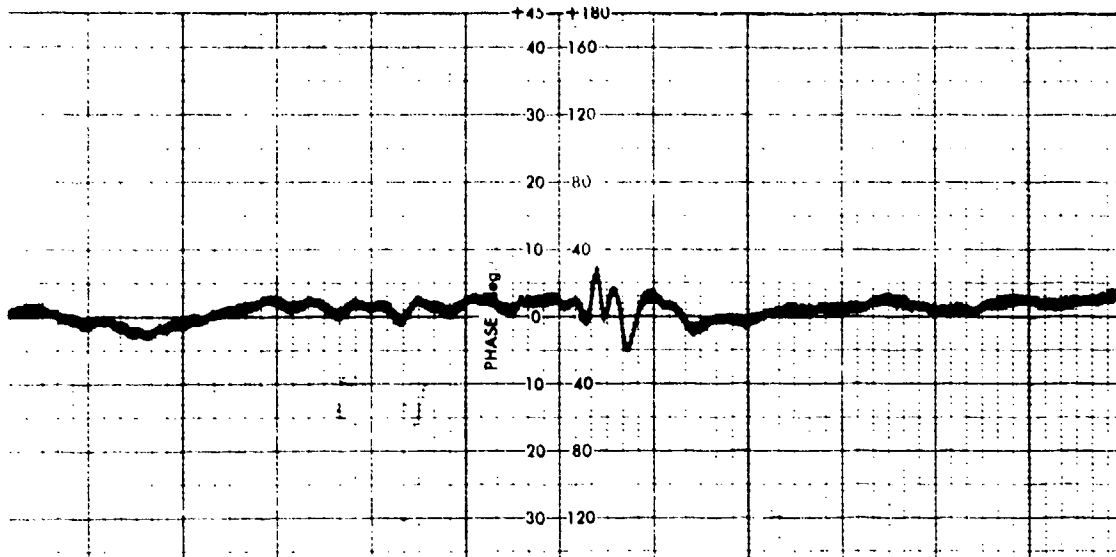
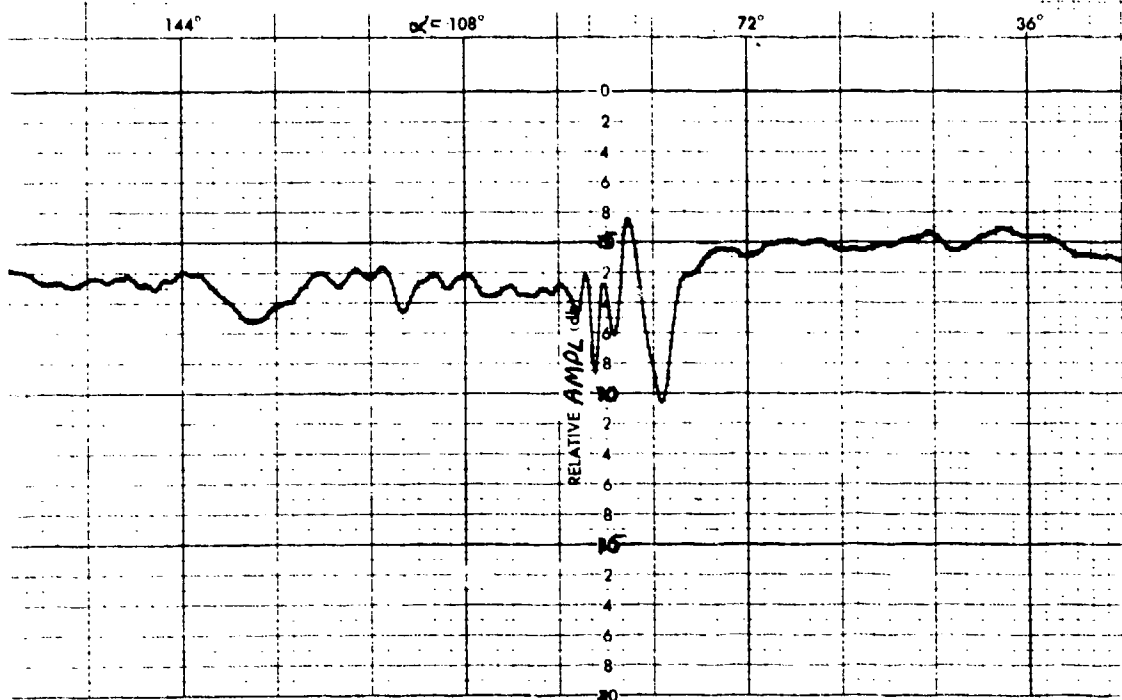


FIG. III-36. PHASE AND AMPLITUDE VARIATIONS FOR SMALL COUNTERPOISE AND HORIZONTAL POLARIZATION AT $\theta = 85^\circ$, $\phi = 45^\circ$, $h = 0\lambda$



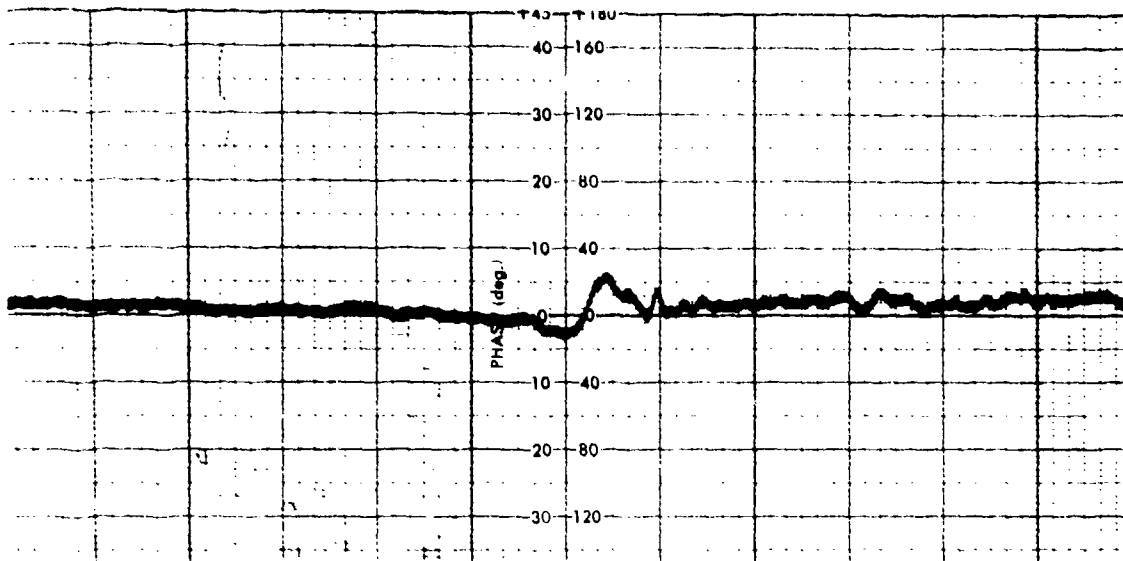
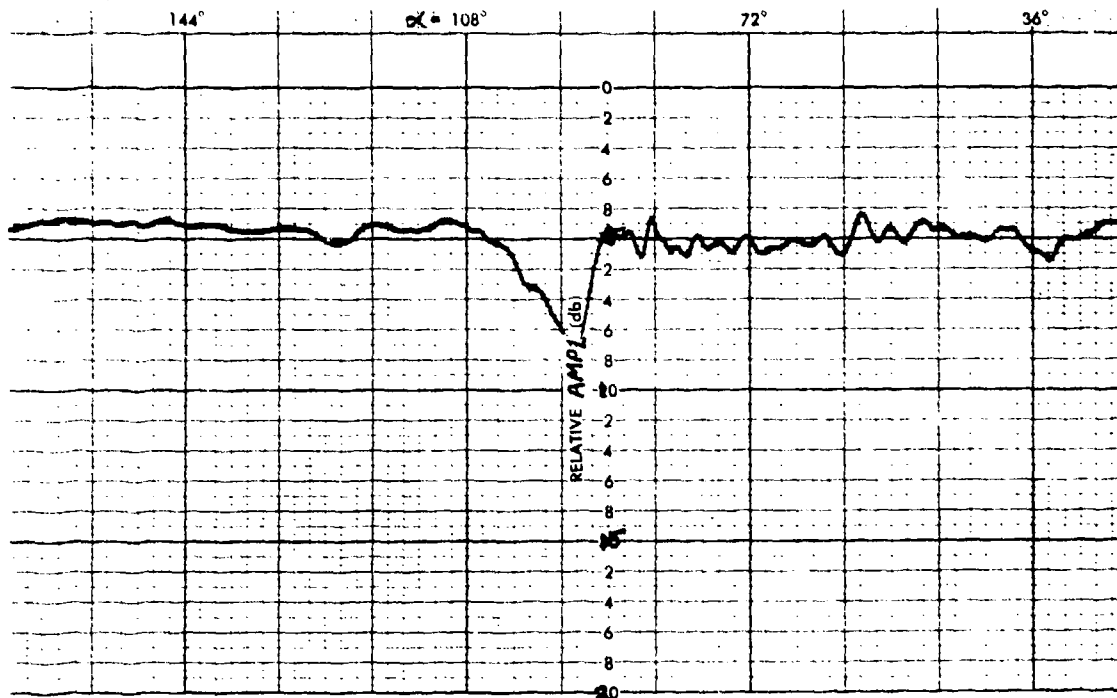


FIG. III-37. PHASE AND AMPLITUDE VARIATIONS
FOR SMALL COUNTERPOISE AND
VERTICAL POLARIZATION AT
 $\theta = 105^\circ$, $\phi = 315^\circ$, $h = 0\lambda$



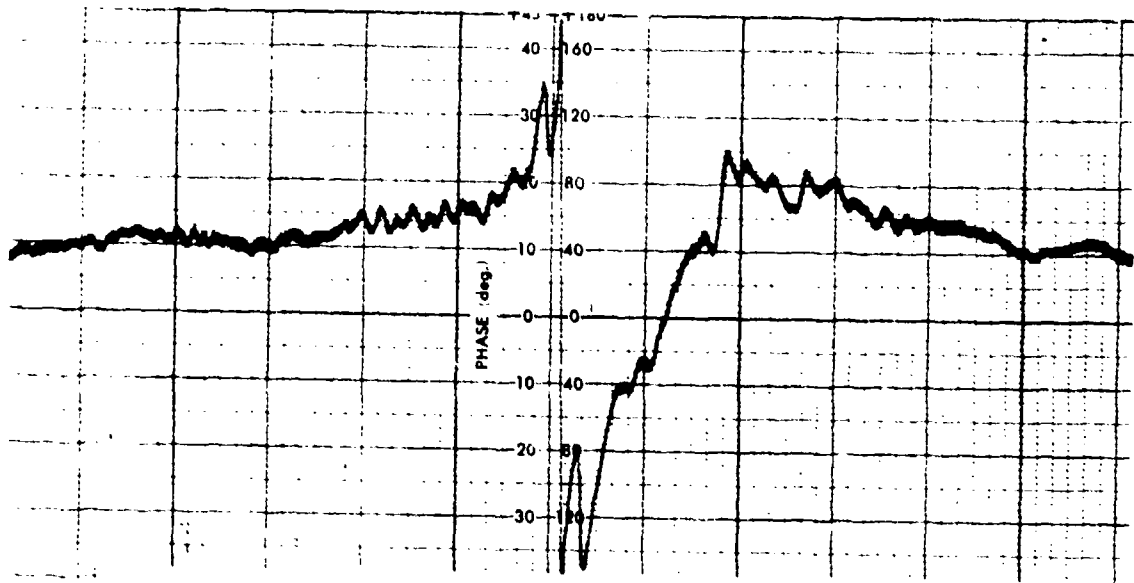
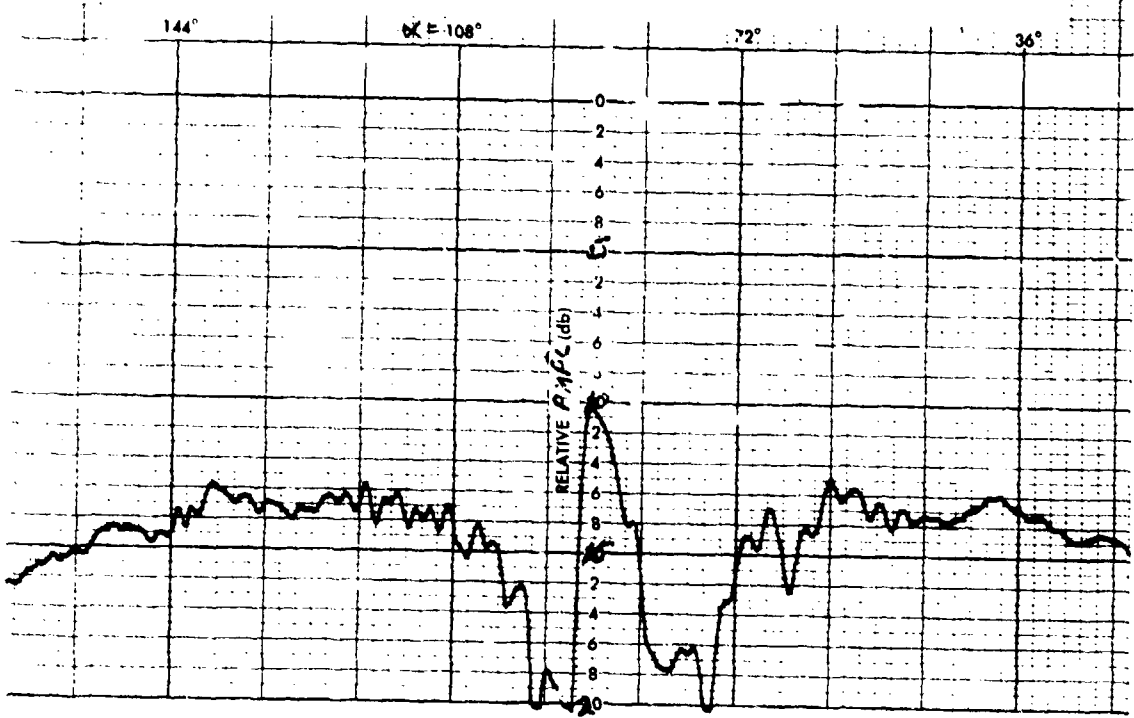


FIG. III-38. PHASE AND AMPLITUDE VARIATIONS FOR SMALL COUNTERPOISE AND HORIZONTAL POLARIZATION AT $\theta = 105^\circ$, $\phi = 0^\circ$, $h = 0 \lambda$



HISA-FM- 2075-75